



Universiteit Utrecht

75
AÑOS



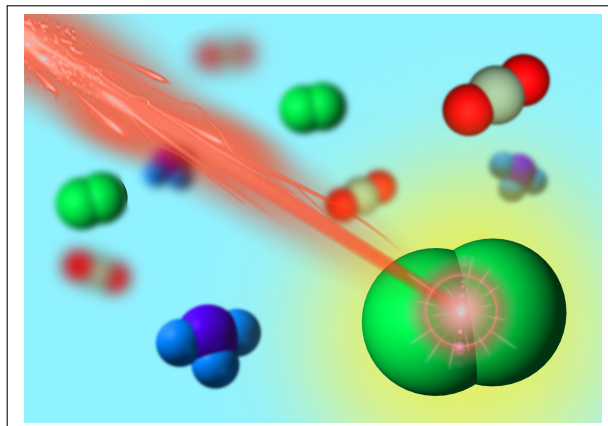
CSIC
CONSEJO SUPERIOR DE INVESTIGACIONES CIENTÍFICAS

Master's Programme
Experimental Physics
Graduate School of Natural Sciences (GSNS)

Characterisation and Modelling of Pulsed Ultra-Long Ring Fiber Laser

MASTER'S THESIS

Fernando SOLÍS FERNÁNDEZ



Supervisors:

Dr. Juan D. ANIA CASTAÑÓN

Instituto de Óptica, CSIC

Dr. Gerhard A. BLAB

Debye Institute for Nanomaterials Science

Dr. Dries VAN OOSTEN

Debye Institute for Nanomaterials Science

June, 2021

Characterisation and Modelling of Pulsed Ultra-Long Ring Fiber Laser

Fernando Solis Fernandez

June, 2021

Contents

Acknowledgements	3
List of abbreviations	3
1 Introduction	4
1.1 Motivation	4
1.2 Goals	5
1.3 Outline	5
2 Theoretical background	6
2.1 Basic concepts of lasers and optical fibers	6
2.2 Fiber lasers and ring lasers	8
2.3 Pulse propagation inside optical fibers	10
2.4 Dispersive effects	17
2.4.1 Group Velocity Dispersion (GVD)	17
2.4.2 Third Order dispersion (TOD)	20
2.5 Nonlinear effects	22
2.5.1 Self-phase modulation (SPM)	22
2.5.2 Cross-phase modulation (XPM)	25
2.5.3 Four wave mixing (FWM)	26

2.5.4	Stimulated Raman Scattering (SRS)	27
2.5.5	Solitons	31
3	The experiment and numerical approach	35
3.1	Experimental setup	36
3.2	Modelling and simulation	38
3.2.1	The Model	38
3.2.2	Simulation	40
3.2.3	Optimization	44
3.3	Results	49
4	Conclusions	55
5	Further research	56
	Appendix A: User Interface guide	59
	Appendix B: The code	63
	References	65

Acknowledgements

Thanks to Inés Cáceres Pablo for providing wonderful insight about the experimental setup and being incredibly helpful with the measurements. Thanks to Noelia Pellejero Cuevas for the marvelous assistance with the artistic illustrations

List of abbreviations

AC - Autocorrelator
BVP - Boundary Values Problem
CW - Continuous Wave
EDFA - Erbium-Doped Fiber Amplifier
FBG - Fiber Bragg Grating
FWHM - Full Width at Half Maximum
FWM - Four Wave Mixing
GVD - Group Velocity Dispersion
IVP - Initial Values Problem
LASER - Light Amplification by Stimulated Emission of Radiation
MMF - Multi-Mode Fiber
NLSE - Non-Linear Schrödinger Equation
NM - Nelder-Mead
NN - Neural Network
ODE - Ordinary Differential Equation
OSA - Optical Spectrum Analyzer
OSNR - Optical Signal-to-Noise Ratio
OTDR - Optical Time Domain Reflectometer
PMD - Polarization Mode Dispersion
RK - Runge-Kutta
SESAM - Semiconductor Saturable Absorber Mirror
SMF - Single-Mode Fiber
SPM - Self-Phase Modulation
SRS - Stimulated Raman Scattering
TIR - Total Internal Reflection
TOD - Third Order Dispersion
UI - User Interface
XPM - Cross-Phase Modulation

1 Introduction

1.1 Motivation

In the past few decades, light technologies have seen an outstanding development. First lasers were created during the 1960's and, since their first appearance, there have been great expectations about their huge potential. In that time, it was said that they would completely change the world, from dentists' tools to telephone wires [1], and they did. Since the 60s, lasers have been highly improved in efficiency, cost and reliability and nowadays we can find them everywhere around. In fact, many of the predictions that were made about lasers when they first came out, have become real. For instance, laser tools for cutting or surgery are now common practice. But among all those predictions that have come to life, maybe the one we are most used to is the replacement of telephone wires (and telecommunications in general) with lines that use laser light to transmit information from one point to another.

Of course, achieving light-based telecommunication systems has not been possible only thanks to lasers. In order to transmit light from one point to another distant one, we need a medium for light to propagate without major losses. This medium is the optical fiber. Optical fibers are a type of guided light system. This had been theorized earlier on, but it was not until 1966 that optical fibers were proposed as a medium for light transmission in telecommunications [2]. However, it was not until the 80s that optical fibers started to be used for telecommunication purposes. In the beginning they were still quite lossy (around 20 dB/km) but more sooner rather than later, they were highly improved [3] and nowadays they have been implemented in telecommunication systems all around the world.

A necessity that arises in the field of telecommunications is not just to achieve lossless transmission, in the sense that the output power equals the input power. But to prevent the signal from decaying and getting a signal gain curve as flat as possible. This can be achieved by periodically amplifying at certain points of the systems, as it is done with telephone or WiFi signal repeaters. However, this does not avoid signal attenuation and it adds an important drawback: the amplification of noise along with the signal. This problem can be avoided if, instead of periodical amplification, distributed amplification is used, so gains and losses are compensated at every point. One way to achieve this distributed amplification is through the Raman effect (we will discuss it on section 2.5.4) in systems like the one J.D. Ania-Castañón and his team are developing.

A very brief explanation on lasers and optical fiber working principles will be given in section 2, but so far, we have made clear the close relation between lasers and optical fiber in the field of telecommunications. Since the 80s, a lot of research has been made on this topic in an effort to make these systems more and more efficient and reliable. Following this effort, pulsed lasers were quickly introduced. Pulsed lasers present many advantages compared with continuous wave lasers in the telecommunications field. Since the energy of the pulse is concentrated in a short period of time, higher peak powers are achieved. In addition, pulsed lasers are more compatible with the binary architecture that most digital systems use. However, higher peak powers and the long interaction lengths provided by optical fibers come along with nonlinear effects that could be, in principle, detrimental for the system performance. But they can also be studied and used in our favour. J.D. Ania-Castañón et al. are working to achieve a virtually lossless system [4] that uses nonlinear effects to compensate for fiber losses. Properly managing fiber losses and nonlinear effects would allow for soliton¹ transmission over a fiber span.

¹We will talk about solitons a little later on section 2

1.2 Goals

The main goal of the project is to study an ultra-long ring cavity fiber laser that operates in an ultra-short pulse (hundreds of fs) regime. The characteristics of this type of lasers are ideal for the appearance of numerous nonlinearities. We intend to study its applicability in solitonic, lossless transmission. While trying to achieve that, we will be pursuing several goals:

- Study the behaviour of the ring laser in different pumping conditions.
- Learn what nonlinear effects have greater relevance under different conditions.
- Create a numerical model of the laser that can be numerically solved to obtain simulated results.
- Compare simulated and experimental results and correct the model if necessary.
- Finish with a design of a more stable and reliable fs laser

The goals stated up here are the ones that J.D. Ania-Castañón's team and myself are pursuing. However, I have set some personal goals for myself apart from the collective ones. I consider these ones more related to my own formation and learning process:

- Design a code to simulate the model that can be used after my collaboration is over. Therefore, it should be versatile, robust and user-friendly.
- Learn about the nonlinear effects that appear as a result of high peak powers. Since it is my first contact with these type of phenomena, it is my main intention to achieve an understanding of them as deep as possible by the end of my time with J.D. Ania-Castañón's team.
- Understand the experiment design and the different parts of the setup while taking rigorous experimental measurements that will be compared with my own simulation's results.
- Use these experimental results to correct the model if necessary and try to end up with a model as accurate as possible.

During the time spent under the supervision of J.D. Ania-Castañón and his team, I did my best to fulfill all of my personal goals and help as much as possible with the team's goals.

1.3 Outline

In chapter 2, explanations on the different effects that have to be considered when studying the propagation of a light pulse through a silica fiber are given. This includes dispersive effects (section 2.4) and nonlinear effects (2.5).

On section 3 I will give a detailed explanation of the whole setup and the experiment. I will also focus on the part of the setup that I have been working on. I will show the experimental results and compare them with the simulated data. In this section, I will also talk about the mathematical model and how it has been solved to obtain numerical results.

On section 4 I will sum up all the information obtained both from simulations and experiments and give an educated opinion on the whole experiment and topic.

Finally, on section 5 I will mention some of the applications that this setup might have once it is finished and stable as well as some research lines that could come out of it in a near future.

2 Theoretical background

2.1 Basic concepts of lasers and optical fibers

As mentioned in the introduction (section 1), the combined effects of a laser and an optical fiber span will be used in our setup to produce a virtually lossless system. Hence, it is useful to provide a very brief reminder of their working principles to set a base for the effects that will be later described. Because my work is more centered around the study of the role that the fiber span plays in our system, I will elaborate more on this topic than on lasers.

Laser is an acronym for Light Amplification by Stimulated Emission of Radiation. This means that they generate, or more usually, amplify a small amount of light that is injected into it (called ‘pumping’). To obtain a laser, one needs at least three elements: a medium, that will provide a large amount of atoms that will radiate during de-excitation; a pumping process, to generate a population inversion (take the majority of these atoms to excited states); and an optical feedback to allow for the beam to pass once through the medium or bounce back and forth between its endings [5]. All three elements should provide something like figure 2.1.1

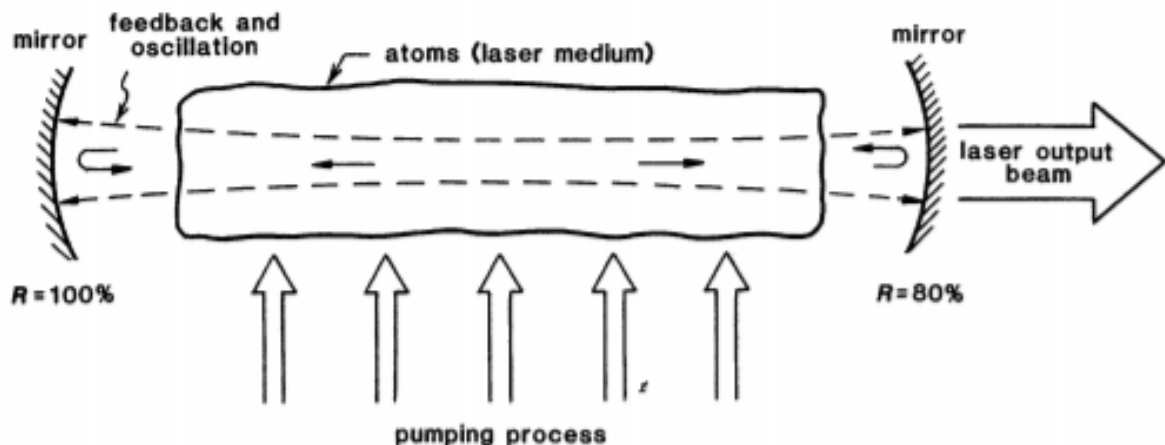


Figure 2.1.1: Scheme of a laser’s working principle. Extracted from [5]

Obtaining the necessary population inversion in the medium when trying to generate laser light can be challenging. This is typically achieved by using four-level lasers. In this type of lasers, atoms are excited from their ground state to an excited state. From said excited state, the atoms will decay in a non-radiative way to a lower-energy state. Then, the spontaneous emission takes place when atoms decay a second time from the low-energy excited state to an even lower energy state. Finally, atoms will decay again in a non-radiative way to the ground state. This is illustrated in figure 2.1.2. The excitement and decaying process is a natural phenomenon called spontaneous emission, but when a pump sufficiently high is used to excite the atoms, a threshold is surpassed and spontaneous emission becomes stimulated emission. In this regime, a population inversion takes place, which means that the majority of the atoms are in a high-energy level. Then, stimulated by said pump, the atoms decay providing an intense source of light which is coherent and very monochromatic. This phenomenon can be enhanced with a feedback mechanism. For instance, reflectors can be included at the ends of the medium, creating a resonator. Light would then bounce off of them going back and forth, stimulating the emission of more light.

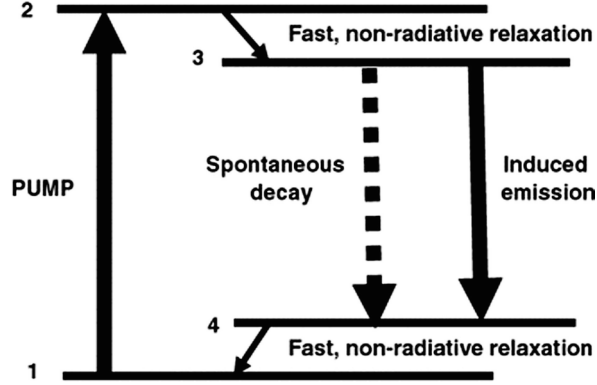


Figure 2.1.2: Scheme of a laser’s working principle. Extracted from [6]

One last note I would like to add on this topic is the different working regimes that different lasers may have. There are mainly two of them: continuous wave regime and pulsed regime. Different operating modes will adequate to different purposes. For instance, pulsed lasers are widely used in materials processing or photonics applications [7–9], whereas continuous wave lasers can be found in mechanical or engineering, and also photonics applications [10–12]. The regime in which a laser works, usually depends on parameters of the active medium such as the lifetime of the excited states [5]. Depending on this, it might be impossible to maintain the continuous cycle of population inversion and decaying. Typically, pulsed lasers are achieved with a pulsed pumping method or by using techniques such as Q-Switching [13] or mode-locking [14]. Pulsed lasers can generate a wide range of pulse widths and the exploration of the lower limits of this width has become a popular topic in the past few years. The reason why this is so is because many interesting physical phenomena take place when really short pulses are reached [15]. On the one hand, small pulses focus the energy of the pulse in a very short time, hence providing really high peak powers. On the other hand, when interacting with matter, short pulses can reveal interesting phenomena derived from this extremal light-matter interaction.

The characteristics of the light that exits the laser cavity have granted it a solid place in every laboratory around the world. Thanks to these devices, we can obtain powerful, colimated, coherent and almost monochromatic light. Plus, nowadays, we can find a wide variety of lasers regarding their main wavelength, working regime, portability, cost, etc. A lot could be said about lasers and I encourage the reader, if in need or interested, to search through the literature. Reference [16] gives a little more insight on the basics of lasers and reference [5] provides very extensive knowledge of the theoretical foundations of lasers. The reader may also check references [6] for more advanced, fiber-focused laser knowledge; or reference [17] to learn about the latest techniques that have been developed.

Because we are working with a fiber laser and I will be focused in the fiber span acting as a cavity during my project, I think it is useful to include also a little summary of fiber optics working principle. Fiber optics rely on a rather simple phenomenon: total internal reflection (TIR). TIR arises from Snell’s law of refraction (2.1.1). If the refractive indices of the media fulfill the condition $n_1 > n_2$, TIR is achieved in the interface for angles greater than a critical angle given by eq. 2.1.2

$$n_1 \sin \theta_1 = n_2 \sin \theta_2 \tag{2.1.1}$$

$$\theta_c = \arcsin \frac{n_2}{n_1} \tag{2.1.2}$$

This phenomenon is used to make light bounce off of the internal surface of the fiber on and on as it propagates through the span. This is illustrated in figure 2.1.3

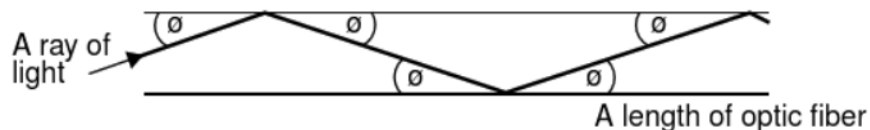


Figure 2.1.3: Scheme of a fiber optics' working principle. Extracted from [18]

Because of the necessary condition for TIR, light needs to propagate within a medium with higher refractive index than air. Generally silica glass is used for this purpose, but a variety of materials, such as plastics, can be used as well. There are numerous types of fiber optics with different properties, suitable for different applications. However, they can all be sorted into two main categories: single mode fiber (SMF) and multimode fiber (MMF). Depending on the fiber's nature, light might be able to propagate in only one way (SMF) or in several ways (MMF). These different ways in which light can travel inside the fiber are called modes (see fig. 2.1.4).

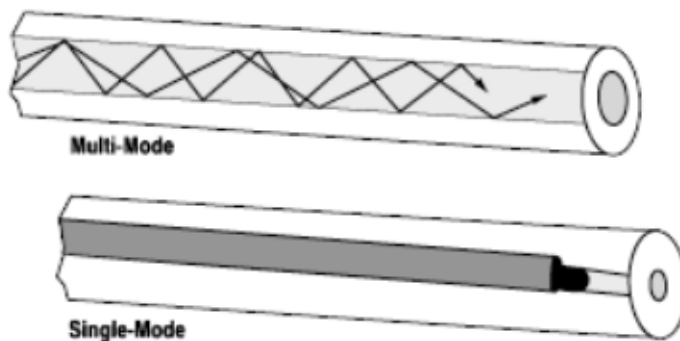


Figure 2.1.4: Fiber modes in SMF and MMF. Extracted from [19]

The fact that the optical fiber provides a material medium for light to propagate is a source of interesting phenomena by itself. These are usually referred to as dispersive effects and have to do with the dependence of λ with the refractive index. But if we also consider the high-peak powers obtained from pulsed lasers, we will be able to see other type of phenomena equally, if not even more, interesting, called nonlinear effects. Both, dispersive and nonlinear effects will be discussed during sections 2.4 and 2.5.

As with lasers, a lot more could be said on this topic and I, again, encourage the reader to go through the references if required or if willing to learn more about fiber optics. Reference [18] provides a very basic, applied approach. In references [20] and [21] you can find broader, yet still quite fundamental explanations about the main topics surrounding fiber optics. And in reference [2] a more advanced insight is given.

2.2 Fiber lasers and ring lasers

We have provided the basics on laser and optical fibers working principles. So it is time to put both of them together and learn a little about fiber lasers. And specially, since the system I will be working with is a ring fiber laser, I will also explain the main features of this type of lasers.

An optical fiber is a great option to produce and study nonlinear phenomena. This is not because of the material the fiber is made of itself (as silica is actually very “linear”), but rather because of the long interaction length between the pulse and the medium and the small core area of the fiber. More on this will be discussed through section 2.5, but one of these nonlinear phenomena that might appear in the fiber is the stimulated Raman scattering (SRS). Very briefly (more is given in section 2.5.4), in the presence of a pump wave, SRS can be responsible for the appearance of a so-called Stokes wave, which is downshifted from said pump. If this Stokes radiation is enclosed by mirrors, creating a cavity, a Raman oscillator is made [22]. Adding specific elements to this cavity can allow us to tune the oscillator over the broad Raman gain curve. And once the threshold power pump has been surpassed, power conversion from the pump to the Stokes wave begins to occur and an effective gain is achieved at the Stokes frequency.

The difference between a regular laser and a fiber laser is that the first ones use atomic energy levels to create the three (or more usually four) level scheme to work, as was explained in section 2.1. But, fiber Raman lasers rely on the phenomenon of Raman scattering, which involves vibrational molecular energy levels and photon-phonon interaction to produce the stimulated emission. Thanks to it, a regular span of single mode fiber can be converted into a somewhat tunable laser source, although to achieve said conversion, one must dope the fiber with rare earths (typically erbium, ytterbium, neodymium...[23–25]). But they present important advantages; for instance, since the active medium is a flexible material, it is much easier to store and transport. Also, since the SRS phenomenon occurs throughout the whole fiber span, Raman lasers produce a distributed gain though all the fiber.

One of the main components of the laser is the resonator. The resonator is what allows radiation to build up inside the cavity as light bounces on and off the mirrors at the ends. Now, we can substitute the linear resonant cavity by a cavity with the shape of a ring. In such cavity, light instead of going back and forth from one mirror to the other, propagates in the same direction uninterrupted. However, the ring cavity allows for two independent propagation directions (see fig. 2.2.1). Ring lasers can be advantageous with respect to regular line lasers because of several reasons, a major one being that, because there are no mirrors with normal incidence, light can never go back directly into the source [26]. This can be critical in lasers that are highly affected by feedback from the cavity

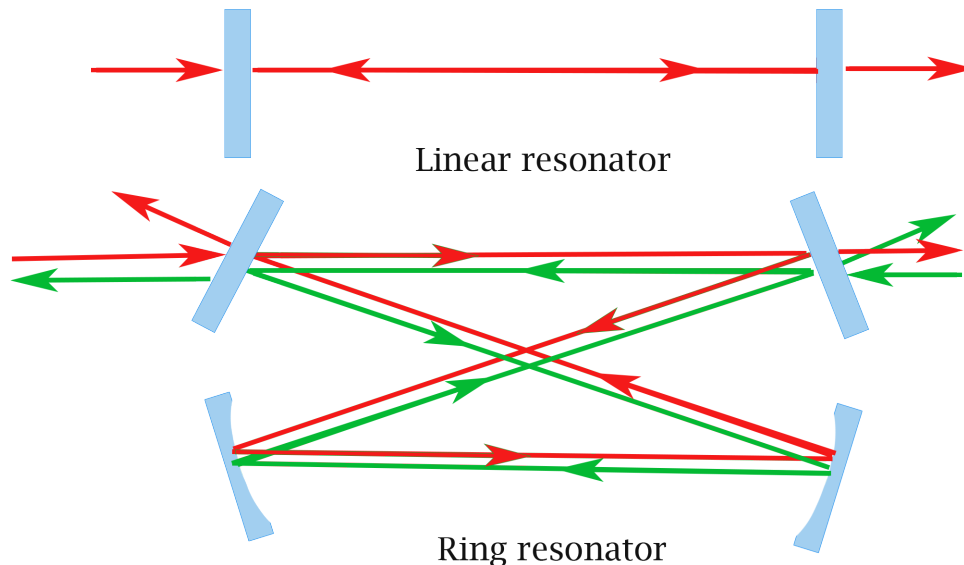


Figure 2.2.1: Resonator types. Linear (up) and ring (down) with the propagation directions they allow for

Combining fiber lasers and ring cavities results in ring fiber lasers, which unite the advantages of ring resonators with those of fiber lasers. Furthermore, the ring resonator in a fiber ring laser is obtained through TIR, which happens naturally inside the fiber. So there is no need to include mirrors inside the fiber (although it can be done for tuning or signal cleaning). That makes ring fiber lasers a great option for many applications

2.3 Pulse propagation inside optical fibers

In this and the next sections (2.3 - 2.5) fairly detailed explanations are given on a series of dispersive and nonlinear effects. The documentation for these sections has been mainly based on Govind P. Agrawal's book of nonlinear fiber optics. [27]. Agrawal's book provides very exhaustive and top-quality explanations that have been immensely helpful to understand and write the content of these sections.

The propagation of a light pulse within a material medium is defined by Maxwell's laws (2.3.1 - 2.3.4) and the constitutive relations (2.3.5 - 2.3.6)

$$\nabla \times \mathbf{E} = -\frac{\partial \mathbf{B}}{\partial t} \quad (2.3.1)$$

$$\nabla \times \mathbf{H} = \mathbf{J} + \frac{\partial \mathbf{D}}{\partial t} \quad (2.3.2)$$

$$\nabla \cdot \mathbf{D} = \rho_f \quad (2.3.3)$$

$$\nabla \cdot \mathbf{B} = 0; \quad (2.3.4)$$

$$\mathbf{D} = \epsilon_0 \mathbf{E} + \mathbf{P} \quad (2.3.5)$$

$$\mathbf{H} = \frac{\mathbf{B}}{\mu_0} - \mathbf{M} \quad (2.3.6)$$

Where \mathbf{E} is the electric field; \mathbf{H} , the magnetic field; \mathbf{D} the electric flux density; \mathbf{B} , the magnetic flux density; \mathbf{P} , the electric polarization; \mathbf{M} , the magnetization; \mathbf{J} , the current density; μ_0 and ϵ_0 are electric permittivity and magnetic permeability of vacuum respectively; and magnitudes in bold letters represent vectors.

The response of the medium (optical fiber in this case) to an electric field is governed by the electric polarization \mathbf{P} . And specially, since optical fibers are not magnetic, their electric polarization becomes our main concern. In general, a quantum-mechanical approach would be necessary to address the form and value of \mathbf{P} , but if we are working with frequencies far away from the resonant frequencies of the medium, a more classical, phenomenological approach can be used. Therefore, we can obtain the polarization vector from eq. 2.3.7

$$\mathbf{P} = \epsilon_0 \left(\chi^{(1)} \cdot \mathbf{E} + \chi^{(2)} : \mathbf{E}\mathbf{E} + \chi^{(3)} : \mathbf{E}\mathbf{E}\mathbf{E} \dots \right) \quad (2.3.7)$$

Here, χ is the electric susceptibility. In general $\chi^{(i)}$ is a tensor or rank $i + 1$. Note that there is no dot between the \mathbf{E} s in the second and third terms of the equation, meaning that they are operated with the dyad product, whereas the two or three vertical dots in said terms represent the double and triple dot product. A

very good conceptual approach to the basic ideas regarding tensors can be found in reference [28] and much broader and profound insight on the topic can be found on reference [29].

Naturally, the major contribution to the polarization with this description is due to $\chi^{(1)}$, the linear susceptibility. The effect of the linear susceptibility is reflected in the familiar linear refractive index, n . The next biggest contribution should be due to $\chi^{(2)}$, but this is nonzero only for media with no inversion symmetry on a molecular level (which is not the case for optical fibers). Hence, the second term of eq. 2.3.7 can be taken to be zero. So, the next term we need to consider is the one with $\chi^{(3)}$. This will be responsible for the nonlinear phenomena described in section 2.5 and will be reflected in the nonlinear refractive index, \tilde{n}_2 .

Knowing that the main two contributions to the polarization come from $\chi^{(1)}$ (linear) and $\chi^{(3)}$ (nonlinear), we can rewrite the polarization as $\mathbf{P}(\mathbf{r}, t) = \mathbf{P}_L(\mathbf{r}, t) + \mathbf{P}_{NL}(\mathbf{r}, t)$, where \mathbf{P}_L and \mathbf{P}_{NL} are given by equations 2.3.8 and 2.3.9.

$$\mathbf{P}_L(\mathbf{r}, t) = \epsilon_0 \int_{-\infty}^{\infty} \chi^{(1)}(t - t') \cdot \mathbf{E}(\mathbf{r}, t') dt' \quad (2.3.8)$$

$$\mathbf{P}_{NL}(\mathbf{r}, t) = \epsilon_0 \iiint_{-\infty}^{\infty} \chi^{(3)}(t, t_1, t_2, t_3) \cdot \mathbf{E}(\mathbf{r}, t_1) \mathbf{E}(\mathbf{r}, t_2) \mathbf{E}(\mathbf{r}, t_3) dt_1 dt_2 dt_3 \quad (2.3.9)$$

Due to the high complexity of these expressions, we will need to apply significant simplifications to use them. The first simplification we can make is use the fact that the nonlinear contribution is usually much weaker than the linear contribution, so we can treat the first as a small perturbation to the latter. The second simplification is assuming that \mathbf{E} is linearly polarized (for example along the x direction), so that the only contributing terms of $\chi^{(1)}$ and $\chi^{(3)}$ are, respectively, $\chi_{xx}^{(1)}$ and $\chi_{xxxx}^{(3)}$. Another significant simplification can be made if we assume that the medium's nonlinear response to the field is instantaneous. In that case, the time dependence of $\chi^{(3)}$ is given by the product of three delta functions $\delta(t - t_i)$ (with $i = 1, 2, 3$) and equation 2.3.9 reduces to eq. 2.3.10. Note that this equation holds for pulses broader than 1 ps. Electronic response to the medium is persé much faster than the nuclear response and we consider the electronic response to be fast and the nuclear response to be slow. For fibers, the response of the nuclei (Raman or vibrational response) is in the order of 0.1 ps. If the pulse is wider than that, both, the nuclear and electronic responses can be considered fast and the approximation does not hold anymore. This assumption neglects the Raman contribution to the nonlinear polarization, but it will be included later on, in section 2.5.4.

$$\mathbf{P}_{NL}(\mathbf{r}, t) = \epsilon_0 \chi^{(3)} \cdot \mathbf{E}(\mathbf{r}, t) \mathbf{E}(\mathbf{r}, t) \mathbf{E}(\mathbf{r}, t) \quad (2.3.10)$$

Making use of the Maxwell equations and the constitutive relations (eqs. 2.3.1 - 2.3.6), we can arrive at the wave equation inside the fiber (2.3.11)

$$\nabla^2 \mathbf{E} - \frac{1}{c} \frac{\partial^2 \mathbf{E}}{\partial t^2} = \mu_0 \frac{\partial^2 \mathbf{P}_L}{\partial t^2} + \mu_0 \frac{\partial^2 \mathbf{P}_{NL}}{\partial t^2} \quad (2.3.11)$$

c being the speed of light

If we use the first simplification we mentioned (treating \mathbf{P}_{NL} as a weak perturbation) and assume that losses in the fiber are negligible (low absorption coefficient), the first step would be to solve the wave equation 2.3.11 without the nonlinear term. This is much more easily done in the frequency domain. So, taking the

Fourier transform of equation 2.3.11 (without the nonlinear term), we arrive at the well-known Helmlotz equation 2.3.12:

$$\nabla^2 \tilde{\mathbf{E}} + n^2(\omega) \frac{\omega^2}{c^2} \tilde{\mathbf{E}} = 0 \quad (2.3.12)$$

Where, $n(\omega)$ is the refractive index and ω is the frequency. The refractive index is related to the permittivity, ϵ , through 2.3.13:

$$\epsilon(\omega) = \left(n + i \frac{\alpha c}{2\omega} \right)^2 \quad (2.3.13)$$

At the same time, ϵ is related to the Fourier transform of the susceptibility ($\tilde{\chi}$) through 2.3.14

$$\epsilon(\omega) = 1 + \tilde{\chi}^{(1)}(\omega) \quad (2.3.14)$$

If the absorption, α is small, equations 2.3.13 and 2.3.14 lead to the known relations 2.3.15

$$n(\omega) = \sqrt{1 + \text{Re}[\tilde{\chi}^{(1)}(\omega)]}, \quad \alpha(\omega) = \frac{\omega}{nc} \text{Im}[\tilde{\chi}^{(1)}(\omega)] \quad (2.3.15)$$

Since our current goal is to solve Helmholtz's equation (2.3.12) inside a fiber, the easiest way is to take advantage of the cylindrical symmetry of the medium and switch to cylindrical coordinates (eq. 2.3.16). Doing so, allows us to find a general solution in the frequency domain using separation of variables that has the form of 2.3.17

$$\frac{\partial^2 \tilde{\mathbf{E}}}{\partial \rho^2} + \frac{1}{\rho} \frac{\partial \tilde{\mathbf{E}}}{\partial \rho} + \frac{1}{\rho^2} \frac{\partial^2 \tilde{\mathbf{E}}}{\partial \phi^2} + \frac{\partial^2 \tilde{\mathbf{E}}}{\partial z^2} + n^2 k_0^2 \tilde{\mathbf{E}} = 0 \quad (2.3.16)$$

$$\tilde{E}_z(r, \omega) = A(\omega) F(\rho) e^{il\phi} e^{\beta z} \quad (2.3.17)$$

Where k_0 is the wave number $\frac{\omega}{c} = \frac{2\pi}{\lambda}$; $l = 0, 1, 2, \dots$, is an integer; β , is the propagation constant, A is a function that depends only on ω and $F(\rho)$ is the solution to 2.3.18

$$\frac{d^2 F}{d\rho^2} + \frac{1}{\rho} \frac{dF}{d\rho} + \left(n^2 k_0^2 - \beta^2 - \frac{l^2}{\rho^2} \right) F = 0 \quad (2.3.18)$$

To solve equation 2.3.18 one must consider two separate regions. Inside the core, the solution must not diverge as $r \rightarrow 0$, and outside the core, the solution should decay exponentially to account for the lack of losses of the fiber (light travels bouncing on the core-cladding interface thanks to TIR, so no light escapes the fiber and no energy should be lost). These considerations also impose a condition on the propagation constant [30]. The propagation constant of a mode β_{lm} can be understood as the longitudinal component of the wave vector. So, the existing constraints when solving eq. 2.3.18 imply that condition 2.3.19 must be satisfied

$$n_2 k < \beta < n_1 k \quad (2.3.19)$$

being n_1 and n_2 , the refractive indices of core and cladding respectively;

The solutions to equation 2.3.18 with the considerations mentioned above, are the well-known Bessel functions 2.3.20. This solution along with condition 2.3.19 reveal the existence of a cut-off frequency (wavelength) above which (below which) no modes can propagate without losses.

$$F(\rho) = \begin{cases} J_l(p\rho), & \rho \leq a \\ K_l(q\rho), & \rho \geq a \end{cases} \quad (2.3.20)$$

Where $p = \sqrt{n_1^2 k_0^2 - \beta^2}$ and $q = \sqrt{\beta^2 - n_2^2 k_0^2}$ and a , the fiber core radius

We can follow the same procedure and solve the wave equation (2.3.16) in cylindrical coordinates for the magnetic component of the field \vec{H} . Then applying that tangential components (\vec{E}_z and \vec{H}_z) must be continuous across the core-cladding interface and angular components (\vec{E}_ϕ and \vec{H}_ϕ) must be equal to each other at $\rho = a$, we arrive at an eigenvalues equation 2.3.21 that will allow us to determine the propagation constant β .

$$\left[\frac{J'_l(U)}{U J_l(U)} + \frac{K'_l(W)}{W K_l(W)} \right] \left[\frac{J'_l(U)}{U J_l(U)} + \frac{n_c^2}{n_1^2} \frac{K'_l(W)}{W K_l(W)} \right] = l^2 \left(\frac{1}{U^2} + \frac{1}{W^2} \right) \left(\frac{1}{U^2} + \frac{n_c^2}{n_1^2} \frac{1}{W^2} \right) \quad (2.3.21)$$

Where $U = pa$ and $W = qa$ so that the relation 2.3.22 defines a very important parameter of optical fibers: the V parameter

$$\sqrt{U^2 + V^2} = k_0 a \sqrt{n_1^2 - n_2^2} = V \quad (2.3.22)$$

Equation 2.3.21 gives multiple solutions for β for each integer value of l . These different solutions are named β_{lm} and each one represents a different way in which the pulse propagates within the fiber. They are called modes and only two types (HE_{lm} and EH_{lm}) can propagate through the fiber. These modes are analogous to the TE and TM modes that appear in dielectric planar wave guides (see references [31, 32] or [33] for more information and detailed derivation on wave guide modes), only that HE_{lm} and EH_{lm} modes have nonzero longitudinal components except for the $l = 0$ modes. For modes with $l \geq 1$, all six components of the magnetic and electric fields are nonzero. The V parameter determines the number of modes that can propagate within a certain fiber and it is related with the cut-off frequencies mentioned earlier. Specifically, the cut-off frequencies for each mode can be derived from equation 2.3.21 in the limit $q \rightarrow 0$ (or $W \rightarrow 0$). Over a certain cut-off frequency, only one mode can propagate, the HE_{11} , which is called the fundamental mode. Fibers that only allow for propagation of the fundamental mode are referred to as Single Mode Fibers, whereas if more than one modes are supported, they are called Multimode Fiber. The critical value V_c that separates SMFs from MMFs can be calculated as mentioned above and turns out to be $V_c \approx 2.405$. Since V depends mainly on fiber parameters (a, n_1, n_2), it can be tailored to the desired value during fiber manufacturing. This allows us to control the number of modes that can propagate inside the fiber.

The solution of equation 2.3.11 without the nonlinear term provides the basis to solve the complete equation with the perturbative nonlinear term. But it also defines a key variable of pulse propagation inside the fiber: the propagation constant β . β should be obtained from equation 2.3.21 but its form is rarely known, so it is usually expanded in Taylor series around the carrier frequency ω_0 to yield 2.3.23

$$\beta(\omega) = \beta_0 + (\omega - \omega_0) \beta_1 + \frac{1}{2} (\omega - \omega_0)^2 \beta_2 + \frac{1}{6} (\omega - \omega_0)^3 \beta_3 + \dots \quad (2.3.23)$$

Where, β_0 is the dispersion constant at the carrier frequency ($\beta_0 = \beta(\omega_0)$) and the β_m terms are defined as [2.3.24](#)

$$\beta_m = \left(\frac{d^m \beta}{d\omega^m} \right) \quad (2.3.24)$$

At this point we can go back to equation [2.3.11](#) and solve the complete equation, including the nonlinear term. In order to do this, first we separate the electric field and polarization as in [2.3.25](#). This is called the slowly varying amplitude method because \mathbf{E} and \mathbf{P} are separated in a part that varies rapidly with time (given by the exponential proportional to ω) and a part that varies slowly compared to the first one (given by the scalars E, P_L, P_{NL}).

$$\begin{aligned} \mathbf{E}(\mathbf{r}, t) &= \frac{1}{2} \hat{x} [E(\mathbf{r}, t) e^{-i\omega_0 t} + c.c.] \\ \mathbf{P}_L(\mathbf{r}, t) &= \frac{1}{2} \hat{x} [P_L(\mathbf{r}, t) e^{-i\omega_0 t} + c.c.] \\ \mathbf{P}_{NL}(\mathbf{r}, t) &= \frac{1}{2} \hat{x} [P_{NL}(\mathbf{r}, t) e^{-i\omega_0 t} + c.c.] \end{aligned} \quad (2.3.25)$$

Where, \hat{x} is the polarization unit vector and c.c. stands for complex conjugate.

The slowly varying part of P_L can be obtained by substituting the electric field from [2.3.25](#) in [2.3.8](#) and using the convolution theorem ² [[34](#), [35](#)] to give [2.3.26](#). And substituting the electric field from [2.3.25](#) in the simplified equation for the nonlinear polarization [2.3.10](#) gives the expression for the slowly varying part of the nonlinear polarization [2.3.27](#), where the nonlinear permittivity, ϵ_{NL} is defined as [2.3.28](#)

$$P_L(\mathbf{r}, t) = \frac{\epsilon_0}{2\pi} \int_{-\infty}^{\infty} \tilde{\chi}_{xx}^{(1)}(\omega) \tilde{E}(\omega - \omega_0) e^{-i(\omega - \omega_0)t} d\omega \quad (2.3.26)$$

$$P_{NL}(\mathbf{r}, t) \approx \epsilon_0 \epsilon_{NL} E(\mathbf{r}, t) \quad (2.3.27)$$

$$\epsilon_{NL}(\mathbf{r}, t) = \frac{3}{4} \chi_{xxxx}^{(3)} |E(\mathbf{r}, t)|^2 \quad (2.3.28)$$

With these definitions, we can try to solve the wave equation with the nonlinear term [2.3.11](#) in the Fourier space. In general this is not possible because of the intensity dependence of the nonlinear term. However, we can, as a first approach, take ϵ_{NL} as a constant during the process to get to the propagation equation. This is a sensible approach because of the slowly varying envelope and perturbative approximations used for the nonlinear term. With these considerations, we arrive again at the Helmholtz equation

$$\nabla^2 \tilde{E} + \epsilon(\omega) k_0^2 \tilde{E} = 0 \quad (2.3.29)$$

Where, this time $\epsilon(\omega)$ is given by [2.3.30](#)

$$\epsilon(\omega) = 1 + \tilde{\chi}_{xx}^{(1)} + \epsilon_{NL} \quad (2.3.30)$$

² $h(x) = \{f * g\}(x) = \mathcal{F}^{-1}\{\mathcal{F} \cdot G\}$

We can use this $\epsilon(\omega)$ to redefine the refractive index and absorption coefficient and include in them the effects of the nonlinear polarization, so relations 2.3.15 become 2.3.31

$$\tilde{n} = n + \tilde{n}_2 I, \quad \tilde{\alpha} = \alpha + \alpha_2 I \quad (2.3.31)$$

Using relations 2.3.13, 2.3.28 and 2.3.30; the nonlinear refractive index coefficient, \tilde{n}_2 and the two-photon absorption coefficient, α_2 are given by 2.3.32

$$\tilde{n}_2 = \frac{3}{8n} \text{Re} \left(\chi_{xxxx}^{(3)} \right), \quad \alpha_2 = \frac{3\omega_0}{4nc} \text{Im} \left(\chi_{xxxx}^{(3)} \right) \quad (2.3.32)$$

In a similar way as we proceeded to solve the linear wave equation 2.3.11 we can try to solve the nonlinear equation 2.3.29 in the Fourier space with an electric field of the form 2.3.33. This leads to equations 2.3.34 and 2.3.35 for the mode profile function, F and the slowly varying envelope, \tilde{A} respectively

$$\tilde{E}(\mathbf{r}, \omega - \omega_0) = F(x, y) \tilde{A}(z, \omega - \omega_0) e^{i\beta_0 z} \quad (2.3.33)$$

$$\frac{\partial^2 F}{\partial x^2} + \frac{\partial^2 F}{\partial y^2} + \left[\epsilon(\omega) k_0^2 - \tilde{\beta}^2 \right] F = 0 \quad (2.3.34)$$

$$2i\beta_0 \frac{\partial \tilde{A}}{\partial z} + \left(\tilde{\beta}^2 - \beta_0^2 \right) \tilde{A} = 0 \quad (2.3.35)$$

The eigenvalue equation 2.3.34 can be solved with a similar procedure to the one used for 2.3.18 but using perturbation theory to replace ϵ with 2.3.36

$$\epsilon = (n + \Delta n)^2 \approx n^2 + 2n\Delta n \quad (2.3.36)$$

Where the small perturbation Δn is given by 2.3.37

$$\Delta n = \tilde{n}_2 |E|^2 + \frac{i\tilde{\alpha}}{2k_0} \quad (2.3.37)$$

For a single mode fiber, F is the spatial distribution of the fundamental mode, which can be usually approximated by a Gaussian shape $F(x, y) \approx e^{-\frac{x^2+y^2}{w}}$. In the equation for \tilde{A} (2.3.35), we must apply perturbation theory too on the propagation parameter, so $\tilde{\beta}$ becomes 2.3.38, where $\Delta\beta$ is defined as in eq. 2.3.39

$$\tilde{\beta}(\omega) = \beta(\omega) + \Delta\beta(\omega) \quad (2.3.38)$$

$$\Delta\beta(\omega) = \frac{\omega}{c} \frac{\iint_{-\infty}^{\infty} \Delta n(\omega) |F(x, y)|^2 dx dy}{\iint_{-\infty}^{\infty} |F(x, y)|^2 dx dy} \quad (2.3.39)$$

Then, approximating $\tilde{\beta}^2 - \beta_0^2$ by $2\beta_0(\tilde{\beta} - \beta_0)$, equation 2.3.35 can be rewritten in the form of equation 2.3.40

$$\frac{\partial \tilde{A}}{\partial z} = i[\beta(\omega) + \Delta\beta(\omega) - \beta_0] \tilde{A} \quad (2.3.40)$$

Just like we did with the propagation constant, $\Delta\beta$ is expanded in Taylor series 2.3.41, where $\Delta\beta_m$ is defined as 2.3.42

$$\Delta\beta(\omega) = \Delta\beta_0 + (\omega - \omega_0)\Delta\beta_1 + \frac{1}{2}(\omega - \omega_0)^2\Delta\beta_2 + \dots \quad (2.3.41)$$

$$\Delta\beta_m = \left(\frac{d^m \Delta\beta}{d\omega^m} \right)_{\omega=\omega_0} \quad (2.3.42)$$

We can now take equation 2.3.40 back to the time domain to and use 2.3.39 to obtain the value of $\Delta\beta$, leading to 2.3.43

$$\frac{\partial A}{\partial z} + \beta_1 \frac{\partial A}{\partial t} + \frac{i\beta_2}{2} \frac{\partial^2 A}{\partial t^2} + \frac{\alpha}{2} A = i\gamma |A|^2 A \quad (2.3.43)$$

Where γ is referred to as the nonlinear parameter and is given by 2.3.44:

$$\gamma(\omega_0) = \frac{\omega_0 \tilde{n}_2 \iint_{-\infty}^{\infty} |F(x, y)|^4 dx dy}{c \iint_{-\infty}^{\infty} |F(x, y)|^2 dx dy} \quad (2.3.44)$$

The nonlinear parameter is usually redefined as in equation 2.3.45

$$\gamma(\omega_0) = \frac{\omega_0 n_2}{c A_{\text{eff}}} \quad (2.3.45)$$

where n_2 and A_{eff} are given by expressions 2.3.46 and 2.3.47

$$n_2 = \frac{2\tilde{n}_2}{\epsilon_0 n c} \quad (2.3.46)$$

$$A_{\text{eff}} = \frac{\left(\iint_{-\infty}^{\infty} |F(x, y)|^2 dx dy \right)^2}{\iint_{-\infty}^{\infty} |F(x, y)|^4 dx dy} \quad (2.3.47)$$

n_2 is usually referred to as the Kerr coefficient and A_{eff} is the mode effective area. For SMFs, for example, if the fundamental mode profile is approximated by a Gaussian, the effective area would be $A_{\text{eff}} = \pi w^2$. Equation 2.3.43 is usually called Nonlinear Schrödinger equation (NLSE) and it describes the evolution of the longitudinal pulse profile along the fiber. The second and third terms of the left hand side describe propagation including dispersive effects up to second-order (which are responsible for the group velocity dispersion, GVD). The last term in the left hand side describes attenuation of the pulse due to fiber absorption. And the right hand side represents the nonlinear effects, such as self-phase modulation (SPM). Dispersive

effects are governed by the propagation polynomial ($\beta_0, \beta_1, \beta_2 \dots$) and nonlinear effects are governed by the nonlinear coefficient, γ . The NLSE can be modified to include higher-order dispersive and nonlinear effects such as third-order dispersion or spontaneous Raman scattering (SRS). These will be treated in the following sections, but with the exception of SRS, most of them provoke a negligible effect in our current experimental setup.

This concludes the necessary general explanations to understand the reasons behind the appearance of nonlinear and dispersive phenomena and should be enough to obtain a clear conceptual idea of the main effects of this types that are significant when working with fiber optics. In the next sections (2.4.1 - 2.5.4) I will briefly explain some of this phenomena and the effect they have on our setup, as well as provide reasons why they should or should not be accounted for in the models that describe our system.

2.4 Dispersive effects

Dispersive phenomena appear due to the different terms in the propagation polynomial (2.3.23) and are independent of the intensity. This means that even for long pulses (low peak-powers) dispersive effects will play an important role in the propagation of the pulse through the fiber. Dispersive effects up to any order can be considered by expanding 2.3.23 up to the desired order. However, usually most terms are negligible and we only consider up to the β_2 term. This is responsible for the group velocity dispersion (GVD) and represents the major contribution to the dispersive effects. Nonetheless, under certain circumstances (i.e. near the zero-dispersion wavelength, where β_2 vanishes), it might be crucial to include at least up to β_3 . This gives rise to the third order dispersion (TOD).

2.4.1 Group Velocity Dispersion (GVD)

The second term of the propagation polynomial (2.3.23), β_1 is obtained from setting $m = 1$ in 2.3.24, and therefore, $\beta_1 = d\beta/d\omega$. But the group velocity of a wave is defined as $v_g = d\omega/dk$ and β is just the longitudinal component of the wave vector, k . Therefore, the group velocity is related with the propagation polynomial like 2.4.1. But $\beta_2 = \frac{d^2\beta}{d\omega^2} = \frac{d}{d\omega}\beta_1$. So, $\beta_2 = \frac{d}{d\omega}\frac{1}{v_g}$. β_2 depends on the variation of the group velocity with the frequency. Hence the name group velocity dispersion.

$$v_g = \frac{d\omega}{dk} = \frac{1}{\beta_1} \quad (2.4.1)$$

If we look at the NLSE (2.3.43) and disregard the terms with β_1 and α (group velocity and losses), there are two remaining terms: one proportional to β_2 (the group velocity dispersion) and the other proportional to γ , the nonlinear parameter. The behaviour of a pulse inside the fiber will depend drastically on which of these two terms dominates the equation. Therefore, it is extremely useful to know *a priori* which of the two terms will be the strongest. We can get a nice feel about this by defining in 2.4.2, the dispersion length, L_D , and the nonlinear length, L_{NL}

$$L_D = \frac{T_0^2}{|\beta_2|}, \quad L_{NL} = \frac{1}{\gamma P_0} \quad (2.4.2)$$

Where T_0 and P_0 are the pulse width and peak power respectively.

If the length of the fiber reaches one of the lengths, the corresponding effects will start to be significant for pulse propagation. That leaves us four regimes of propagation depending on the fiber and pulse parameters:

1. $L \ll L_D, L_{NL}$
Fiber is not long enough for either dispersive or nonlinear effects to be significant and both terms will be negligible in the NLSE
2. $L \sim L_D$ but $L \ll L_{NL}$
Fiber is long enough for dispersive effects to become significant but is still too short for relevant nonlinear effects to appear. In this regime, the NLSE is governed by the GVD (β_2) term
3. $L \sim L_{NL}$ but $L \ll L_D$
Fiber is too short for dispersive effects to cause a major impact, but long enough to be obliged to consider nonlinear effects
4. $L \gg L_D, L_{NL}$
Fiber is long enough for both nonlinear and dispersive effects to take place. Both terms of the NLSE equation will compete and there will be no clear dominant term in the equation, so pulse propagation is highly affected by both

For simplicity, let us study the effects of the GVD by itself. That is, let us assume we operate the setup within the dispersion-dominant regime, which is reached when $\frac{L_D}{L_{NL}} = \frac{\gamma P_0 T_0^2}{|\beta_2|} \ll 1$. We can study this regime by setting to zero the nonlinear parameter and using the change of variables [2.4.3](#)

$$\tau = \frac{T}{T_0} = \frac{t - z/v_g}{T_0}, \quad A(z, \tau) = \sqrt{P_0} e^{-\alpha \frac{z}{2}} U(z, \tau) \quad (2.4.3)$$

τ and U are normalized time scale and amplitude respectively and the exponential factor in $A(z, \tau)$ accounts for losses in the fiber due to absorption. With these changes, second and last terms of the left hand side of the NLSE equation are absorbed by τ and U and [2.3.43](#) can be rewritten as [2.4.4](#)

$$\frac{\partial U}{\partial z} = -\frac{i\beta_2}{2} \frac{\partial^2 U}{\partial T^2} \quad (2.4.4)$$

As usual, this equation can be much more easily solved in the Fourier space to give the general solution [2.4.5](#)

$$U(z, T) = \frac{1}{2\pi} \int_{-\infty}^{\infty} \tilde{U}(0, \omega) e^{\frac{i}{2}\beta_2 \omega^2 z - i\omega T} d\omega \quad (2.4.5)$$

$\tilde{U}(0, \omega)$ is the Fourier transform of the initial pulse (at $z = 0$), which can be any shape we desire. For example, a Gaussian or a sech. To see what the GVD causes, let us use as an example, a Gaussian input pulse of the form [2.4.6](#):

$$U(0, T) = \exp\left(-\frac{T^2}{2T_0}\right) \quad (2.4.6)$$

Substitution of [2.4.6](#) in [2.4.5](#) and integration leads to the pulse shape at every point z along the fiber length [2.4.7](#):

$$U(z, T) = \frac{T_0}{\sqrt{T_0^2 - i\beta_2 z}} e^{-\frac{T^2}{2(T_0^2 - i\beta_2 z)}} \quad (2.4.7)$$

Therefore, the pulse maintains its Gaussian shape while propagating through the fiber, but it broadens as 2.4.8:

$$T(z) = T_0 \sqrt{1 + \left(\frac{z}{L_D}\right)^2} \quad (2.4.8)$$

Figure 2.4.1 shows the broadening of the pulse for two different values of the normalized length z/L_D . But the GVD also has effect on the pulse phase. If we compare 2.4.6 and 2.4.7, we will notice that an imaginary exponential factor appears after propagation. This means that, even if the original pulse is unchirped³, it will become chirped during propagation

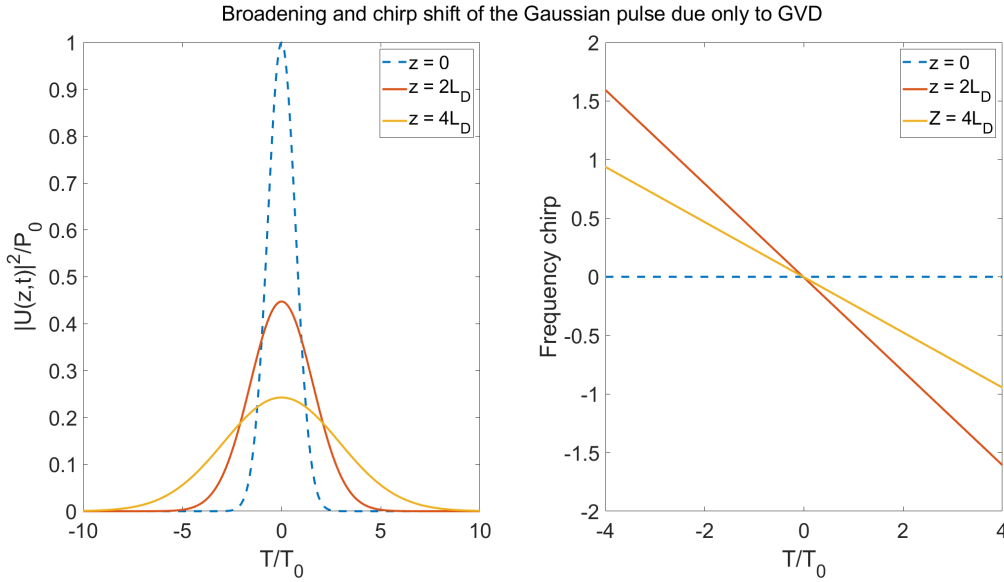


Figure 2.4.1: Broadening of an initially Gaussian pulse due to GVD. Reproduced from [27]

So, the effect of the GVD is to broaden the pulse. In fact, depending on certain conditions, it will broaden or narrow the pulse. If the original pulse is unchirped, the pulse will broaden by the factor given in 2.4.8. But if the pulse is chirped, as in 2.4.9 (linearly chirped pulse), the effect of the GVD will depend on the signs of β_2 and the chirp parameter, C .

$$U(0, T) = \exp\left(-\frac{1 + iC}{2} \frac{T^2}{T_0^2}\right) \quad (2.4.9)$$

When the pulse is down-chirped ($C < 0$) the instantaneous frequency decreases linearly from the leading to the trailing edge of pulse. That means that, for a down-chirped pulse, wavelengths at the front of the pulse are slightly shorter than at the end of the pulse. And when the pulse is up-chirped ($C > 0$) the opposite happens. Instantaneous frequencies increase linearly from the leading to trailing edge of the pulse, and wavelengths at the front of the pulse are larger than those at the end. If chirp parameter, C and β_2 have

³Chirped pulses are those that have a time-dependent phase, $\phi(t)$. They have become quite popular in the past years and have many applications. See refs [36–39]

the same sign, the GVD-induced chirp adds to the original chirp and the pulse broadens monotonically, but faster than in the unchirped case. On the other hand, if C and β_2 have different signs, the GVD-induced chirp compensates the initial chirp and the pulse narrows at the beginning of propagation until the initial chirp is fully compensated. Afterwards, the pulse broadens as in the previous case. This can be seen in figure 2.4.2 and has been conceptually illustrated in figure 2.4.3

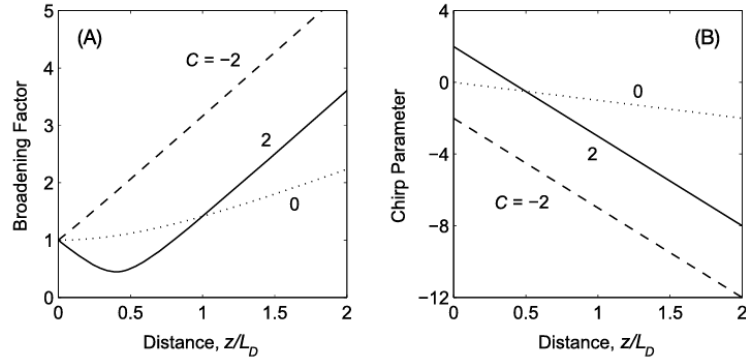


Figure 2.4.2: Broadening factor (A) and chirp parameter (B) as a function of the normalised distance z/L_D for anomalous GVD. Extracted from [27]

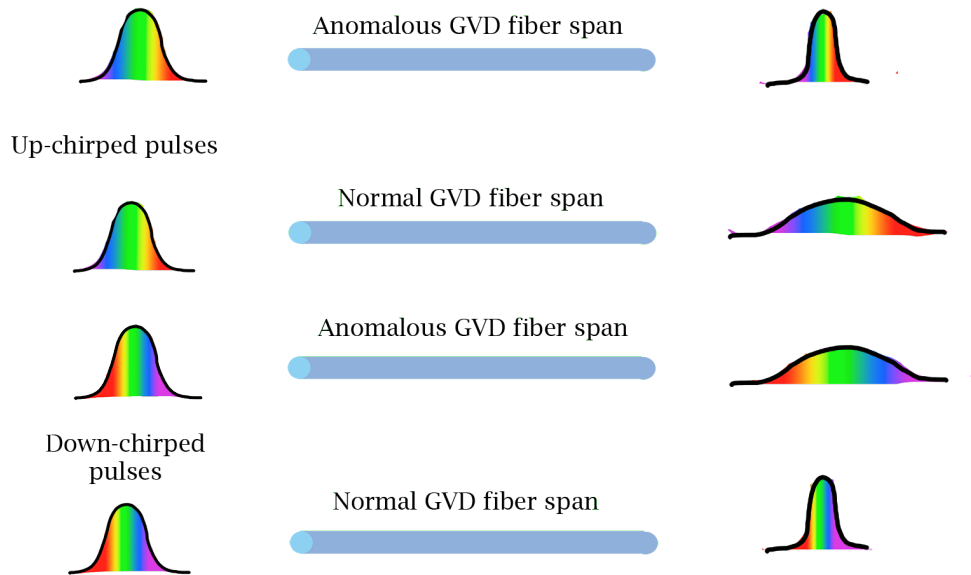


Figure 2.4.3: GVD effect in pulse propagation

2.4.2 Third Order dispersion (TOD)

The GVD and β_2 parameter explained in section 2.4.1 usually governs the dispersive effects on the pulse as it propagates. However, under certain circumstances, it might be necessary to consider up to the third order

term of the dispersion polynomial, β_3 . This is the case, for example, when the GVD parameter is nearly zero. If $\beta_2 \approx 0$, the third order dispersion (TOD) parameter, β_3 gains notorious relevance. In general, this begins to happen in the vicinity of the so-called zero dispersion wavelength, λ_0 . Its name, of course, arises from the fact that when a pulse of this wavelength is launched into the fiber, it suffers no dispersion (not GVD at least). Including the TOD parameter might be also useful when the pulse width is rather short (typically lower than 1 ps). As we did with the GVD, it is useful to introduce a third order dispersion length, L'_D defined as 2.4.10

$$L'_D = \frac{T_0^3}{|\beta_3|} \quad (2.4.10)$$

As long as $L'_D \geq L_D$, TOD can be neglected. In the occasions where TOD can't be neglected, we can study its effect by adding a second term to the right hand side of equation 2.4.7 to yield 2.4.11

$$\frac{\partial U}{\partial z} = -\frac{i\beta_2}{2} \frac{\partial^2 U}{\partial T^2} + \frac{\beta_3}{6} \frac{\partial^3 U}{\partial T^3} \quad (2.4.11)$$

This equation (2.4.11) can be solved in the Fourier space to give Airy function-like solutions. This provokes an oscillatory effect in the trailing edge when β_3 is positive and in the leading edge when β_3 is negative. If this occurs near the zero dispersion wavelength, this effect is intensified and the oscillations even drop intensity to zero. This can be seen in figure 2.4.4

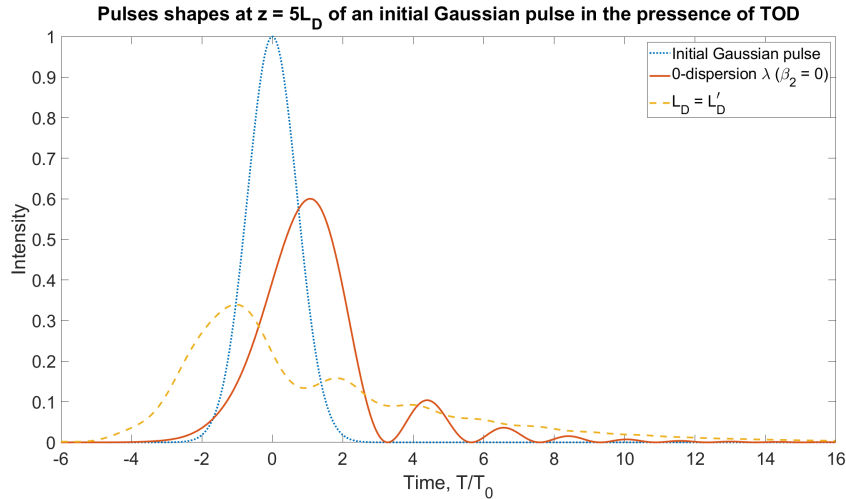


Figure 2.4.4: TOD oscillating effect. Reproduced from [27]

Third order dispersion also produces pulse broadening. Furthermore, unlike the GVD, the TOD always broadens the pulse, regardless of the chirp parameter or β_3 signs. This leads to a curious result. The broadening factor might be bigger for $\beta_2 = 0$ than for $\beta_2 \neq 0$. With a nonzero GVD parameter, the pulse might be narrowed in the beginning. But this is never the case if the main contribution to dispersion is due to TOD. The broadening of the pulse during propagation can be seen in figure 2.4.5

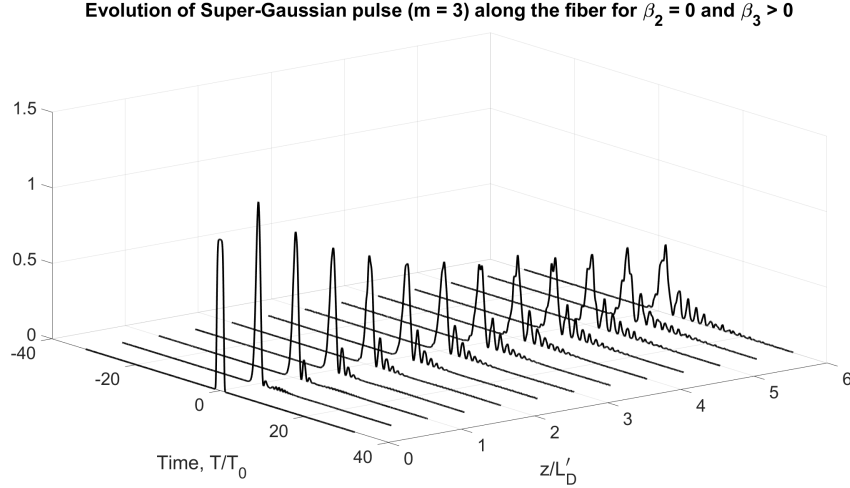


Figure 2.4.5: TOD effect in pulse propagation. Reproduced from [27]

2.5 Nonlinear effects

As explained in section 2.3, nonlinear effects arise from the intensity-dependent refractive index and are closely related with γ , the nonlinear coefficient. Commonly, nonlinear effects are disregarded because they appear with really high powers, But due to the high length of the fibers, nonlinear effects begin to build up and gain importance. The most relevant of the nonlinear effects are the self-phase modulation (SPM) and the spontaneous Raman scattering (SRS), which I will discuss in sections 2.5.1 and 2.5.4 respectively. But other effects such as cross-phase modulation (XPM) or four wave mixing (FWM) will be also briefly talked about.

2.5.1 Self-phase modulation (SPM)

As we did when we studied the GVD effects, for simplicity, we consider now the case where $L_{NL} < L \ll L_D, L'_D$ (These three characteristic lengths were defined by equations 2.4.2 and 2.4.10). So, we do not take into consideration the effects of group velocity dispersion or TOD. Under these circumstances, equation 2.3.43 leads to 2.5.1

$$\frac{\partial U}{\partial z} = \frac{ie^{-\alpha z}}{L_{NL}} |U|^2 U \quad (2.5.1)$$

Equation 2.5.1 can be solved with the substitution $U = Ve^{i\phi_{NL}}$ and then equating real and imaginary parts on both sides of the expression 2.5.2

$$\frac{\partial V}{\partial z} = 0; \quad \frac{\partial \phi_{NL}}{\partial z} = \frac{e^{-\alpha z}}{L_{NL}} V^2 \quad (2.5.2)$$

Solving these two equations (2.5.2) leads to expressions 2.5.3 and 2.5.4 for the amplitude and phase:

$$U(L, T) = U(0, T) \exp[i\phi_{\text{NL}}(L, T)] \quad (2.5.3)$$

$$\phi_{\text{NL}}(L, T) = |U(0, T)|^2 \left(\frac{L_{\text{eff}}}{L_{\text{NL}}} \right) \quad (2.5.4)$$

Where the effective length, L_{eff} is defined as 2.5.5

$$L_{\text{eff}} = \frac{1 - e^{-\alpha L}}{\alpha} \quad (2.5.5)$$

As we can see from equation 2.5.4, due to the nonlinearity, the phase acquires an intensity dependence. This dependence is proportional to the effective length, which increases with the fiber length. Therefore, the longer the fiber, the higher the nonlinear phase shift, ϕ_{NL} , will be. And the maximum phase shift occurs at the center of the peak (where $U(0, T)$ is the highest). The fact that the phase depends on T , will cause the appearance of new spectral components. That is, if the phase changes with time, the instantaneous frequency will also change with T and a frequency shift from the central frequency of the pulse will appear. This is given by 2.5.6

$$\delta\omega(T) = -\frac{\partial\phi_{\text{NL}}}{\partial T} = -\left(\frac{L_{\text{eff}}}{L_{\text{NL}}} \right) |U(0, T)|^2 \quad (2.5.6)$$

The time dependence of $\delta\omega$ is referred to as frequency chirping and it increases with length (because it is proportional to L_{eff}). This means that the longer the distance, the larger the frequency shift will be. A higher frequency shift means that frequencies at the edges of the pulse differ more from the central frequency. Therefore, as the pulse propagates, new frequencies appear continuously due to SPM. So, if the pulse is originally unchirped, the SPM-induced frequencies will spectrally broaden it. Nonetheless, the SPM frequency chirp might compensate for an originally chirped pulse. The exact effect of the SPM will critically depend on the pulse shape. However, it is interesting to note from eq. 2.5.6 that $\delta\omega \propto |U(0, T)|^2$, which means that the SPM-induced frequency chirp imitates the shape of the initial pulse. Hence, for an initially Gaussian pulse, the frequency chirp will be Gaussian. And for super-gaussian pulses ⁴ (which are more rectangular with increasing Gaussian order), the frequency chirp will become more and more rectangular with steeper edges as the Gaussian order increases. This can be observed in figure 2.5.1

⁴super-gaussian pulses are those which take the form $U(0, T) = \exp\left[-\frac{1+iC}{2}\left(\frac{T}{T_0}\right)^{2m}\right]$, with C being the chirp parameter and m , the Gaussian order. For $m = 1$, the original regular Gaussian pulse shape is recovered

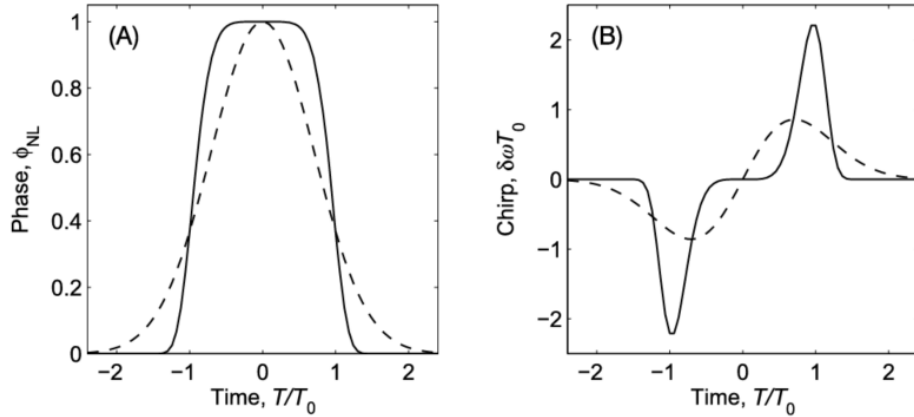


Figure 2.5.1: SPM effect. A: SPM-induced phase-shift for a gaussian (dashed line) and super-gaussian of third order (continuous line) initial pulse. B: SPM-induced frequency shift for a gaussian (dashed line) and super-gaussian of third order (continuous line) initial pulse. Extracted from [27]

It is interesting to get a glimpse of how big the SPM-induced frequency shift can get for a Gaussian pulse. In order to do that, we look for the maximum of equation 2.5.6, which turns out to be 2.5.7:

$$\delta\omega_{\max} = \frac{mf(m)}{T_0} \phi_{\max} \quad (2.5.7)$$

Where ϕ_{\max} is obtained by substitution of the maximum value of the pulse intensity in equation 2.5.4, m ; the Gaussian order ($m = 1$ for Gaussian pulses); and the f function is defined by 2.5.8. For $m = 1$, $f(1) = 0.86$ and using $\frac{1}{T_0} = \Delta\omega_0$, we can write the maximum frequency shift as 2.5.9 for Gaussian pulses. In the case of super-Gaussian pulses, the shape of $\Delta\omega_0$ is not so easy to obtain, although a nice approximation can be achieved with the inverse of the rise time, T_r ⁵, as $\Delta\omega_0 = 1/T_r$.

$$f(m) = 2 \left(1 - \frac{1}{2m}\right)^{1 - \frac{1}{2m}} \exp \left[- \left(1 - \frac{1}{2m}\right) \right] \quad (2.5.8)$$

$$\delta\omega_{\max} = 0.86 \Delta\omega_0 \phi_{\max} \quad (2.5.9)$$

The spectral broadening given by equations 2.5.6 and 2.5.9 can become significantly large, specially for ultrashort pulses. In these cases, it might produce pulses that extend over more than 100 THz (for comparison, 100 THz is, roughly, the whole near IR spectrum region). This phenomenon can be enhanced by other nonlinear effects and is called supercontinuum generation [40–42] and it has developed many applications in the past few years ranging from telecommunications to biophysics or medical imaging [43–46].

The self-phase modulation by itself does not affect the pulse amplitude, and, in principle, does not cause temporal broadening of the pulse. However, spectral changes are often closely related with temporal changes and the spectral broadening will, in most cases, induce a temporal broadening or narrowing. This is, actually, consequence of the interplay between the GVD and the SPM. The SPM generates new frequencies which are then delayed or hasten by the GVD. This combination of phenomena can eventually lead to soliton formation and will be discussed later in this work, in section 2.5.5.

⁵The rise time is the time it takes for the spectral edges to get to the peak intensity and is given approximately by $T_r = T_0/m$

2.5.2 Cross-phase modulation (XPM)

The cross-phase modulation phenomenon is conceptually, closely related with the SPM, but rather more complicated mathematically. XPM is negligible in our setup, mainly because of the low PMD⁶ coefficient of our fibers and even if the PMD coefficient was a little larger, the length of the fiber would not be sufficient for it to be relevant. However, it should be taken into account when studying the propagation of the pulse, specially in fibers with high PMD coefficients. For these reasons, I believe it unnecessary to include the whole mathematical derivation. But, of course, I encourage the interested reader to check chapter 7 of Agrawal's book [27].

Qualitatively, the XPM occurs when two pulses overlap in the fiber during propagation. They might have different wavelengths, different phases or different polarization states. This can be the case for example in a multimode fiber. When two pulses propagate inside the same fiber span overlapping, we need to extend the theory and demonstrations of section 2.3 to two coexisting pulses. This leads to a pair of coupled non-linear Schrödinger equations (2.3.43), which means that the propagation of one pulse has an effect on the second and vice versa. Specifically, if we focus only on one of the pulses, we will observe it is affected by SPM. SPM causes an intensity dependent phase shift (and frequency shift). But with two pulses propagating at the same time inside the fiber, the intensity involved in the SPM equations is not only due to the first pulse, but caused by both pulses.

XPM can appear also when only one pulse propagates through a birefringent fiber. If a pulse is intruded at a certain angle with respect to the optical axes (slow and fast) of the fiber, the pulse will suffer from PMD and can be viewed as decomposed in two pulses: one on the fast axis and one on the slow axis. These “two” pulses can interact through XPM. This is illustrated in figure 2.5.2

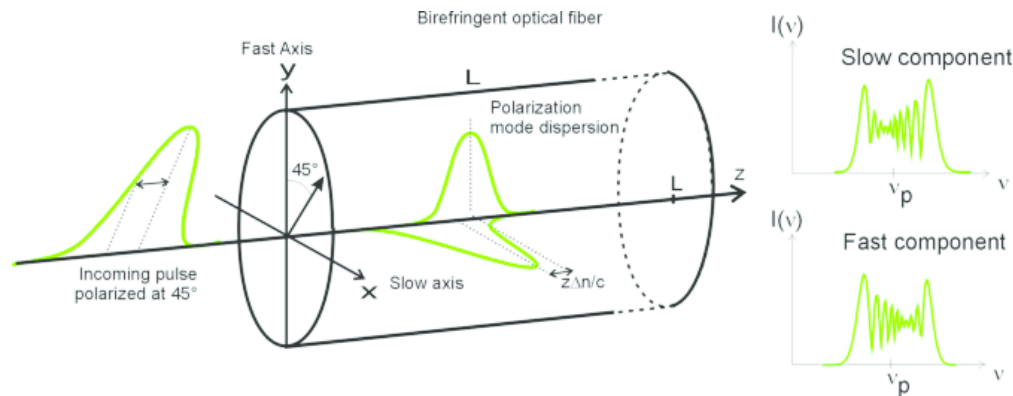


Figure 2.5.2: Effect of the cross-phase modulation on a single pulse that travels through birefringent fiber decomposing into two pulses. Extracted from [49]

So, when two pulses coexist in the same fiber span, they are both affected by SPM due to their own intensity and by XPM due to the intensity of the other pulse. Because this effect arises from the nonlinear terms of the NLSE (2.3.43), the nature of this feedback and the relation between SPM and XPM and the different intensities is rather complicated, but I hope the conceptual underlying basis is now sufficiently clear

⁶PMD: Polarization Mode Dispersion is a phenomenon caused the difference in refractive index depending on the direction. This leads to the appearance of a fast axis and a slow axis and broadening of the pulse caused by the different velocities of the two components of the pulse. More information can be found on [47] or [48]

2.5.3 Four wave mixing (FWM)

Although the theory and equations governing this phenomenon are also rather complex, we can still get a good idea of where this effect comes from without diving too deep in complicated mathematical expressions. The conditions for FWM to occur do not usually happen naturally. Rather than that, the experiment should be designed deliberately to enhance FWM effects, and this is not the case for our setup. Therefore, FWM will have little to zero impact in our setup and so. For this reason, I do not think it is necessary to include a detailed explanation.

The process of four wave mixing arises from the nonlinear polarization. The different nonlinear terms of the polarization (eq. 2.3.7) are responsible for second-, third- or higher-order nonlinearities depending on the relevant susceptibility ($\chi^{(i)}$). Second-order nonlinear effects such as second harmonic generation are not usually relevant in fiber optics because fibers have inversion symmetry and $\chi^{(2)}$ becomes zero for such kind of media. But the following term ($\chi^{(3)}$) will cause third-order nonlinearities such as third harmonic generation or four wave mixing. Let us consider the case where four continuous waves (CW) propagate inside the fiber with frequencies ω_j , (with $j = 1,2,3,4$) and, for simplicity, they do so with linear polarization along the same axis. We can write the electric fields and polarizations in a similar way as we did in equation 2.3.25 to give 2.5.10:

$$\begin{aligned} \mathbf{E} &= \frac{1}{2} \hat{x} \sum_{j=1}^4 E_j \exp [i (\beta_j z - \omega_j t)] + c.c \\ \mathbf{P} &= \frac{1}{2} \hat{x} \sum_{j=1}^4 P_j \exp [i (\beta_j z - \omega_j t)] + c.c \end{aligned} \quad (2.5.10)$$

Substitution of 2.5.10 in the nonlinear term of 2.3.7 leads to the coefficients P_j having the form of 2.5.11, where $j = 4$ has been used as an example:

$$P_4 = \frac{3\epsilon_0}{4} \chi_{xxxx}^{(3)} [|E_4|^2 E_4 + 2 (|E_1|^2 + |E_2|^2 + |E_3|^2) E_4 + 2E_1 E_2 E_3 e^{i\theta_+} + 2E_1 E_2 E_3^* e^{i\theta_-} + \dots] \quad (2.5.11)$$

Where the θ_+ and θ_- phases are given by 2.5.12

$$\begin{aligned} \theta_+ &= (\beta_1 + \beta_2 + \beta_3 - \beta_4) z - (\omega_1 + \omega_2 + \omega_3 - \omega_4) t \\ \theta_- &= (\beta_1 + \beta_2 - \beta_3 - \beta_4) z - (\omega_1 + \omega_2 - \omega_3 - \omega_4) t \end{aligned} \quad (2.5.12)$$

The first four terms in equation 2.5.11 are actually responsible for SPM (the first) and XPM (the other three) and the other terms, that combine the different frequencies of all four waves, are the ones that cause FWM. FWM will only be considerable if the phase mismatching between E_j and P_j is nearly zero. For this to happen, both frequencies and wave vectors need to match (phase matching condition). Physically, FWM occurs when three or two photons interact (annihilate) to generate another or another two photons. In the process of four wave mixing, apart from the phase matching (wave vector matching) condition, frequency matching must be complied. This means that the sum of the frequencies of the “incoming” photons must equal the sum of the frequencies of the “outgoing” photon(s). As a consequence of this, only two types of FWM can occur. One that involves the θ_+ phase in which three photons of different or the same frequency (third harmonic generation) annihilate to generate just one photon whose frequency is the sum of the other three. The other is related with the θ_- phase and it destroys two photons of frequencies ω_1 and ω_2 to give

rise to another two photons of frequencies ω_3 and ω_4 with the condition $\omega_1 + \omega_2 = \omega_3 + \omega_4$. This has been illustrated in figure 2.5.3

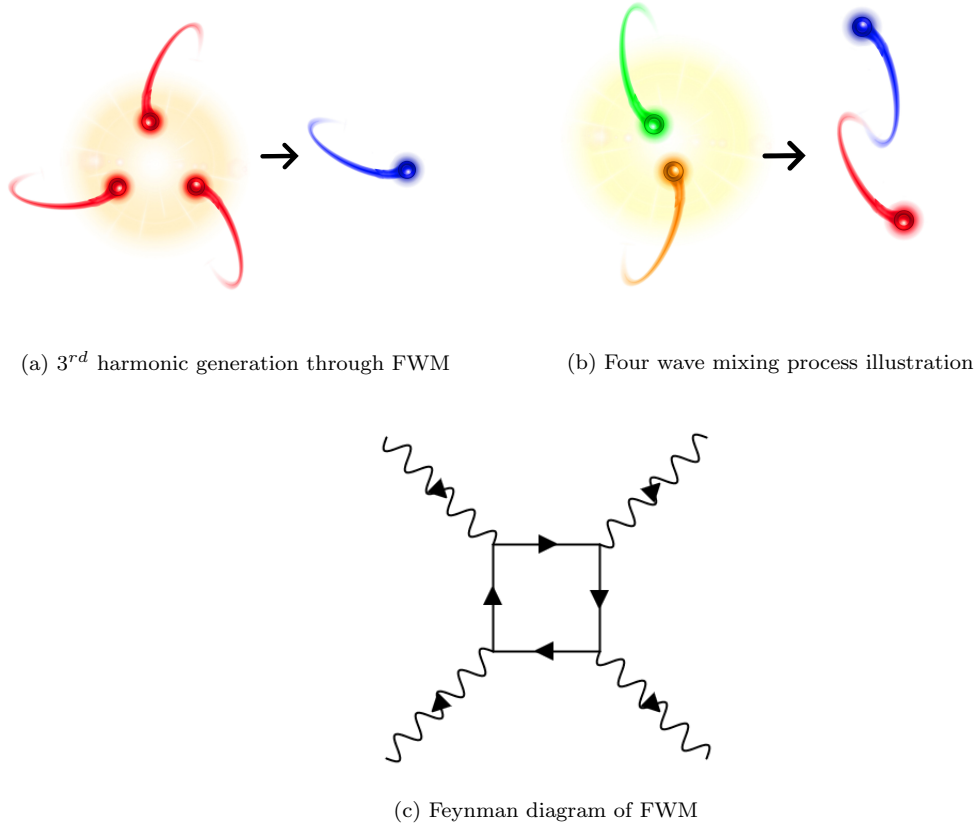


Figure 2.5.3: Illustration of the process of four wave mixing

In general, the phase-matching condition is not fulfilled unless on purpose. So, FWM has little effect on setups not designed to enhance this phenomenon. FWM has several applications, for example, in tomography, phase-conjugation (which can have many applications such as holography), or single-photon experiments [50–52]. And once again, if interested, I encourage the reader to learn more about this topic by seeing the full Agrawal’s demonstration [27] or references [53] and [54]

2.5.4 Stimulated Raman Scattering (SRS)

When an optical field propagates inside a fiber, a small fraction of its power can be converted into light at lower frequency due to spontaneous Raman scattering. This phenomenon was discovered by Raman [55] (hence the name). It is a quantum effect caused by the conversion of a photon from the pump wave to another from the so-called Stokes or anti-Stokes wave. Usually, the amount of the pump pulse affected by spontaneous Raman scattering is very low (around 10^{-6}). But if the pump power is large enough, it might provoke stimulated Raman scattering (SRS) which has a significant impact on the pump and pulse propagation.

The anti-Stokes wave is blue-shifted (higher frequency than the original) and the Stokes wave is red-shifted (lower frequency than the original), although the latter is much more common. The process behind the creation of the Stokes or anti-Stokes wave is a photon-phonon interaction. Phonons are particle-like vibrations of the atomic lattice of the medium. So, when a photon of the pump beam hits the atomic lattice, two things might happen. In the first case, the energy of the photon will be employed in sending a molecule to an excited state, and creating a phonon that propagates through the lattice. Then, the molecule will go back to the ground state emitting a photon of lower energy (red-shifted) than that of the pump. This is called Stokes Raman scattering. In the other case, the photon might hit the molecule at the same time that a phonon arrives at it. Consequently, the molecule will absorb the energy of both the phonon and the photon and jump to a higher excited state. Immediately after, it will decay to the ground level again, but this time, emitting a photon which has higher energy (blue-shifted) than that of the pump. This is the anti-Stokes Raman scattering. An illustration of the phenomenon can be found on figure 2.5.4

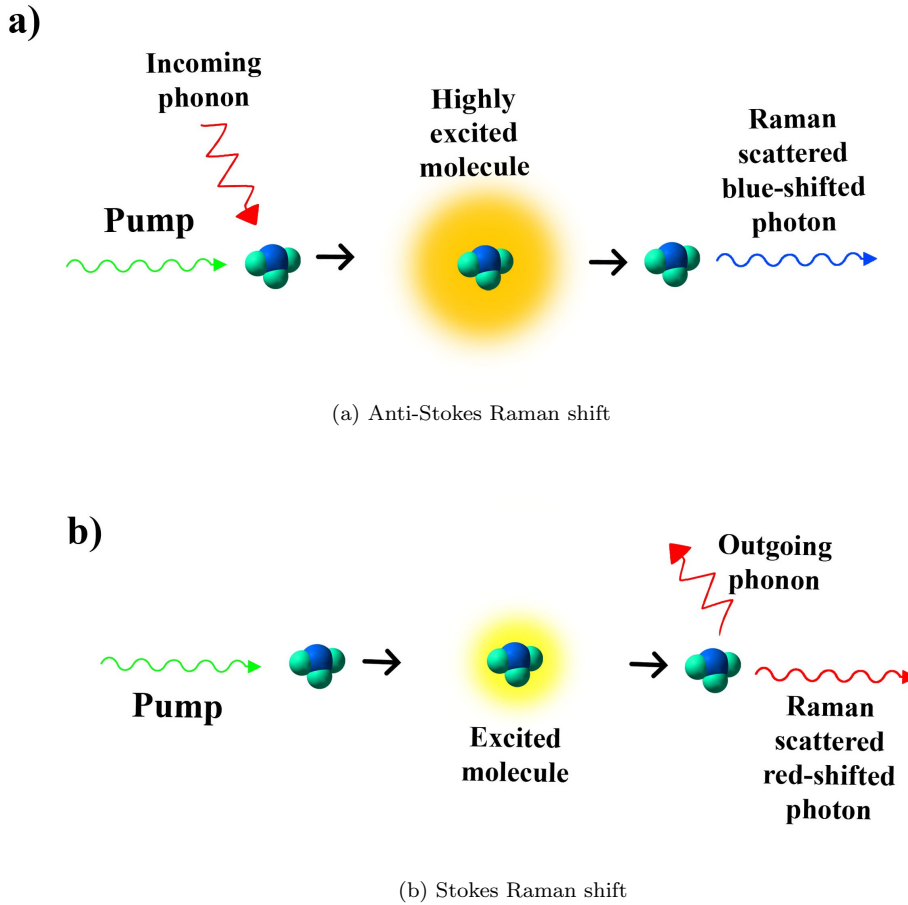


Figure 2.5.4: Illustration of the Raman effect

At a very fundamental level, we can characterize the build-up of the Stokes wave with equation 2.5.13

$$\frac{dI_s}{dz} = g_R(\Omega)I_pI_s \quad (2.5.13)$$

Where $g_R(\Omega)$ is the Raman gain and Ω is the frequency shift between the pump and the Stokes wave

($\Omega = \omega_p - \omega_s$). The Raman gain, g_R is the main parameter to describe the SRS. It depends on several factors such as material of the core, dopants in the fiber or relative polarization of the Stokes and the pump waves. So, it is usually found experimentally. For silica fibers, this has been thoroughly studied and the Raman gain dependence on the frequency shift looks like figure 2.5.5

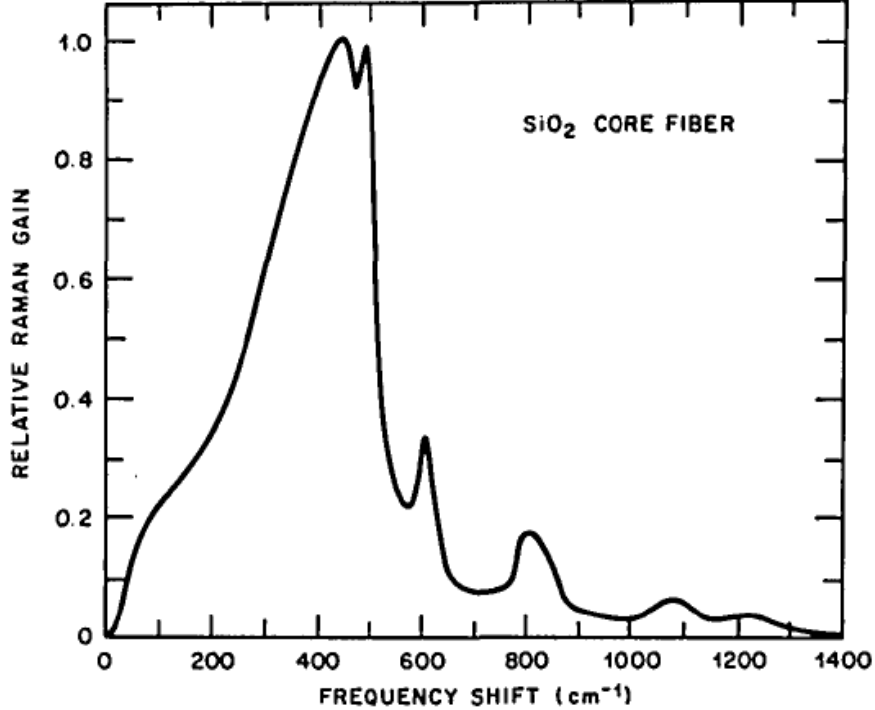


Figure 2.5.5: Raman gain dependence on frequency shift. Extracted from [56]

If a probe beam is introduced in the fiber along with the pump, it will be amplified whenever the frequency shift between pump and probe lies within the Raman gain bandwidth. The main peak of the graph in 2.5.5 is located at about 13 THz, so, naturally, if said shift matches the peak, the amplification effect will be maximum. If no probe is introduced, spontaneous Raman scattering will act itself as a probe and will be amplified during propagation. In this case, spontaneous Raman scattering is generated at all frequencies of the Raman gain bandwidth, but at a much greater rate at the gain peak (~ 13 THz). So the Stokes wave generated by spontaneous Raman scattering is downshifted 13 THz from the pump.

One of the first questions we can ask ourselves about this phenomenon is at what point the spontaneous process becomes stimulated. To find out, let us revisit equation 2.5.13 and account for the fact that there are losses in the fiber and that the pump and the Stokes wave will interact non-linearly with each other. Then, we arrive at 2.5.14

$$\begin{aligned} \frac{dI_s}{dz} &= g_R I_p I_s - \alpha_s I_s \\ \frac{dI_p}{dz} &= -\frac{\omega_p}{\omega_s} g_R I_p I_s - \alpha_p I_p \end{aligned} \tag{2.5.14}$$

Where α_p and α_s represent losses at the pump and Stokes frequencies respectively. In a first approach, we can consider there is no pump depletion and neglect the first term of the Right hand side of the second

equation in 2.5.14. This gives an easy solution for said equation of the form $I_p(z) = I_p(0)e^{-\alpha_p z}$, which we can substitute in the first equation of 2.5.14 to give 2.5.15

$$\frac{dI_s}{dz} = g_R I_0 e^{-\alpha_p z} I_s - \alpha_s I_s \quad (2.5.15)$$

Where, I_0 is the pump intensity. Equation 2.5.15 can be easily solved to arrive at 2.5.16

$$I_s(L) = I_s(0) \exp(g_R I_0 L_{\text{eff}} - \alpha_s L) \quad (2.5.16)$$

Where $L_{\text{eff}} = [1 - e^{-\alpha_p L}] / \alpha_p$ is the effective length. $I_s(0)$ is the input intensity, which would be our probe beam. But let us consider for a moment that this $I_s(0)$ is the one due to inserting just one photon per mode. With this consideration, the power of the Stokes wave is given by 2.5.17

$$P_s(L) = \int_{-\infty}^{\infty} \hbar \omega \exp[g_R(\omega_p - \omega) I_0 L_{\text{eff}} - \alpha_s L] d\omega \quad (2.5.17)$$

This can be solved approximately thanks to the fact that the biggest contribution to g_R is due only to small region of the whole bandwidth. Doing so, we arrive at an expression for the power of the Stokes wave 2.5.18

$$P_s(L) = P_{s0}^{\text{eff}} e^{g_R(\Omega_R) I_0 L_{\text{eff}} - \alpha_s L} \quad (2.5.18)$$

Where, P_{s0}^{eff} , the effective input power is given by 2.5.19

$$P_{s0}^{\text{eff}} = \hbar \omega_s B_{\text{eff}}, \quad B_{\text{eff}} = \left(\frac{2\pi}{I_0 L_{\text{eff}}} \right)^{1/2} \left| \frac{\partial^2 g_R}{\partial \omega^2} \right|_{\omega=\omega_s}^{-1/2} \quad (2.5.19)$$

Where B_{eff} is the effective bandwidth of the Raman gain. Now, we can define a Raman threshold at the point where the Stokes wave power built-up by the spontaneous Raman scattering at the end of the fiber reaches the pump power. With such condition ($P_s(L) = P_p(L)$), the threshold power can be found to be given approximately by 2.5.20

$$P_{th} \approx 16 \frac{A_{\text{eff}}}{g_R L_{\text{eff}}} \quad (2.5.20)$$

Where A_{eff} is the effective core area as defined in 2.3.47.

Of course, if we want to have a better understanding of the SRS, we should take into account effects that have already been mentioned in previous sections such as SPM, XPM, GVD or FWM. This can be done by applying the complete NLSE 2.3.43 to both the pump and Stokes wave. By doing so, and after a lot of algebra, we arrive at equations 2.5.21 and 2.5.22 that describe pulse propagation including SRS effect

$$\frac{\partial A_p}{\partial z} + \frac{1}{v_{gp}} \frac{\partial A_p}{\partial t} + \frac{i\beta_{2p}}{2} \frac{\partial^2 A_p}{\partial t^2} = -\frac{\alpha_p}{2} A_p + i\gamma_p(1 - f_R)(|A_p|^2 + 2|A_s|^2)A_p + R_p(z, t) \quad (2.5.21)$$

$$\frac{\partial A_s}{\partial z} + \frac{1}{v_{gs}} \frac{\partial A_s}{\partial t} + \frac{i\beta_{2s}}{2} \frac{\partial^2 A_s}{\partial t^2} = -\frac{\alpha_s}{2} A_s + i\gamma_s(1 - f_R)(|A_s|^2 + 2|A_p|^2)A_s + R_s(z, t) \quad (2.5.22)$$

In fact, we can clearly identify each contribution in equations 2.5.21 and 2.5.22. On the left hand side, second and third terms are due to dispersion (group velocity and GVD respectively). On the right hand side, the first term is caused by losses in the fiber and second and third terms, are caused by SPM and XPM respectively. The last term is the one due to SRS (although SRS also contributes with the f_R factor in the second and third terms).

The SRS and the Raman effect in general has found many applications since its discovery specially in spectroscopy [57–59], but also in biological imaging [60] and, of course, lasing [61]. If the reader would like to know a little more, extra information can be found on Agrawal’s book [27] or references [62–64]

2.5.5 Solitons

Under certain circumstances, the interplay between nonlinear and dispersive effects may have a really interesting consequence: the formation of a wave packet that can propagate for very long distances without losses or changes in its spectrum. This kind of waves are called solitons. Solitons appear in many branches of physics and have drawn a lot of attention onto them since they were first observed in 1834 by John Scott Russell [65], who followed “a solitary elevation, a rounded, smooth and well-defined heap of water which continued its course along the channel apparently without change of form or diminution of speed [...] for one or two miles”, as described by himself. More than a century later, the existence of solitons in fiber was observed [66] and attributed to a compensation between nonlinear and dispersive effects [67]

To begin with the study of this interesting phenomenon, we take the nonlinear Schrödinger equation (2.3.43) but we consider only GVD and SPM effects and neglect losses⁷. With those assumptions, equation 2.3.43 reduces to 2.5.23

$$i\frac{\partial A}{\partial z} = \frac{\beta_2}{2}\frac{\partial^2 A}{\partial T^2} - \gamma|A|^2A \quad (2.5.23)$$

We can find the stationary state solution for this equation by making the time derivative equal to zero, which yields to a simple ODE whose solution can be easily found to be $A = \sqrt{P_0}e^{i\phi_{NL}}$, where $\phi_{NL} = \gamma P_0 z$, is the nonlinear phase-shift induced by the SPM. Note that this simplified equation and its solution is the same that would be obtained from solving 2.5.23 for a CW because for the continuous wave case, the amplitude, A , does not depend on the time. To check if this solution is stable we need to apply a small perturbation to the amplitude, so that $A = (\sqrt{P_0} + a)e^{i\phi_{NL}}$. Substituting this perturbed amplitude in 2.5.23 and linearizing around a , we obtain equation 2.5.24

$$i\frac{\partial a}{\partial z} = \frac{\beta_2}{2}\frac{\partial^2 a}{\partial T^2} - \gamma P_0(a + a^*) \quad (2.5.24)$$

This equation can be solved in the Fourier space to give 2.5.25:

$$a(z, T) = a_1 e^{i(Kz - \Omega T)} + a_2 e^{-i(Kz - \Omega T)} \quad (2.5.25)$$

Where K and Ω are the wave number and frequency of the perturbation. Substitution of 2.5.25 in 2.5.24

⁷The assumption of lossless propagation, although it might seem bizarre, is actually quite descriptive since solitons do not change in amplitude (hence do not lose energy)

yields to the pair of coupled equations 2.5.26

$$\begin{aligned} \left[K - \left(\gamma P_0 + \frac{\beta_2 \Omega^2}{2} \right) \right] a_1 - \gamma P_0 a_2^* &= 0 \\ \left[K + \left(\gamma P_0 + \frac{\beta_2 \Omega^2}{2} \right) \right] a_2 - \gamma P_0 a_1^* &= 0 \end{aligned} \quad (2.5.26)$$

Which has a nontrivial solution only when the dispersion relation 2.5.27 is satisfied

$$K = \pm \frac{1}{2} |\beta_2 \Omega| \sqrt{\Omega^2 + \text{sgn}(\beta_2) \Omega_c^2} \quad (2.5.27)$$

Where sgn is the mathematical function sign, which takes the value 1 or -1 depending on whether its argument is positive or negative respectively; and Ω_c is a critical frequency defined by 2.5.28

$$\Omega_c = \frac{4\gamma P_0}{|\beta_2|} = \frac{4}{|\beta_2| L_{\text{NL}}} \quad (2.5.28)$$

The dispersion relation 2.5.27 defines two very distinct regimes. If the fiber presents normal GVD ($\beta_2 > 0$), K will be real for any value of Ω . But in the case of anomalous GVD ($\beta_2 < 0$), for some frequencies, Ω might be smaller than Ω_c and K will take imaginary values. In the first case the solution is stable against small perturbations. But in the second case, the perturbation will grow exponentially and lead to temporal modulation. This is called instability modulation. Therefore, even if a CW beam is propagating inside a fiber with anomalous GVD, the instability modulation will automatically break the beam into a train of pulses. To see how the instability evolves exactly, it is necessary to find its gain and, eventually, as the instability grows, solve the NLSE (2.5.24) numerically. This feature was applied as soon as in 1989 to create pulse widths of around 130 fs with repetition rates of 2 THz.

It is clear that the case where the GVD parameters is negative is drastically different from the positive GVD. But, apart from the modulation instability that can give rise to ultrashort pulses, equation 2.5.23 happens to have specific solutions that do not change during propagation through the fiber, or change in a periodic way (so that the initial shape of the pulse is recovered after some distance). These solutions are called solitary waves or solitons (to stress their particle-like nature). Equation 2.5.23 can be solved with the inverse scattering method [68, 69]. To do so, it is better to previously normalize the equation with the parameters defined in 2.5.29

$$U = \frac{A}{\sqrt{P_0}}; \quad \xi = \frac{z}{L_D}; \quad \tau = \frac{T}{T_0}; \quad N = \sqrt{\frac{L_D}{L_{\text{NL}}}} = \sqrt{\frac{\gamma P_0 T_0^2}{|\beta_2|}} \quad (2.5.29)$$

Where a new parameter, N , has been introduced so equation 2.5.23 can be written as 2.5.30 after choosing the sign of β_2 to be -1 since that is our case of interest.

$$i \frac{\partial U}{\partial \xi} = \text{sgn}(\beta_2) \frac{1}{2} \frac{\partial^2 U}{\partial \tau^2} - N^2 |U|^2 U \quad (2.5.30)$$

Which can be taken to the standard form 2.5.31 by using $u = NU = \sqrt{\gamma L_D} A$:

$$i \frac{\partial u}{\partial \xi} + \frac{1}{2} \frac{\partial^2 u}{\partial \tau^2} + |u|^2 u = 0 \quad (2.5.31)$$

This equation can now be solved with the inverse scattering method to give general solutions for solitons of the form [2.5.32](#)

$$u(\xi, \tau) = -2 \sum_{j=1}^N \lambda_j^* \psi_{2j}^* \quad (2.5.32)$$

The λ_j coefficients in equation [2.5.32](#) are given by [2.5.33](#) and the ψ_{2j} functions are obtained by solving the set of algebraic linear equations given by [2.5.34](#)

$$\lambda_j = \sqrt{c_j} e^{i\zeta_j \tau + i\zeta_j^2 \xi} \quad (2.5.33)$$

$$\begin{aligned} \psi_{1j} + \sum_{k=1}^N \frac{\lambda_j \lambda_k^*}{\zeta_j - \zeta_k^*} \psi_{2k}^* &= 0 \\ \psi_{2j}^* + \sum_{k=1}^N \frac{\lambda_j \lambda_k^*}{\zeta_j - \zeta_k^*} \psi_{1k} &= \lambda_j^* \end{aligned} \quad (2.5.34)$$

In equations [2.5.33](#) and [2.5.34](#), ζ_j are the eigenvalues of the scattering problem (inverse scattering) associated with the NLSE ([2.5.31](#)). The inverse scattering method involves residues calculation theorem and a solid understanding of complex variable calculus. The c_j in [2.5.33](#) is actually the residues at the j -th pole and there are as many eigenvalues as complex poles. In general, the eigenvalues will be complex ($\zeta_j = \delta_j + i\eta_j$). The number poles, N defines the order of the soliton. So, the fundamental soliton ($N = 1$) appears when the scattering problem presents only one pole.

Making $j = k = N = 1$ in equations [2.5.32](#) to [2.5.34](#) we can find the shape of the fundamental soliton. This is the only one whose shape is preserved at all times during propagation. Higher-order solitons recover the initial shape periodically. We can, therefore, write the expression for a general soliton as in [2.5.35](#)

$$u(\xi, \tau) = \eta \operatorname{sech}[\eta(\tau - \tau_s + \delta\xi)] \exp \left[i(\eta^2 - \delta^2) \frac{\xi}{2} - i\delta\tau + i\phi_s \right] \quad (2.5.35)$$

Where the parameters δ and η are the real and imaginary parts of the eigenvalue ζ respectively and τ_s and ϕ_s are defined through [2.5.36](#)

$$-\frac{c_1}{\eta} = e^{\eta\tau_s - i\phi_s} \quad (2.5.36)$$

So, in fact, a four-parameter family of fundamental solitons is supported inside the fiber. The four parameters η, δ, τ_s and ϕ_s have a physical meaning. They represent, respectively, the amplitude, frequency, position and phase of the soliton. But equation [2.5.35](#) can be much simplified with a wise choice of the parameters. For instance, an overall constant phase has no physical significance, so we can drop the term with ϕ_s . τ_s represents the position of the maximum of the pulse, but we can choose our origin of times so that $\tau = 0$ when $\xi = 0$ which leads to τ_s being zero as well. δ can be seen as a frequency shift from the carrier frequency ω_0 which will change the original frequency to $\omega' = \omega_0 + \delta/T_0$ and provoke a change in the group velocity ($\beta'_1 = \beta_1 + \delta|\beta_2|/T_0$). But it can also be removed from [2.5.35](#) by choosing the right carrier frequency. Lastly, the parameter η determines the amplitude of the soliton and its width (as a matter of fact,

amplitude and width of the soliton are inversely related) and it can be chosen to be equal to 1 by making $u(0,0) = 1$. With all these considerations, equation 2.5.35 reduces to 2.5.37

$$u(\xi, \tau) = \text{sech}(\tau)e^{i\xi/2} \quad (2.5.37)$$

As mentioned before, higher-order solitons, with values of N larger than 1 are supported in the fiber. The power requirements to launch a soliton of the N -th order into the fiber can be obtained from equation 2.5.29 and it will be N^2 times the power needed for the fundamental soliton. Higher-order solitons recover the original shape periodically with a period $\xi_0 = \pi/2$, as we can see in figure 2.5.6

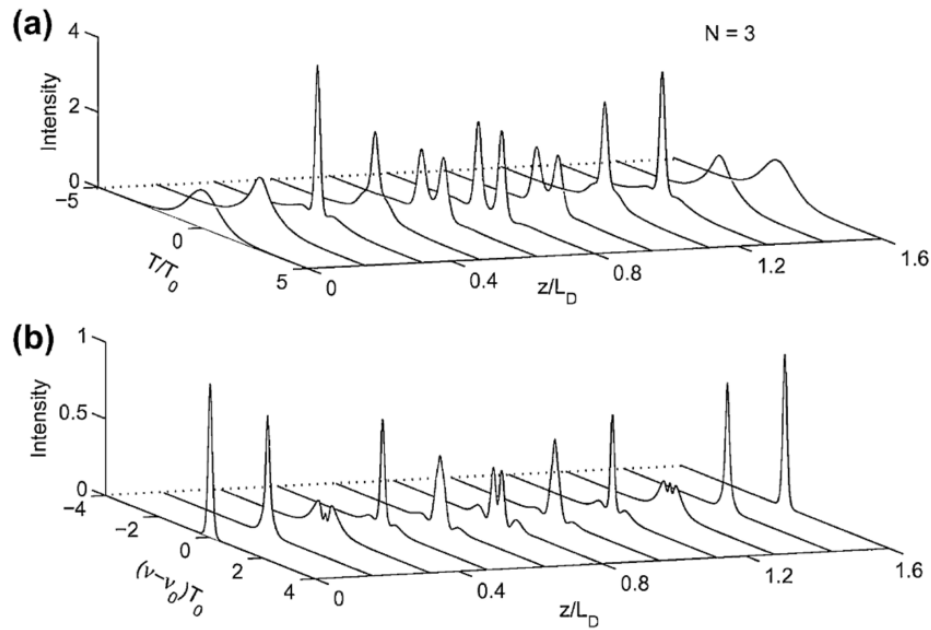


Figure 2.5.6: Evolution of pulse shape and pulse spectrum of a third order soliton. Extracted from [27]

A really interesting feature of the solitonic behaviour is that if the power with which the pulse is launched into the fiber is slightly higher than the required for a certain order soliton, the pulse will adjust itself (and disperse some energy) to match the proper value. We can see this in figure 2.5.7 where the pulse is launched with $N = 1.2$ instead of $N = 1$ and the pulse gradually changes its peak power to reach the correct value of $N = 1$

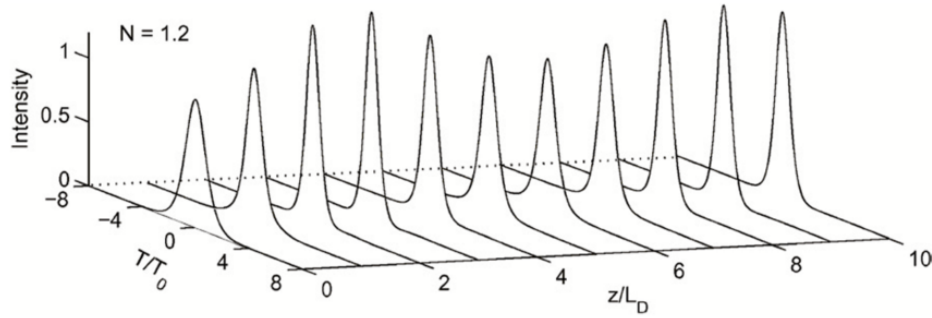


Figure 2.5.7: Evolution of pulse shape that initially presented a value of $N = 1.2$. The pulse gradually evolves into the fundamental soliton ($N = 1$). Extracted from [27]

A lot more information can be found to get a more profound insight on this topic. Agrawal's book [27] contains more detailed explanations and mathematical demonstrations. References [70] and [71] explore deeper into the mechanic soliton (in a material medium) like the one observed by John Scott Russel; and references [72] and [73] deal entirely with optical solitons. Solitons have numerous application not just in the field of optics [74, 75], but also in electronics [76] or magnetism [77]

3 The experiment and numerical approach

We have now given short, but hopefully insightful explanations of the main phenomena that can take place inside an optical fiber span when a pulse (or CW) of light propagates through it. Once that the necessary clarifications have been made, it is time to present the experiment itself.

The motivation behind this experiment is to get the laser to generate ultra-short pulses in a stable way, for which solitonic transmission in the fiber span must be achieved. As we saw in section 2.5.5, solitons are waves that can travel long distances maintaining their shape and spectrum due to an interplay between nonlinear and dispersive effects. Therefore, to obtain this kind of transmission, one must provide a virtually lossless medium. Even though fibers are themselves a rather low-loss medium, even for short distances ($\sim 1\text{km}$), losses are sufficiently high to prevent solitonic transmission from happening.

One way to overcome the losses inherent to the fiber is to amplify the signal, so that gains compensate for losses. Probably the first option that comes to the reader's mind to do this is to amplify the signal periodically (lumped amplification) every time a certain distance is traveled. This is actually the scheme nowadays in telecommunication applications. However, it is an unsuitable method for solitonic transmission. This is because in the space between two optical amplifiers, the signal will have decayed enough for the signal to lose its solitonic behaviour. So, even if you end up with an output signal power equal to the input signal power, lossless solitonic transmission would not have taken place. Of course, you could put the amplifiers close enough to compensate losses soon and maintain a soliton during transmission, but that would require an exorbitant amount of lump amplifiers to cover a significant length.

On the other hand, one may also wonder why it is really necessary to achieve the lossless, solitonic transmission, if we can already send a signal thousands of kilometers across by amplifying at certain points. The answer is that lumped amplification has two major setbacks. First, it needs a number of optical amplifiers that elevate the cost and maintenance tasks of the system. Second, when the signal decays, the optical-signal-to-noise ratio (OSNR) might drop to values near 1. That is, the power of the signal might

become comparable to the noise. Then, when the signal is amplified, it is amplified along with the noise, leading to a rather noisy signal which might be source of errors while decoding it. For these reasons, achieving solitonic transmission in long distances would be not only extremely interesting from a scientific point of view, but also extremely useful from an applied perspective.

3.1 Experimental setup

A way to overcome the disadvantages of lumped amplification is to use distributed amplification [78–81]. In these kind of setups, the gain is not provided to the signal at specific points, but spread throughout the whole fiber span. With this, we get to compensate for the losses ideally at every point of the fiber, so the signal never gets to decay and solitonic transmission is achieved. The main mechanism to obtain distributed amplification is through Raman amplification, which is based on the SRS (section 2.5.4). The idea behind this kind of setups is to use a Raman cascade. A pump is introduced in the fiber at a wavelength close to the Raman gain peak so that a Stokes wave is created at the signal wavelength, and the signal is amplified. The experimental setup we have used is included below in figure 3.1.1. The Erbium-Doped fiber amplifier (EDFA) generates the signal and the semiconductor saturable absorber mirror (SESAM) is used to adjust the length of the cavity so that it matches an integer multiple of the soliton period, and to clean the signal from noise [82]

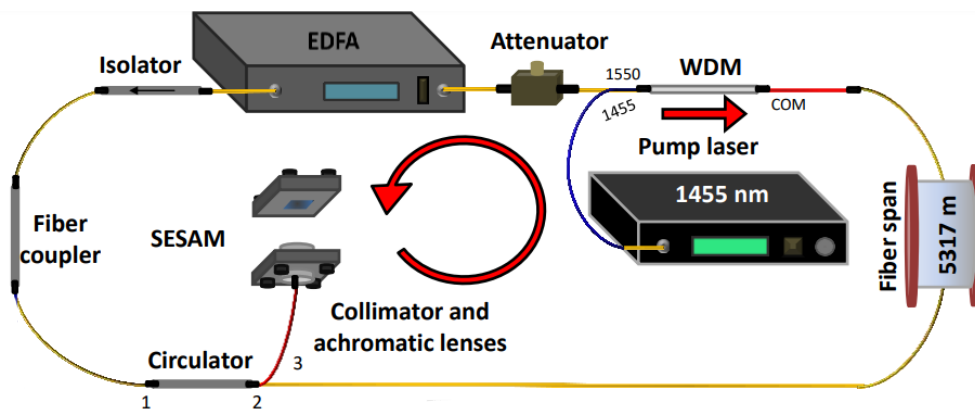


Figure 3.1.1: Schematic depiction of the experimental setup.

The right part of this setup, between the attenuator and the circulator is what I will be focusing on during my work and what simulations are based on. The main elements of this part are the pump laser and the fiber span. Although it is not the case, the fiber span can act as a resonant cavity when FBGs are placed on its end, but mainly it is there where we can test if lossless transmission is achieved. And the pump laser is the responsible for generating the Raman cascade mentioned earlier. For the experimental measurements two different pumping modes will be used with three different lengths: 5.317 km, 10.000 km and 18.807 km. All of them of the same type of fiber, so that their properties don't change from one to the others. With these three fibers, one of the pumping schemes that will be used is primary backward pumping (see figure 3.1.2 (a)). That is, a 1455 nm pump is injected in the counter-propagating direction (with respect to the signal propagation direction) which, by SRS, generates radiation at the signal wavelength (1550 nm), amplifying it.

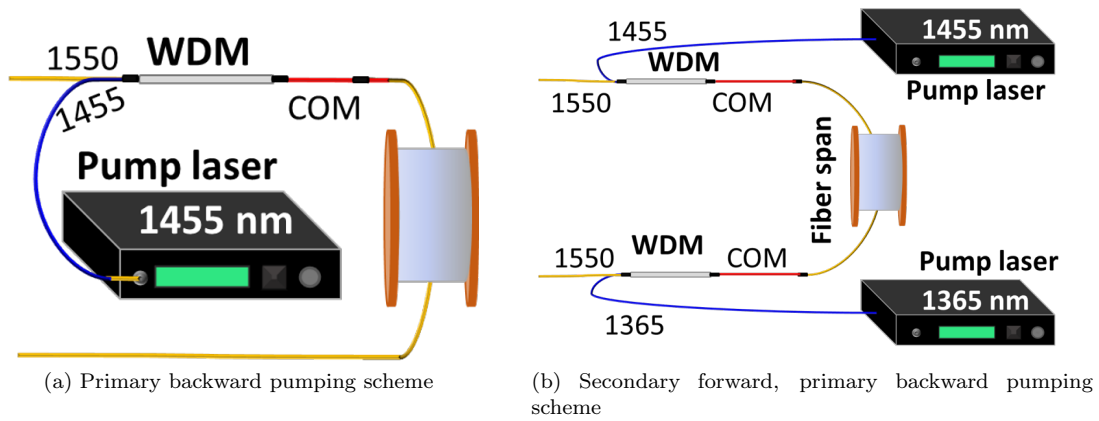


Figure 3.1.2: Pumping schemes of the experiment

The other configuration is a secondary forward, primary backward pumping scheme (fig. 3.1.2 (b)). This means that the pump is injected in both the forward and backward directions. In the forward direction, a double Raman cascade takes place. In other words, a primary pump is injected at 1366 nm at the beginning of the fiber span that generates radiation at 1455 nm which acts itself as a secondary pump creating radiation at 1550 nm that amplifies the signal. In the other end, a 1455 nm pump is injected as in the previous case.

For the sake of data acquisition, the setup (fig. 3.1.1) is slightly modified to replace the EDFA with an optical time domain reflectometer (OTDR) (see fig. 3.1.3). The OTDR now provides the signal and collects experimental measurements of signal power evolution. The ‘cavity’ in fig. 3.1.3 can be any of the three lengths mentioned before and, by switching on or off the 1365 nm laser, we can alternate between the two pumping schemes depicted in fig. 3.1.2

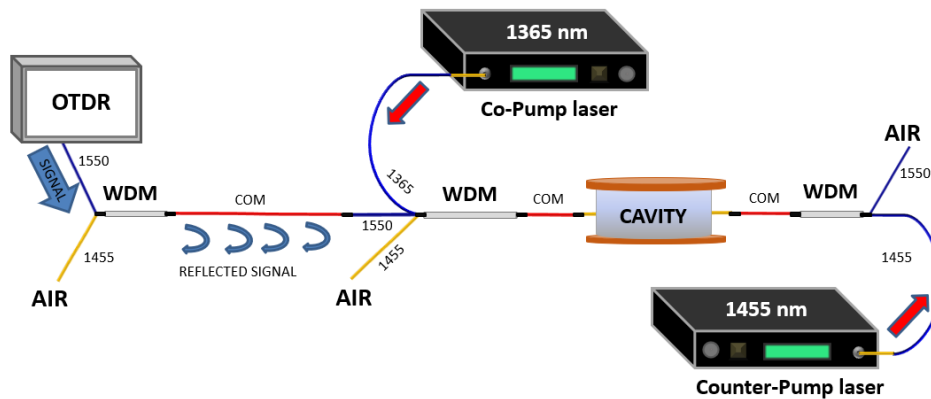


Figure 3.1.3: Experimental setup with the OTDR

3.2 Modelling and simulation

The main goal of this project was to simulate the experimental system in order to compare some theoretical results with experimental results. The idea behind this simulation should be not only to get a numerical or graphic representation of the system, but also to optimize it. That is, we are looking for the set of parameters that provide the flattest signal gain curve while fulfilling the necessary boundary conditions.

The first thing we need to simulate the system is a mathematical model that physically describes our experimental setup. This will be dealt with in section 3.2.1. Once the mathematical model is clear, we need to find a way to integrate (or propagate) it through the fiber to reach a satisfactory solution, which we explain in section 3.2.2. Lastly, in section 3.2.3, once a solution has been found, we try to optimize the system.

3.2.1 The Model

Through section 2 we have seen that light propagation inside a fiber can become a rather complex problem. The effects that have been presented in sections 2.4 and 2.5 must be taken into account when studying the propagation of pulses. For this purpose, equations 2.5.21 and 2.5.22 should be solved with all of its terms, as these are the equations that include all the effects previously described. However, because of the high complexity of these equations, an alternative way to assess the problem is needed. So, instead of trying to directly solve equations 2.5.21 and 2.5.22, we study the evolution of the average signal and pump powers in the stationary state. By doing so, the time dependence is erased and modulation effects are left out of the study. That means that the effects of GVD, SPM and XPM disappear. Furthermore, in our setup, TOD can be neglected because we are working far from the zero dispersion wavelength and FWM can be neglected as well because the conditions for phase and frequency matching are not fulfilled. So, from the dispersive and nonlinear effects explained in sections 2.4 and 2.5, only SRS plays a role in the power evolution equations. The reason to study the power evolution is that, it will allow us to obtain an effective gain $\alpha_{\text{eff}}(z)$ that we can then use to solve the propagation equations in a much simpler way. With this consideration, the differential equations governing the model are given by [4, 83] equations 3.2.1 - 3.2.7.

$$\frac{dP_{P1}^+}{dz} = -\alpha_1 P_{P1}^+ - g_1 \frac{\nu_1}{\nu_2} P_{P1}^+ \left(P_{P2}^+ + P_{P2}^- + 4h\nu_2 \Delta\nu_2 \left(1 + \frac{1}{e^{h(\nu_1 - \nu_2)/K_B T} - 1} \right) \right) + \epsilon_1 P_{P1}^- \quad (3.2.1)$$

$$\frac{dP_{P1}^-}{dz} = \alpha_1 P_{P1}^- + g_1 \frac{\nu_1}{\nu_2} P_{P1}^- \left(P_{P2}^+ + P_{P2}^- + 4h\nu_2 \Delta\nu_2 \left(1 + \frac{1}{e^{h(\nu_1 - \nu_2)/K_B T} - 1} \right) \right) - \epsilon_1 P_{P1}^+ \quad (3.2.2)$$

$$\begin{aligned} \frac{dP_{P2}^+}{dz} &= -\alpha_2 P_{P2}^+ + g_1 \left(P_{P2}^+ + 2h\nu_2 \Delta\nu_2 \left(1 + \frac{1}{e^{h(\nu_1 - \nu_2)/K_B T} - 1} \right) \right) (P_{P1}^+ + P_{P1}^-) \\ &\quad - g_2 \frac{\nu_2}{\nu_S} P_{P2}^+ \left(P_S + N_S^+ + N_S^- + 4h\nu_S \Delta\nu_S \left(1 + \frac{1}{e^{h(\nu_2 - \nu_S)/K_B T} - 1} \right) \right) + \epsilon_2 P_{P2}^- \end{aligned} \quad (3.2.3)$$

$$\begin{aligned} \frac{dP_{P2}^-}{dz} &= \alpha_2 P_{P2}^- - g_1 \left(P_{P2}^- + 2h\nu_2 \Delta\nu_2 \left(1 + \frac{1}{e^{h(\nu_1 - \nu_2)/K_B T} - 1} \right) \right) (P_{P1}^+ + P_{P1}^-) \\ &\quad + g_2 \frac{\nu_2}{\nu_S} P_{P2}^- \left(P_S + N_S^+ + N_S^- + 4h\nu_S \Delta\nu_S \left(1 + \frac{1}{e^{h(\nu_2 - \nu_S)/K_B T} - 1} \right) \right) - \epsilon_2 P_{P2}^+ \end{aligned} \quad (3.2.4)$$

$$\frac{dP_S}{dz} = -\alpha_S P_S + g_2 P_S (P_{P_2}^+ + P_{P_2}^-) \quad (3.2.5)$$

$$\frac{dN_S^+}{dz} = -\alpha_S N_S^+ + g_2 \left(N_S^+ + 2h\nu_S \Delta\nu_S \left(1 + \frac{1}{e^{h(\nu_2 - \nu_S)/K_B T} - 1} \right) \right) (P_{P_2}^+ + P_{P_2}^-) + \epsilon_S N_S^- \quad (3.2.6)$$

$$\frac{dN_S^-}{dz} = \alpha_S N_S^- - g_2 \left(N_S^- + 2h\nu_S \Delta\nu_S \left(1 + \frac{1}{e^{h(\nu_2 - \nu_S)/K_B T} - 1} \right) \right) (P_{P_2}^+ + P_{P_2}^-) - \epsilon_S (P_S + N_S^+) \quad (3.2.7)$$

Where $P_{P_1}^\pm$ are the primary forward (+) and backward (-) pumps; $P_{P_2}^\pm$ are the secondary forward (+) and backward (-) pumps; P_S is the signal power; ν_i are the frequencies of primary and secondary pump and signal; $\Delta\nu_i$ are the bandwidths of the pumps and signal (or the FBG when necessary) α_i are the attenuation coefficients; ϵ_i are the backscattering coefficients; g_i are the Raman gain coefficients; N_S^\pm are the forward (+) and backward (-) noise; z , the distance; h , Planck's constant; K_B , Boltzmann's constant and T , the temperature

This set of coupled ODEs that describe the system is subject to boundary conditions that vary slightly depending on the cavity configuration (presence or absence of FBGs, double or single pumping) and will be specified in section 3.2.2. Alternatively, the model can be simplified if we consider single pumping only, which leads to equations 3.2.8 - 3.2.12

$$\frac{dP_P^+}{dz} = -\alpha_P P_P^+ - \frac{\nu_P}{\nu_S} \frac{g}{A_{eff}} \left(P_S^+ + N_S^+ + N_S^- + 4h\nu_S \Delta\nu_S \left(1 + \frac{1}{e^{h(\nu_P - \nu_S)/K_B T} - 1} \right) \right) P_P^+ \quad (3.2.8)$$

$$\frac{dP_P^-}{dz} = \alpha_P P_P^- + \frac{\nu_P}{\nu_S} \frac{g}{A_{eff}} \left(P_S^+ + N_S^+ + N_S^- + 4h\nu_S \Delta\nu_S \left(1 + \frac{1}{e^{h(\nu_P - \nu_S)/K_B T} - 1} \right) \right) P_P^- \quad (3.2.9)$$

$$\frac{dP_S}{dz} = -\alpha_S P_S + \frac{g}{A_{eff}} (P_P^+ + P_P^-) P_S \quad (3.2.10)$$

$$\frac{dN_S^+}{dz} = -\alpha_S N_S^+ + \frac{g}{A_{eff}} (P_P^+ + P_P^-) \left(N_S^+ + 2h\nu_S \Delta\nu_S \left(1 + \frac{1}{e^{h(\nu_P - \nu_S)/K_B T} - 1} \right) \right) + \epsilon N_S^- \quad (3.2.11)$$

$$\frac{dN_S^-}{dz} = \alpha_S N_S^- - \frac{g}{A_{eff}} (P_P^+ + P_P^-) \left(N_S^- + 2h\nu_S \Delta\nu_S \left(1 + \frac{1}{e^{h(\nu_P - \nu_S)/K_B T} - 1} \right) \right) - \epsilon (N_S^+ + P_S) \quad (3.2.12)$$

This simplification becomes specially useful when we run the simulation as simpler models are easier to integrate and less computationally expensive.

3.2.2 Simulation

As seen in equations 3.2.1 - 3.2.7, the complete model is characterized by a set of seven ordinary differential equations. But it is not defined uniquely by this set of equations. The real problem implies finding a solution that not only satisfies the equations, but also fulfills the boundary conditions imposed by the physical constraints of the system. These boundary conditions vary slightly depending on cavity design, so they have been summarized in table 3.2.1 and equations 3.2.13

Pumping mode	Primary	Secondary
FBG at beginning	$P_{P1}^+(0) = R_1 P_{P1}^-(0)$ $P_{P1}^-(L) = P_{P1,in}^-$ $P_{P2}^+(0) = P_{P2}^-(0) = 0$ $P_{P2}^+(L) = P_{P2}^-(L) = 0$	$P_{P1}^+(0) = P_{P1,in}^+$ $P_{P1}^-(L) = P_{P1,in}^-$ $P_{P2}^+(0) = R_1 P_{P2}^-(0)$ $P_{P2}^-(L) = P_{P2,in}^-$
FBG at end	$P_{P1}^+(0) = P_{P1,in}^+$ $P_{P1}^-(L) = R_2 P_{P1}^+(L)$ $P_{P2}^+(0) = P_{P2}^-(0) = 0$ $P_{P2}^+(L) = P_{P2}^-(L) = 0$	$P_{P1}^+(0) = P_{P1,in}^+$ $P_{P1}^-(L) = P_{P1,in}^-$ $P_{P2}^+(0) = P_{P2,in}^+$ $P_{P2}^-(L) = R_2 P_{P2}^+(L)$
FBG at both ends	$P_{P1}^+(0) = R_1 P_{P1}^-(0)$ $P_{P1}^-(L) = R_2 P_{P1}^+(L)$ $P_{P2}^+(0) = P_{P2}^-(0) = 0$ $P_{P2}^+(L) = P_{P2}^-(L) = 0$	$P_{P1}^+(0) = P_{P1,in}^+$ $P_{P1}^-(L) = P_{P1,in}^-$ $P_{P2}^+(0) = R_1 P_{P2}^-(0)$ $P_{P2}^-(L) = R_2 P_{P2}^+(L)$
No FBGs	$P_{P1}^+(0) = P_{P1,in}^-$ $P_{P1}^-(L) = P_{P1,in}^-$ $P_{P2}^+(0) = P_{P2}^-(0) = 0$ $P_{P2}^+(L) = P_{P2}^-(L) = 0$	$P_{P1}^+(0) = P_{P1,in}^+$ $P_{P1}^-(L) = P_{P1,in}^-$ $P_{P2}^+(0) = P_{P2,in}^+$ $P_{P2}^-(L) = P_{P2,in}^-$

Table 3.2.1: Different boundary conditions depending on cavity design

$$P_S(0) = P_{S,in}; \quad N_S^+(0) = N_0; \quad N_S^-(L) = 0 \quad (3.2.13)$$

Now, when solving a system of ODEs, the common practice is to use some integrator to get from the initial point (at $z = 0$) to the last point of the integration interval ($z = L$). There are several numerical integration methods (like Bulirsch-Stoer method, predictor-corrector methods, etc. [84]), but one of the most common is the Runge-Kutta (RK) method.

Actually the Runge-Kutta methods are a broad family of methods (Euler method, Runge-Kutta-Fehlberg method [85], etc.), each of which might be better than others for certain systems. Their working principle is, in fact, rather simple and straight-forward and very easy to implement. The main idea is to take Euler-style steps⁸, but to make them more accurate, the derivative is not just calculated with the starting and ending points of the step. Rather than that, a half-step is taken to calculate the derivative at the midpoint and use that information to take the real step. This would give a second-order RK method. This is illustrated in figure 3.2.1

⁸The Euler method computes the value of a function at point $n + 1$ given the value of it at the point n . It uses the derivative to go from n to $n + 1$ [84]

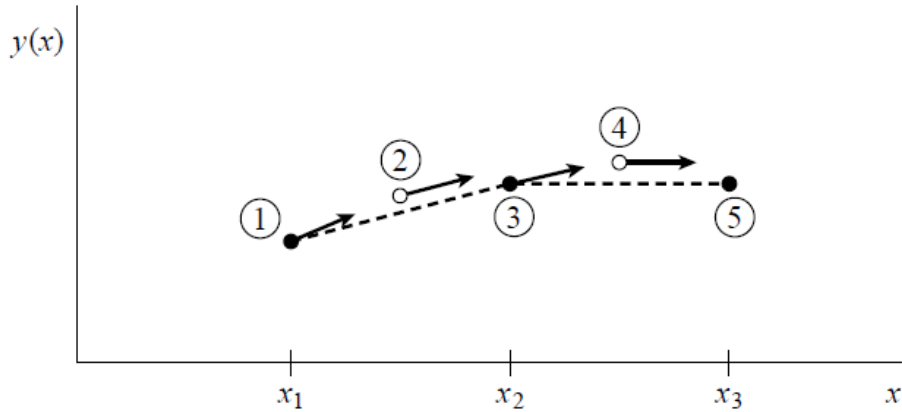


Figure 3.2.1: RK method. Black points represent calculated values of the function. White points represent midpoints, where only the derivative information was used. Figure extracted from [84]

The method can be extended to smaller fractions of the step to improve accuracy, giving higher-order RK methods. Amongst these, probably the all-time favorite is the fourth-order RK method, which can be easily implemented following the equations in 3.2.14

$$\begin{aligned}
 k_1 &= hf(x_n, y_n) \\
 k_2 &= hf\left(x_n + \frac{h}{2}, y_n + \frac{k_1}{2}\right) \\
 k_3 &= hf\left(x_n + \frac{h}{2}, y_n + \frac{k_2}{2}\right) \\
 k_4 &= hf(x_n + h, y_n + k_3) \\
 y_{n+1} &= y_n + \frac{k_1}{6} + \frac{k_2}{3} + \frac{k_3}{3} + \frac{k_4}{6} + O(h^5)
 \end{aligned}
 \tag{3.2.14}$$

Where h is the step size and f would be the derivative of the system

This method in particular is already perfectly implemented in the MATLAB[®] built-in function ‘ode45’. This function takes a system of ODEs, an integration interval and an initial set of values and uses the Rung-Kutta algorithm with an additional improvement: adaptive step-size⁹, to return the evolution of the system through a number of points of the integration interval. This would be just right if we knew the exact values at the beginning of said interval. This is called an initial value problem (IVP). But we do not have an IVP. Our system has boundary conditions, which lead to a boundary values problem (BVP). That is, we are seeking for a solution of our system that fulfills some requirements at $z = 0$ but some other requirements at $z = L$.

MATLAB[®] has as well a built-in function able to numerically solve a system of ODEs subject to a BVP: The ‘bvp4c’ function, which uses ‘ode45’ and a collocation method. The collocation method used by ‘bvp4c’ was introduced in 1972 by Russel and Shampine [86]. Collocation methods are a group of numerical methods utilised to solve BVP. To get an idea of how they work, let us imagine a second-order ODE 3.2.15

⁹The adaptive step-size is an improvement to the RK routine that adjusts the size of the step, h depending on the error to guarantee that the integration is accurate if the function varies rapidly for example

with boundary conditions [3.2.16](#)

$$\frac{d^2y}{dx^2} = f(x, y, y) \quad (3.2.15)$$

$$y(x_a) = a; \quad y(x_b) = b; \quad (3.2.16)$$

One option (used by the shooting method [\[87\]](#) for example) is to transform the BVP into an IVP by iteratively “shooting” the equations to get to a solution and use the difference between the desired values and the obtained values to correct the initial condition and shoot again. Thus, targeting more accurately each time the value of $y(x_a)$ that leads to the correct value of $y(x_b)$. This is a very simple method that works quite well when the system is not very complex or when you want to specify the values of certain variables at the beginning of the interval and the values of the other variables at the end of the interval. In fact, we have tried this method, although unsuccessfully. Most likely, due to the complexity of the system.

So, having discarded the shooting method, another thing one might try to do is, instead of directly matching the initial condition to the ending condition, we subdivide the interval in a number of N subintervals. Every subinterval is enclosed by two points x_i . These are the collocation points. The aim of the collocation method [\[86\]](#) is to adjust these interior points so that they all satisfy the ODE [3.2.15](#). In order to do that, the finite differences approximation [\[88, 89\]](#) is used to obtain numerical values of the derivatives.

But there is one small inconvenience about ‘bvp4c’ with which we must be careful. This function does not allow to specify constraints to the solutions (apart from the boundary conditions), such as restricting the variables to a certain region. In our case, it would have no physical meaning to obtain a solution with negative powers. So we should constrain our variables to only positive values. Since ‘bvp4c’ does not allow us to do so, we need to find a workaround. The easiest we can think of (although probably not the best) is to integrate repeatedly until a solution with no negative values is found. Of course this could end up in an infinite loop which is taken care of by defining a maximum number of iterations. If a solution can not be found within said maximum of iterations, an error is thrown and the user is suggested to try a slightly different starting point.

As mentioned at the beginning of this text (section [1.2](#)), one of my personal goals for this project was to produce a user-friendly, robust and versatile code to run simulations of the system with a high variability in cavity design elements, parameters, etc. With this in mind, the model, along with its different possible boundary conditions have been built into a user interface (UI) created with MATLAB App Designer[®]. This interface allows the user to specify the pumping conditions, signal power, fiber length and all the relevant parameters and simulate the evolution of the system. A screenshot of it is shown in figure [3.2.2](#)

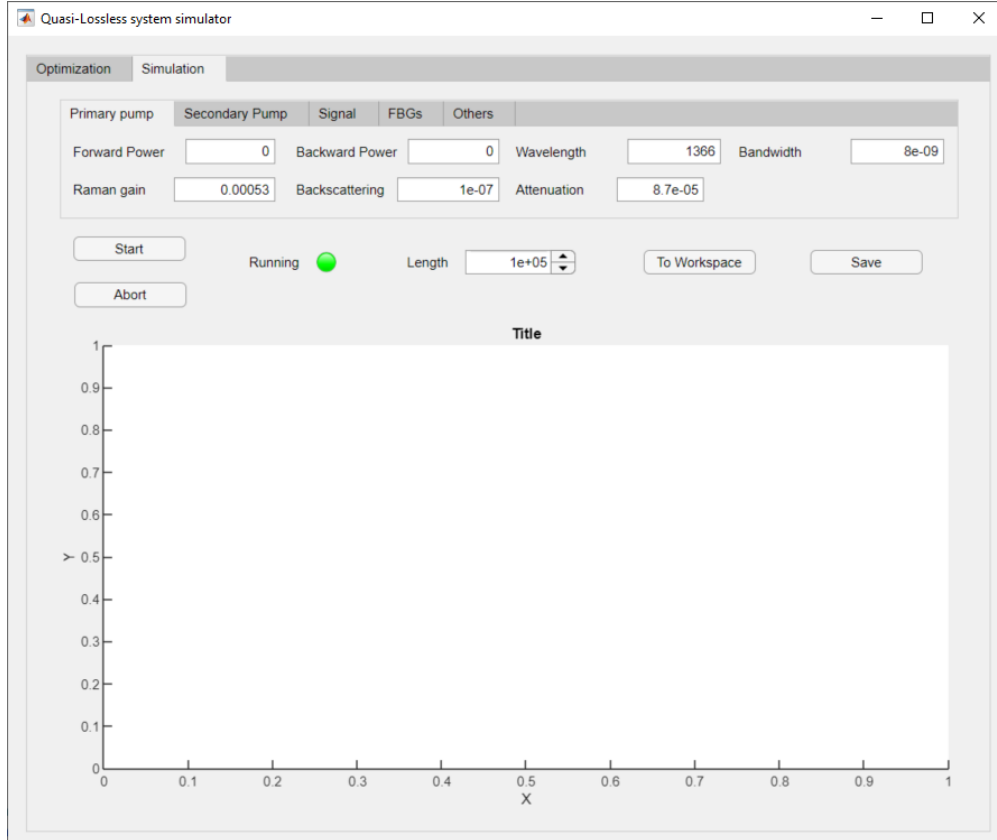


Figure 3.2.2: Screenshot of the simulator user interface

The app or UI takes as input from the user, parameters concerning the primary and secondary pumps and signal such as power, wavelength, Raman gain, backscattering coefficient, attenuation coefficient, etc. It also allows the user to specify whether there are or not FBGs at the beginning and/or at the end of the cavity as well as their reflectivities if applicable. Lastly, under the ‘Others’ tab, the user may modify parameters such as the initial noise, temperature or tolerance¹⁰ of the simulation. Clicking on the ‘Abort’ button will stop the simulation, which can be useful if the user realizes that some parameters are incorrect or if it is taking too long for the simulation to finish. The ‘Running’ lamp turns red when simulation starts and green again when it finishes to let the user know that the job is done. Finally, pushing the buttons ‘To Workspace’ and ‘Save’ will, respectively, save the results of the simulation to your MATLAB® workspace and to a text (‘.txt’) file.

Since we want our UI to be robust and versatile. If the user inputs one of the simpler cases (for example single backward pumping), equations 3.2.8 to 3.2.12 are completed with 3.2.17

$$\frac{dP_{P2}^+}{dz} = 0; \quad \frac{dP_{P2}^-}{dz} = 0 \quad (3.2.17)$$

This allows us to always work in a seven-dimensional variable space so the code becomes more versatile.

¹⁰The tolerance of the simulation is taken into account mainly when fulfilling boundary conditions. So for example if a certain variable should take the value a at a certain point, the simulator will aim to leave that variable between $a - tolerance$ and $a + tolerance$

As a test to check that the simulator works properly, we reproduce the results in [4]. There, they simulated the system of figure 3.2.3. Which is a secondary bidirectional scheme with FBGs on the ends of the span for cavity lengths of 100 km and 60 km. A comparison between that paper and my simulation is shown in figure 3.2.4 and, as we can see, they are in very good agreement, which poses a good starting point for the interface.

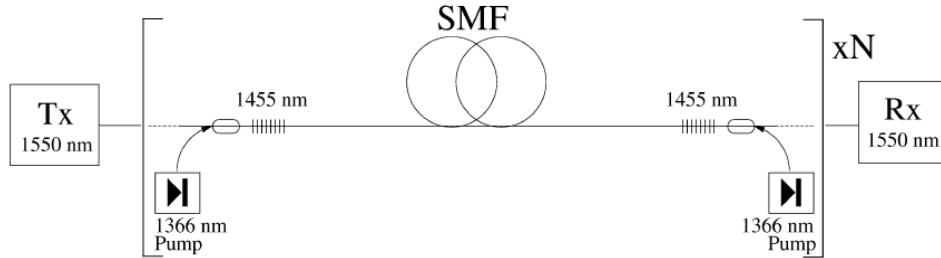


Figure 3.2.3: Schematic setup for which the ‘test’ simulation was run. Extracted from [4].

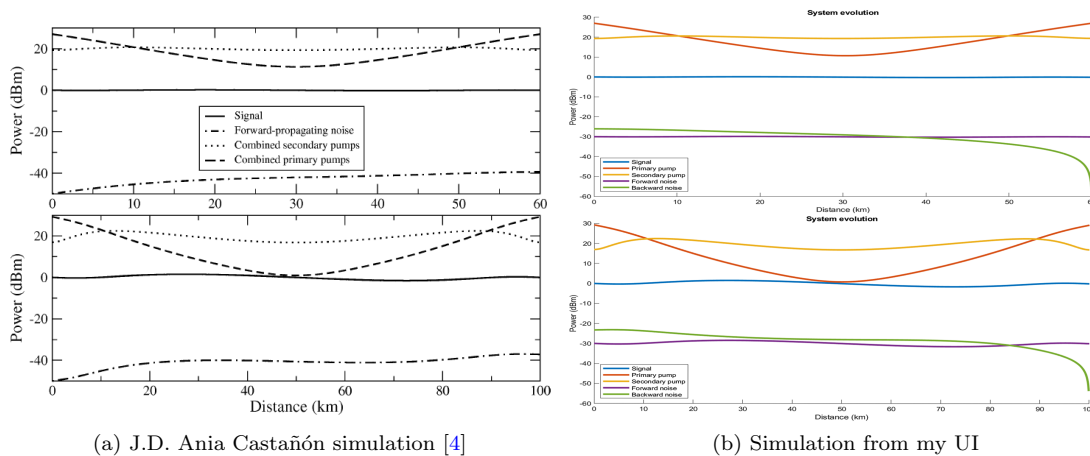


Figure 3.2.4: Comparison between simulations

3.2.3 Optimization

Now that we have found a stable and trustworthy way to simulate our system given certain initial values, our next target is to find the set of parameters that lead to the flattest signal gain curve (while keeping the condition of no losses). The model defined by equations 3.2.1 - 3.2.7 has seven independent variables, so we need to use multidimensional optimization techniques.

There are several numerical optimization algorithms, but most of them rely on the calculation of the derivative (or the gradient in N dimensions). Optimization problems in N -dimensions usually require the evaluation of a certain *cost* function. It is the value of this cost function what we want to maximize or minimize. In addition to the optimization problem, there might be some constraints. Imagine, for example, that we wanted to find the maximum of the function $f(x, y)$ but subject to the region $x, y \geq 0$.

In our case, we want to make the signal gain curve as flat as possible, which means bringing 3.2.18 to its minimum value. But this should be achieved while maintaining a lossless system. So, our problem would be

to optimize 3.2.18 subject to the constraint $|\Delta P_S| < tol$

$$F = P_{S,\max} - P_{S,\min} \quad (3.2.18)$$

The way we have chosen to face the problem is with the Nelder-Mead (NM) method [90] (also known as downhill simplex, amoeba or polytope) as optimization algorithm together with the penalty method [91] to add the lossless condition constraint. Let us briefly explain what these two methods consist of:

The NM algorithm is quite distinct from other optimization algorithms. The fundamental difference is that, unlike most of these algorithms, the NM method does not need information about the derivative or the gradient of the function to optimize, rather than that, it uses only function evaluations at $N + 1$ points (N being the dimensionality of the system). A simplex is the simplest N -dimensional geometrical figure one can construct with $N + 1$ points in an N -dimensional space. That is, in 2D, a triangle is a simplex and in 3D, a tetrahedron would be a simplex (see fig. 3.2.5). Unfortunately, human consciousness is unable to visualize figures in more than 3D, but the abstract idea can be extended to as many dimensions as needed.

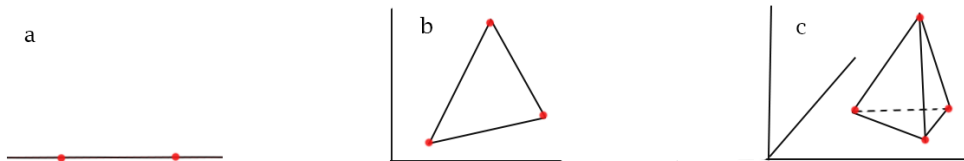


Figure 3.2.5: Simplex in a) one dimension; b) two dimensions; c) three dimensions

So, the NM, amoeba or downhill simplex algorithm evaluates the cost function at every vertex of the simplex and substitutes the worst point according to one of the moves that are shown in figure 3.2.6. In order to do this, the vertices of the simplex need to be sorted from best (lowest in our case) to worst (highest) value of the cost function. And it is the worst point the one that moves at every iteration except when the simplex shrinks. As a result, the simplex moves at every iteration in a way that reminds of an amoeba (hence the name), always reaching towards the best points it finds.

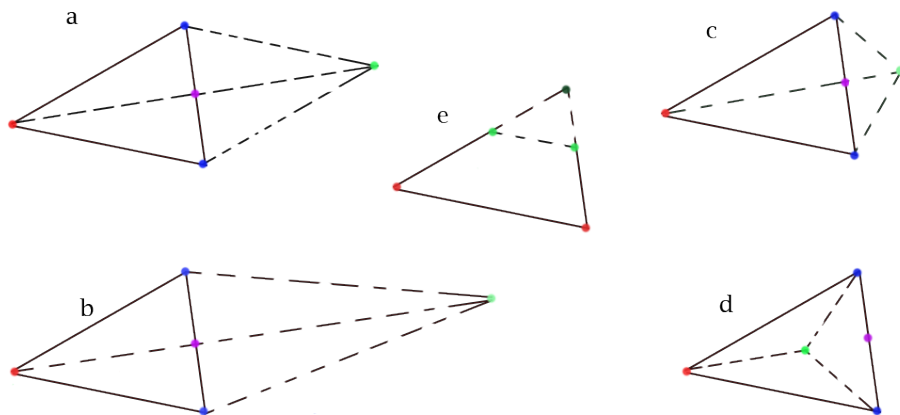


Figure 3.2.6: a) Reflection. b) Expansion. c) Outside contraction. d) Inside contraction. e) Shrinking. Points in red are the ones being substituted by the points in green. In purple, the centroid; and in blue, vertices that remain unchanged in the iteration. The darker green point in e) marks what was the best point before the shrinking. Dashed lines show the simplex after the corresponding move

A little more mathematically, the process begins with sorting the vertices of the simplex so that equation 3.2.19 is fulfilled

$$f(x_1) \leq f(x_2) \leq \dots \leq f(x_{N-1}) \quad (3.2.19)$$

Where x_i are the vertices of the simplex ordered from best to worst, and f is the function to optimize

Once the simplex has been sorted, at every iteration the following steps are followed [92]:

1. Reflection. Compute reflection point with 3.2.20

$$x_r = \bar{x} + \alpha(\bar{x} - x_{N+1}) \quad (3.2.20)$$

If $f(x_1) \leq f(x_r) \leq f(x_N)$, substitute worst point with reflected point

2. Expansion. If $f(x_r) < f(x_1)$ compute expansion point with 3.2.21

$$x_e = \bar{x} + \beta(x_r - \bar{x}) \quad (3.2.21)$$

If $f(x_e) < f(x_r)$, substitute worst point with expanded point. Otherwise, substitute worst point with reflected point.

3. Outside contraction. If $f(x_N) \leq f(x_r) < f(x_{N+1})$, compute outside contraction point with 3.2.22

$$x_{oc} = \bar{x} + \gamma(x_r - \bar{x}) \quad (3.2.22)$$

If $f(x_{oc}) \leq f(x_r)$, substitute worst point with outside contracted point. Otherwise, shrink simplex (step 5)

4. Inside contraction. If $f(x_r) \geq f(x_{N+1})$, compute inside contracted point with 3.2.23

$$x_{ic} = \bar{x} - \gamma(x_r - \bar{x}) \quad (3.2.23)$$

If $f(x_{ic}) < f(x_{N+1})$, substitute worst point with inside contracted point. Otherwise, shrink simplex (step 5)

5. Shrink. When necessary, shrink simplex using 3.2.24 with every vertex of the simplex except the best point

$$x_i = x_1 + \delta(x_i - x_1) \tag{3.2.24}$$

The \bar{x} that appears in equations 3.2.20 - 3.2.24 is the centroid¹¹ of all the vertices of the simplex except the worst one. The α, β, γ and δ parameters are scalar magnitudes characteristic of each move. Their standard values are respectively 1, 2, 1/2 and 1/2 [93–96]. However, high dimensionality can affect the performance of the Nelder-Mead algorithm, so we chose an adaptive set of parameters that depend on it [97] given by 3.2.25.

$$\alpha = 1; \quad \beta = 1 + \frac{2}{N}; \quad \gamma = 0.75 - \frac{1}{2N}; \quad \delta = 1 - \frac{1}{N} \tag{3.2.25}$$

With N being the dimensionality of the problem.

The whole process is illustrated in a flowchart in figure 3.2.7

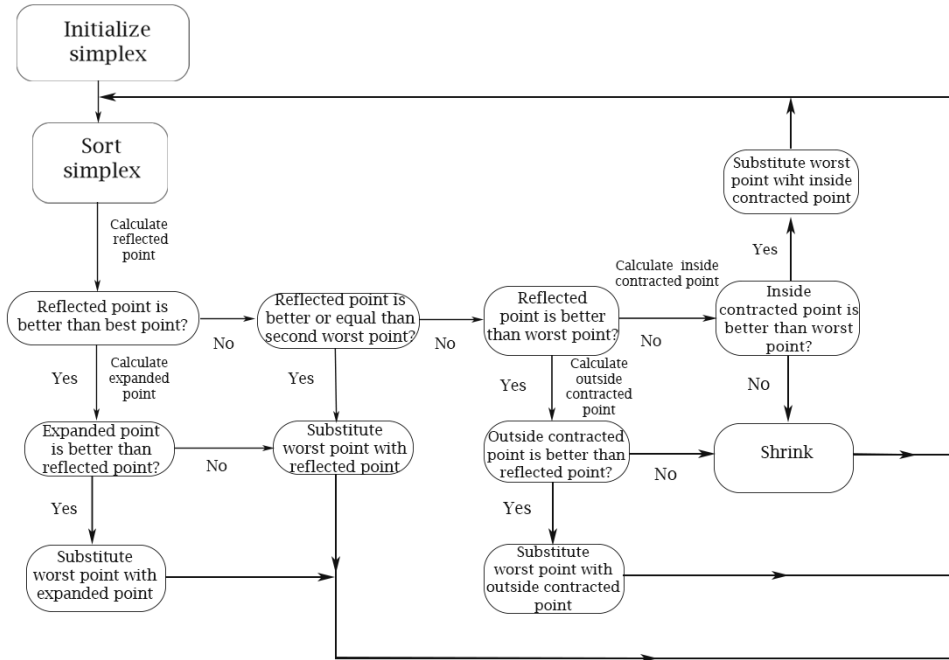


Figure 3.2.7: Flowchart for the Nelder-Mead algorithm

As with any iterative process, we need a way to tell the amoeba when to stop moving and hopefully settle for a point where it has converged to the optimum solution. Otherwise, it would go on and on forever in an infinite loop. How we do this is by implementing a termination criterion, and note that I say termination criterion and not convergence criterion. A convergence criterion is one that is fulfilled when the optimizer has converged to the optimum solution, the one that satisfies our problem with all the possible constraints

¹¹The centroid of a set of points is the mean point of all of them

we may have had to add. A termination criterion is just the one that tells the optimizer to stop because it makes no sense to go on with the iterative process as iterations are now simply revolving the optimizer around a certain point. There are different termination criteria one may choose. The one I used stops the process when the values of the cost function at the best and worst points in the simplex differ by 0.001 or less. This automatically means that all the vertices in the simplex lead to values in a range of just 0.001 from the best point, which implies that all the vertices are sufficiently close to one another. Of course, as every iterative algorithm of this kind, the termination criterion is complemented with a *break* command to stop the process also when a certain number of iterations is reached even if the termination criterion is not fulfilled. This is so to avoid getting the optimizer stuck in an infinite loop. The convergence criterion is probably more straight-forward in our case. We want to minimize 3.2.18, but we know exactly what its minimum value can be: 0. So, we defined the convergence criterion to be fulfilled when the value of the cost function at the best point of the simplex was below a certain tolerance (also fixed at 0.001).

One of the main difficulties one might come across while optimizing a certain function is the existence of local minima (or maxima) that may trick the optimizer into thinking that its work is done and it has converged to an optimum value when, in fact, it has not. To overcome this, as recommended in [84] we “kick” the simplex once the termination or convergence criteria have been fulfilled to begin again from a different starting point. We do this a number of times and store the information of the best point of each kick. After the final kick is finished, the results of every kick are compared and the best final point is picked as the optimum. This ensures that we do not get stuck in local critical points.

As mentioned earlier, we need to optimize the flatness of the signal gain curve. But we need to do so while keeping losses at zero, so the cost function that would be originally 2.3.18 is modified with a penalty factor. To briefly illustrate how the penalty method works, I am going to use an example from [98], which I found quite descriptive. Imagine we have a highway (with a toll) and we want to limit the speed to 120 km/h. We could use signs and forbid going faster than that, which would mean adding a constraint. But we could also make the highway free as long as you keep your speed under 120 km/h, but with a 500 € toll if you surpass that limit. In this case, there would be no rules (no constraints) against going over 120 km/h, and yet, most people will not pass that limit because there is a significant penalty if they do so. This is a way to keep the problem unconstrained but slightly forced to comply with the constraints.

With all these things in mind, the only step left to do is to define our cost function, which, by this point, we should guess it would look like $f = P_{S,\max} - P_{S,\min} + \Delta P_S$. But we have actually modified it a little more. So, our cost function (the one being optimized) is given by 3.2.26

$$f = \underbrace{\frac{P_{S,\max} - P_{S,\min}}{P_{S,\max} + P_{S,\min}}}_{\text{Magnitude to minimize}} + \underbrace{\frac{|P_S(L) - P_S(0)|}{P_S(L) + P_S(0)}}_{\text{Penalty factor}} \quad (3.2.26)$$

We have normalized the cost function so that both of its terms always take values in the range $[0, 1]$. The reason why we do this, apart from making the cost function a bounded function is because with this expression we know that the best value that f can take is zero. This allows us to define a convergence criterion. Note that only if $P_{S,\max} = P_{S,\min}$ and $P_S(0) = P_S(L)$, $f = 0$. Given that, we have defined the convergence criterion as $f \leq tol$, with $tol = 0.001$. This means that for the convergence criterion to be fulfilled, neither of the two terms in 3.2.26 can be higher than 0.001. But, the first term being equal to 0.001 means that $\frac{P_{S,\max}}{P_{S,\min}} = \frac{1.001}{0.999} \Rightarrow P_{S,\max} \approx 1.002P_{S,\min}$. And, analogously, the second term being 0.001 would mean either $P_S(0) \approx 1.002P_S(L)$ or $P_S(0) \approx 0.998P_S(L)$. Therefore, such definitions of the cost function and the convergence criterion seem rather suitable for our problem.

3.3 Results

As specified in section 3.1, we test up to six different configurations in the laboratory and obtain the evolution of the signal for each of them with an OTDR¹². The OTDR is mainly used in on-field applications to localize singular points in the fiber where losses are higher than they should. These kind of events occur at the connections between two spans of fiber or, for example, at points where a macro- or micro-bending is present or the fiber is burnt, etc. It works really well to measure the relative power of the signal at every point of the fiber. However, because of how it works, the measurements obtained from around the first two kilometers of the fiber can not be used. This is sometimes compensated by introducing a ‘launch’ fiber, which is a span of fiber of around that length. But since, fiber length is a critical parameter in the setup, we did not want to modify or alter this. Therefore, we decided to use it without the launch fiber and consider the measurements only after 2.5 km. Also because the initial section is neglected and the input power from the OTDR is not really known (manufacturer says the input pulse is between 150 μW and 300 μW), we decide to represent the power excursion. This is given by the difference, in dB, between the power at any point and the initial power (considering here the initial power as $P_S(z = 2.5\text{km})$) and it is actually a magnitude of interest because the aim of the setup is to achieve solitonic transmission and for that to occur, a lossless system should be achieved but also the signal gain curve should be as flat as possible.

In figure 3.3.1 the power excursion is represented for the three different lengths: 5.317 km, 10.000 km and 18.807 km. For each of these lengths, several powers of primary backward pumping at 1455 nm were tried in the range from 40 mW to 400 mW. The OTDR provides a measurement of the slope, in dB/km of the signal power decay. Although when pumping is introduced, the evolution of the signal can not really be adjusted by a line (in dB scale), it gives a good idea of at what point the signal stops losing power and starts to gain it. The results of these measurements are summed up in table 3.3.1

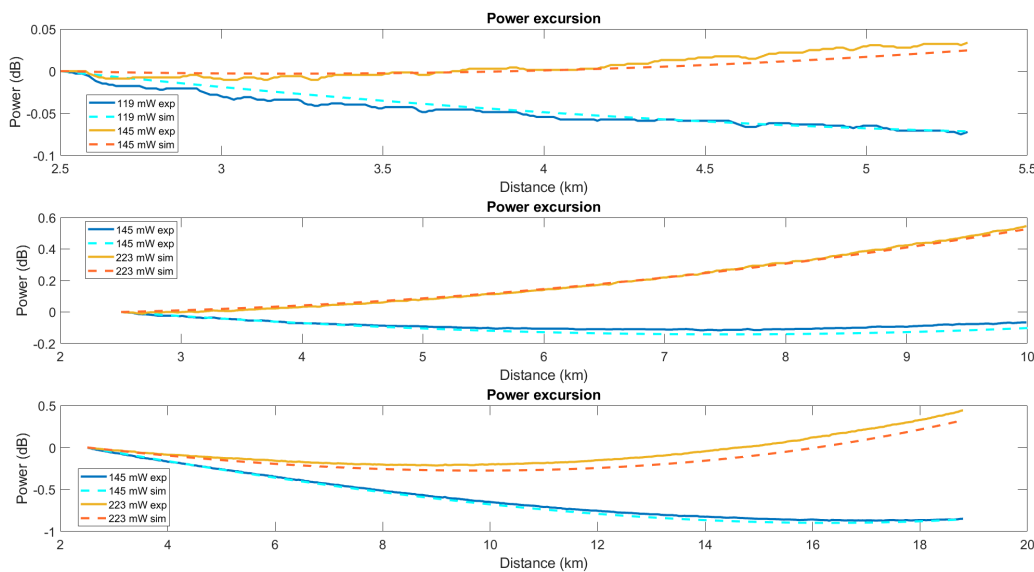


Figure 3.3.1: Comparison between simulation and experimental measurements for three different lengths and two different powers, one that gives overpumping and one that gives underpumping

¹²Stands for Optical Time Domain Reflectometer and it is a device capable of measuring signal power through the fiber based on Rayleigh backscattering

Power (mW)	Slope (dB/km)					
	5.317 km		10.000 km		18.807 km	
	experiment	simulation	experiment	simulation	experiment	simulation
0.00	-0.227	-0.191	-0.220	-0.191	-0.203	-0.191
48.0	-0.152	-0.129	-0.155	-0.134	-0.156	-0.148
119	-0.044	-0.038	-0.066	-0.054	-0.078	-0.084
145	-0.005	-0.006	-0.019	-0.026	-0.058	-0.061
223	0.111	0.090	0.066	0.053	0.030	0.007
296	0.220	0.179	0.161	0.138	0.094	0.069
377	0.297	0.289	0.235	0.227	0.148	0.142

Table 3.3.1: Comparison of experimental and simulated slope measurements for the single backward pumping scheme

Seeing figure 3.3.1 we can notice that the agreement between the experimental (continuous line) and the simulated (dashed line) results is rather good for all of the distances. Furthermore, we can clearly see that, better results are obtained when the distance is higher (10km and 20 km). This has to do with the fact that the OTDR measurements are more accurate when the fiber span is longer, but also with the fact that the model itself is a better approximation when the distance is long enough.

Similar measurements are taken for a different pumping configuration: secondary forward, primary backward pumping. That is, a 1366 nm pump is injected in the same direction as the signal and a 1455 pump is injected in the opposite direction. The results are shown in figures 3.3.2 and 3.3.3. Again we see that simulations fit the experimental data reasonably well, although a little bit worse than for primary pumping schemes. Furthermore, looking at 3.3.3 we notice again that simulation matches the experimental results better when the fiber span is longer.

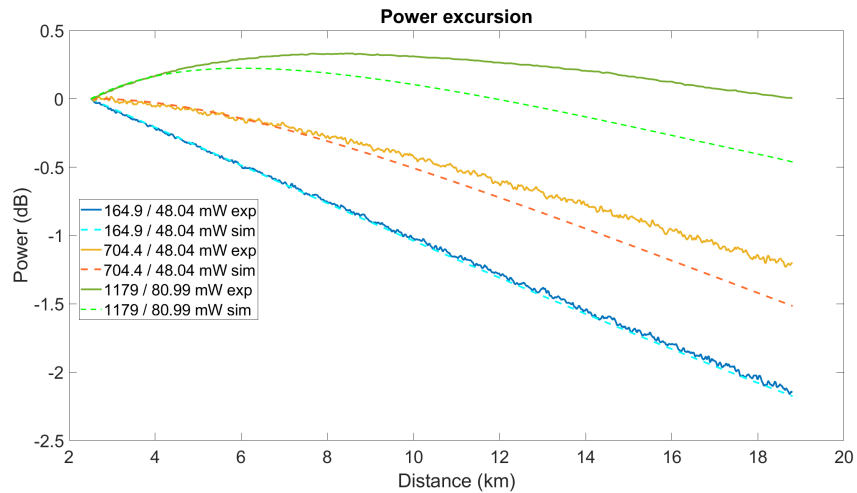


Figure 3.3.2: Comparison between simulation and experimental measurements at a length of 20 km for three different pumping schemes: 164.9 mW forward pumping with 48.04 mW backward pumping; 704,4 mW forward pumping with 48.04 mW backward pumping; and 1179 mW forward pumping with 80.99 mW backward pumping.

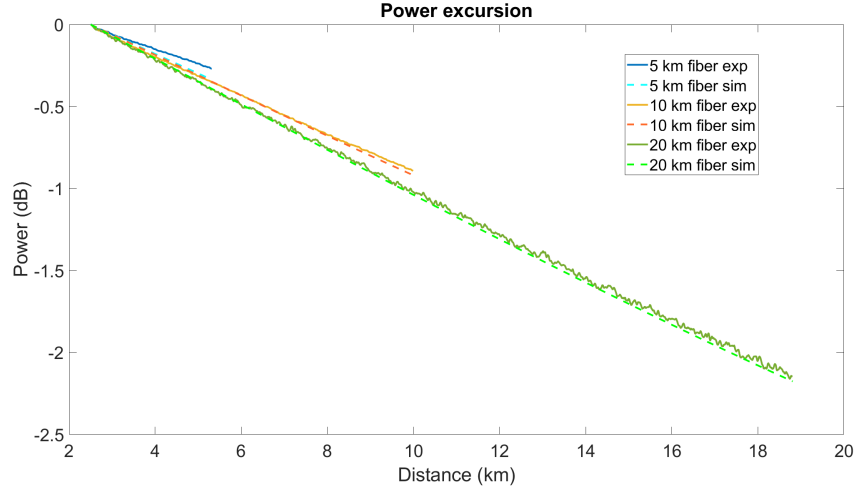
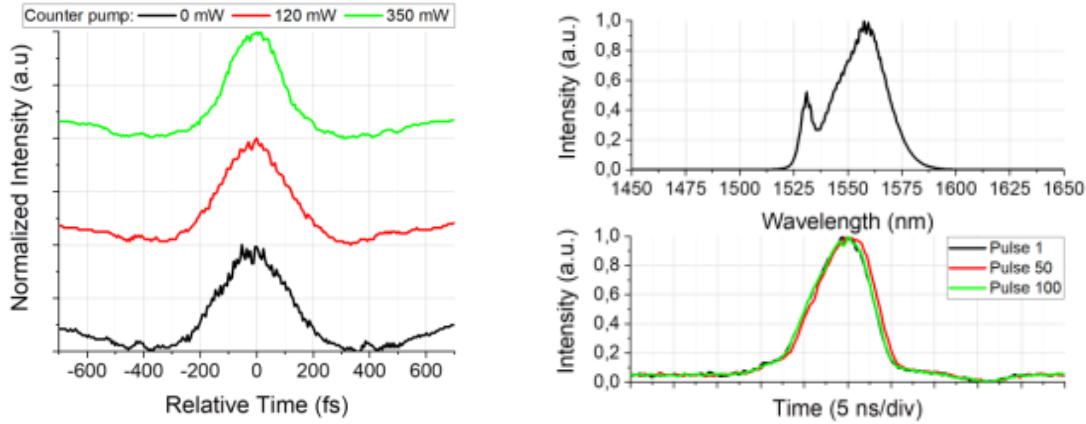


Figure 3.3.3: Comparison between simulation and experimental measurements for three different lengths with the same pumping scheme: 164.9 mW forward pumping with 48.04 mW backward pumping

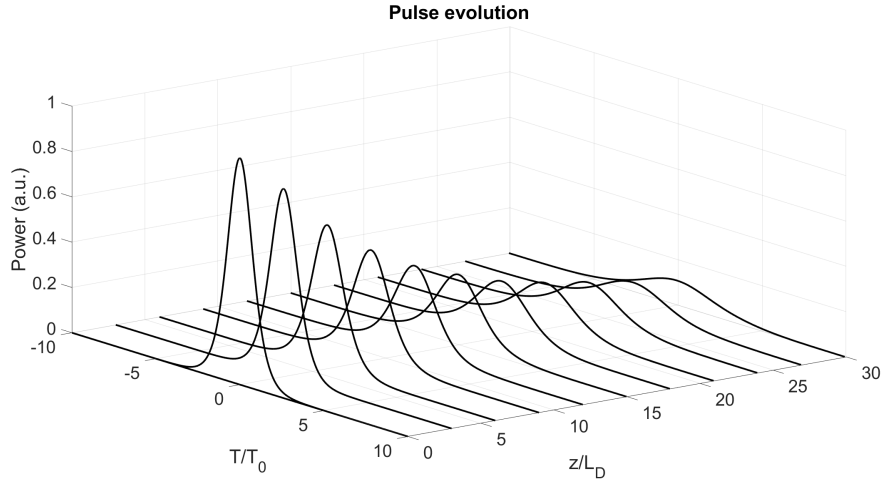
Since the simulations fit well the experimental results, we can use them, to obtain an effective length-dependent attenuation $\alpha_{\text{eff}}(z)$ that can be used to get the evolution of the pulse thanks to the toolbox SSPROP [99] that solves the NLSE. The best-fitting simulation is the one obtained for the 20 km fiber span and 223 mW of backward pumping, so we use that one to extract the effective attenuation and simulate the evolution of a pulse close to a first-order soliton, which can be guaranteed by adjusting the input power. This can be seen in figure 3.3.5, where a comparison between the unpumped and pumped cases is shown. This figure represents the evolution of a pulse like that of figure 3.3.4, with a hyperbolic secant shape and around 100 fs full at width half maximum (FWHM).



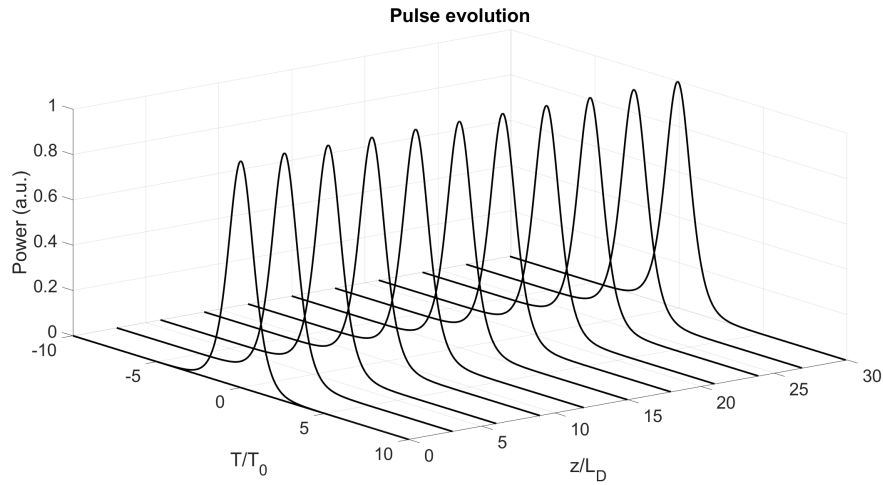
(a) Autocorrelation traces, showing the width of the pulses (around 100 fs)

(b) Optical spectrum (up) and broadened individual pulse (down) obtained after propagation showing the shape of the pulses

Figure 3.3.4: The autocorrelation traces in (a) show the width of the pulse is around 100 fs. The shape of the pulse is obtained by broadening and transforming the original output, so it can be viewed on an oscilloscope. Figures by courtesy of Inés Cáceres Pablo et al.



(a) Pulse evolution in the unpumped case



(b) Pulsed evolution in the pumped case

Figure 3.3.5: Pulse evolution comparison between the pumped and unpumped cases for the 20 km long fiber span

As we can observe, in figure 3.3.5, the effect of the right amount of pumping in the pulse propagation is outstanding. We can clearly see how the pulse maintains its shape perfectly during propagation when it is pumped, while it gradually decreases in amplitude (almost fades away) and increases in width when unpumped.

Although it could not be experimentally contrasted because of the limitations of the OTDR, I find it really illustrating to show the evolution of the signal (simulated) in different pumping situations. This way we can clearly see how the pumping affects the signal and why some pumping schemes might be better than others even if all of them end up compensating the overall losses. This is shown in figure 3.3.6

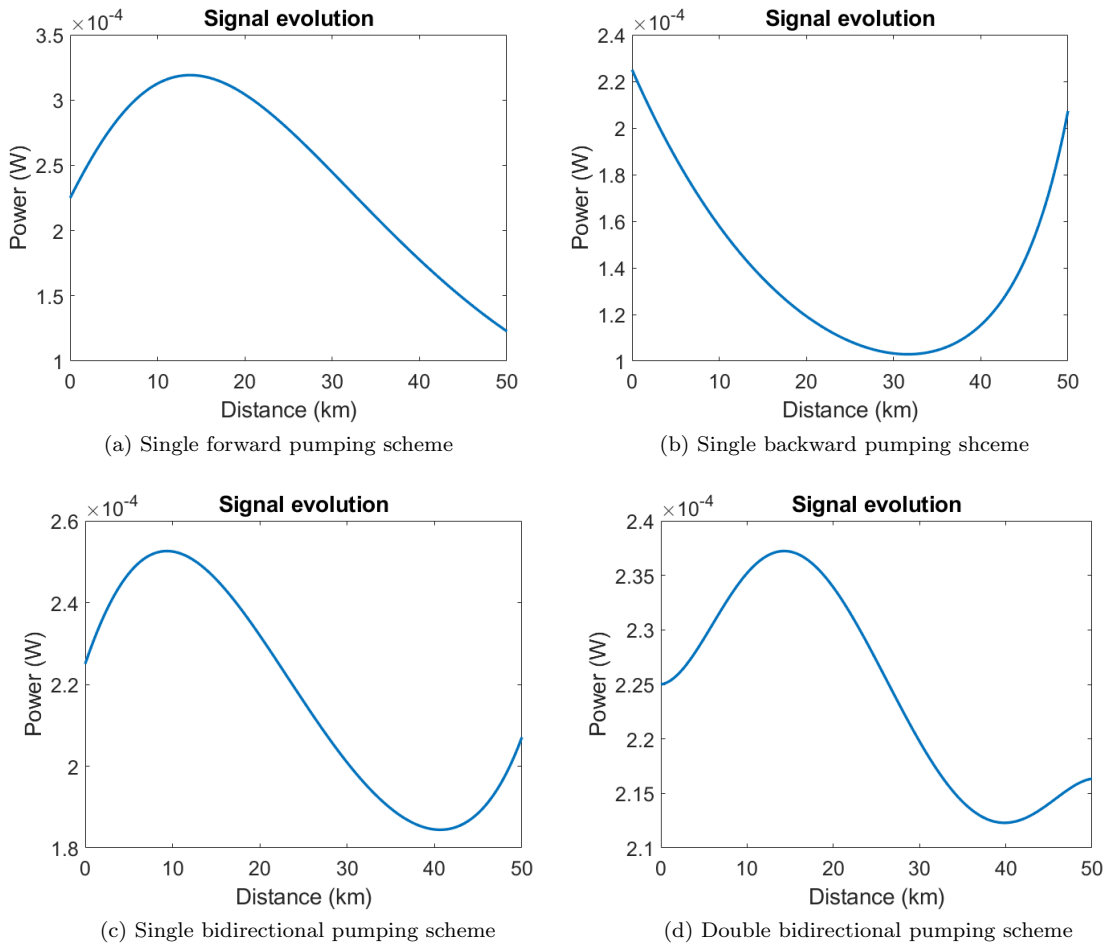


Figure 3.3.6: Signal evolution through 50 km fiber span for different pumping configurations. Pumping powers are not included because this is just for illustrative purposes

In the first row of figure 3.3.6, we can observe how the forward pump creates a gain at the beginning of the fiber that fades away with the distance, so the signal first rises quickly and then after about 15 km decays more slowly. On the other hand, the backward pump creates a gain more towards the end of the fiber so, in this case (up, right panel in fig. 3.3.6), the signal decays for around 30 km and then rises. In both cases the overall variation (max. - min.) is of roughly around 150 microwatts (about 67% of the input signal).

Looking at the second row of fig. 3.3.6 we can notice how the two behaviours described above come together to create a gain at the beginning and the end of the fiber. This way, the signal first increases due to the forward pump for around 10 km; then it decays slowly for around 30 km and from 40 km until the end, the signal increases again due to the backward pump. This is similar for both panels of the bottom row of fig. 3.3.6, but there is an important difference between these two graphs: the overall variation is of roughly $60 \mu\text{W}$ ($\sim 27\%$) for the primary bidirectional pumping scheme but just of about $25 \mu\text{W}$ ($\sim 11\%$) for the secondary bidirectional pumping scheme.

So, choosing between forward, backward or bidirectional pumping will let us select different types of gain curves. For example, imagine that we need to maintain the signal always below the input power. In that

case we would probably choose the primary backward configuration because although it does not provide a really flat signal, it keeps the power below the input power. If we did not have such limitation but instead we could not set a secondary pumping scheme, we would probably decide to use the primary bidirectional pumping scheme as it provides a smaller signal variation than forward or backward configurations. On the other hand, choosing between primary or secondary pumping will have an important effect on the variation of the signal. The use of Raman cascades (secondary pumping. See sections 3.1 and 2.5.4) will smooth out the gain curve a little, while primary pumping schemes present higher signal variations.

Naturally, as in every physical system, its parameters play an important role. The most important of these parameters can easily be modified from the UI. As an example, we have reproduced figure 3.3.6 (up, right) with three different values of the Raman gain and plotted the results in figure 3.3.7. The parameters that were used for all the simulations are listed in table 3.3.2

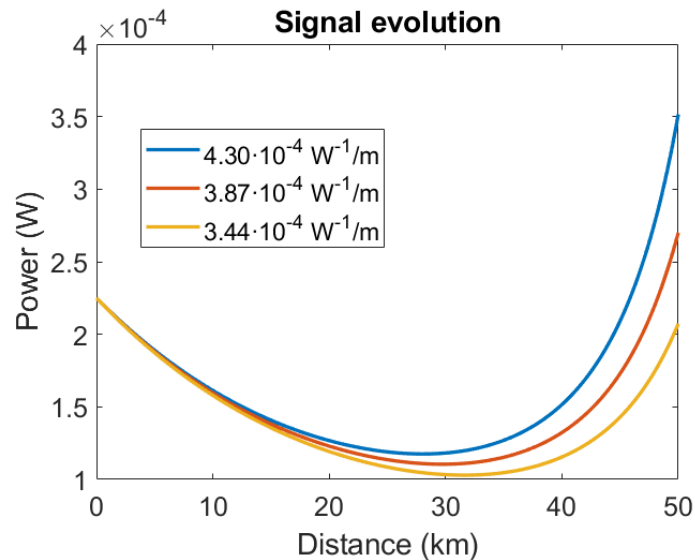


Figure 3.3.7: Comparison between simulations with three different Raman gain coefficients

Parameter	at 1366 nm	at 1455 nm	at 1550 nm
α ($10^{-5}m^{-1}$)	5.2	6.2	4.4
ϵ ($10^{-8}m^{-1}$)	10	6.0	4.3
g_R ($10^{-4}W^{-1}/m$)	5.3	3.4	—
$\Delta\lambda$ (nm)	8.0	8.0	10
Temperature (K)	298		

Table 3.3.2: Simulation parameters

The solution presented in [4], that can be seen in fig 3.2.4 is known to be optimum, because for such system, that is the configuration that provides the lowest power excursion (flattest signal gain curve), which is what they aim for. Since this is a known optimum solution, we decide to test the optimization feature of the UI with this configuration. In [4] the conclusion they reached was that, for the optimum solution, a secondary bidirectional symmetrical pumping of 849 mW at 1366 nm was needed to get a maximum signal variation of 3.08 dB with the parameters shown in table 3.3.3.

Parameter	at 1366 nm	at 1455 nm	at 1550 nm
α (dB/km)	0.38	0.27	0.19
ϵ (km^{-1})	$1.0 \cdot 10^{-4}$	$6.0 \cdot 10^{-5}$	$4.3 \cdot 10^{-5}$
g_R (W^{-1}/km)	0.53	0.43	—

Table 3.3.3: Simulation parameters used in [4]

We specify in the UI that the optimizer searches for the optimum solution near a starting point with the backward and forward pumps at 1366 nm equal to 0.8 W and the parameters shown in table 3.3.3. The optimizer finishes the simulation at an optimum point with a forward primary pump power of 846 mW and backward primary pump power of 852 mW which yields to a maximum signal variation of 3.09 dB.

As we can see, the agreement between the optimum parameters found by the program and those found experimentally by J.D. Ania and his team is very good, which leads us to think that the optimizer is also working properly. However, we also run a test with a starting point a little further from the optimum solution than the first test. This time, with the same configuration, we try a forward and backward pump power of 0.5 W at 1366 nm and the optimizer reaches an optimum solution with 0.170 W of power in the primary forward pump and 1.38 W of power in the primary backward pump, which leads to a 0.74% loss in the signal power and an overall variation of 8.99 dB. This does not mean that the program is not able to successfully find an optimum. What can be inferred from this result is that the space of solutions of the problem is, quite likely, rather “bumpy”, in the sense that it probably has multiple local minima. What minimum the optimizer arrives at will depend critically on the initial guess.

4 Conclusions

Throughout this work I have learnt about how light pulses propagate through optical fibers and the dispersive and nonlinear effects that arise from the interaction between this medium and the light. A system has been presented that is able to achieve lossless transmission with distributed amplification thanks to the Raman effect, therefore becoming a potentially suitable system for solitonic transmission and long-haul telecommunications in general. The equations that govern this system were implemented in a model that we want to be able to solve with different configurations and parameters.

To solve said model, we built a user interface that allows us to specify several characteristic parameters of the system such as length, attenuation and Raman gain coefficients, power of the pump, signal and noise, temperature, etc. The interface consists of two separate features: a simulator and an optimizer. The first one works based on the collocation method and its function is to solve the model given certain boundary conditions and an initial guess. The second one works based on the results of simulations at different points in the variable space and the Nelder-Mead algorithm and its function is to find the set of parameters (initial power values) near an initial guess that provide the flattest signal gain curve.

The results of the simulator appear to fit quite well the experimental measurements and were more accurate for the longer distances and the user interface makes it very comfortable to change parameters and run simulations to “play around” with the system as much as we want.

Although the results might not represent a breakthrough in the field, I believe that the goals that I defined for myself and this project have been fulfilled. All in all, I have learnt a lot about the physics of optical fibers and the interesting and numerous applications that the nonlinear and dispersive phenomena present in this kind of medium can have.

Furthermore, I have also learnt a lot about numerical methods in two fields that I believe will be extremely useful in a near future: simulation and optimization. The expertise I have acquired and the methods I have learnt in both of these areas of computing science seem very handy and interesting to me. Multivariate optimization, integration methods for simulations or machine learning techniques are a powerful resource that I have now added to my scientific toolbox.

5 Further research

The project J.D. Ania-Castañón and his team are developing is a system that will surely let us learn a lot about the formation and propagation of ultra-short pulses in optical fiber, which can find numerous applications in several fields. Not just in telecommunications, but rather in biomedical applications, optics or chemistry

Regarding the experimental part of this project, some further research could be done in the line of comparing simulated and experimental results and testing solitonic transmission. The idea would be to use an extended setup like that of figure 5.0.1 and observe the shape of the pulse at different points of the fiber span and compare them with the simulations.

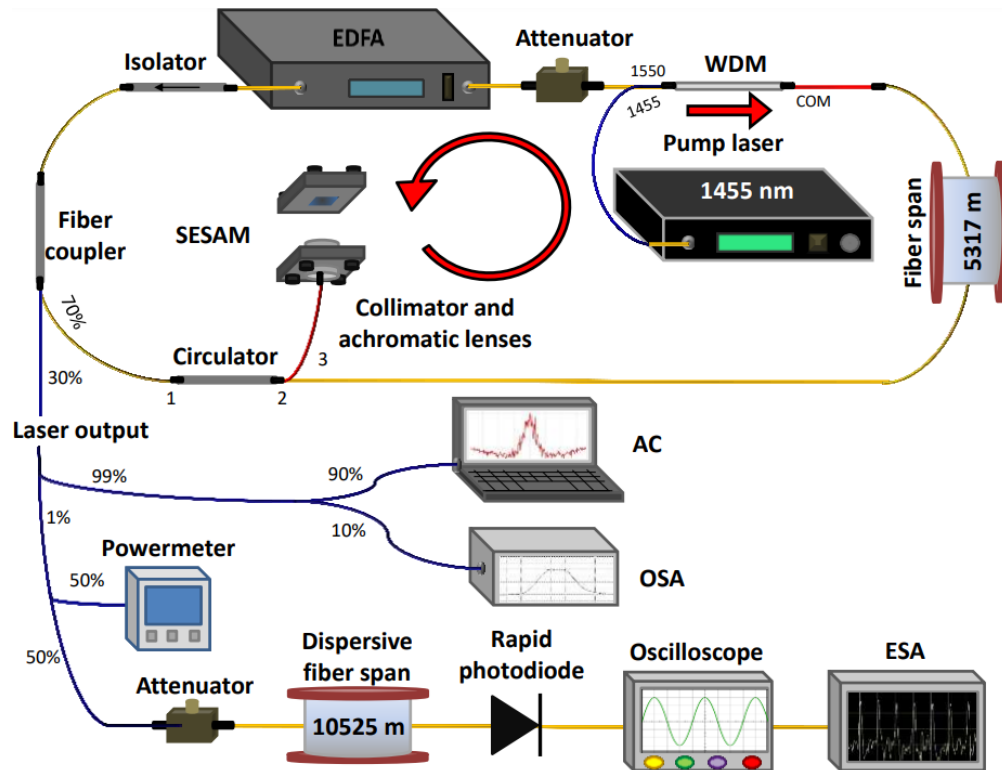


Figure 5.0.1: Extended setup to obtain measurements of pulse shape and compare them with simulations. The autocorrelator (AC) and optical spectrum analyser (OSA) are used to obtain the measurements of pulse shape and pulse spectrum respectively

As for my part in the project, I have been focused mainly on simulated, numerical results. I believe that the goal that I set for myself were successfully fulfilled, but still some aspects could be improved.

Regarding the simulation part of the UI, it could probably be sped up and made more efficient by changing the method used to integrate the system. Let us recall that in the physical problem, solutions that go through making any of the variables negative at any point should not exist. Because MATLAB®'s 'bvp4c' does not allow to specify such restriction (added to the boundary conditions), this was dealt with via running the simulation from a starting point and randomly adjusting said point until a non-negative solution was found. Of course, this is computationally rather expensive. So, the first thing that could be done to improve the UI a little, would be to code an algorithm that implements the collocation method but allows to specify the non-negative constraint in the variables. This could be implemented in two ways: using MATLAB®'s 'ode45' with the parameter 'nonnegative' or programming as well a RK routine that takes this limit into account.

That improvement on the simulator alone would boost the optimizer performance. But still a couple of adjustments could be made in this part of the UI as well. First of all, the optimizer uses the Nelder-Mead algorithm. This is a safe, easy-to-implement algorithm, but it is not known for its efficiency. In fact, many other multivariate optimization methods will outperform the Nelder-Mead algorithm in almost every scenario. This algorithm was chosen because of robustness and simplicity, not because of its speed. So, naturally the first thing that could be done to improve the UI would be to change the optimizer method to some of the others that were mentioned in section 3.2.3.

Lastly, but probably most interestingly, I believe that the performance of the program could be extremely improved with some machine learning techniques. Specifically, using a neural network. Neural networks (NN) are really in vogue these days in many fields of science and technology or even finances [100–103].

Neural networks are a type of machine learning technique inspired by animals' brains (hence the name) proposed around the 1940's by McCulloch and Pitts [104]. They consist of a series of nodes or neurons that can pass a signal from the input to the output. The neurons are layered from the first (input layer) to the last (output layer) with as many hidden layers in between as the user wants. Each neuron is characterised by an activation function (although this can be the same for all the neurons) and a weight. The activation function is usually a sigmoid or an arctangent and is used mainly to keep the data restricted and normalized. The weights are actually the most important part of the NN as it learns through them. The first thing one has to do with a NN is train it, and this is done by supplying inputs whose outputs are known to the NN. Then, the error between the real output and the NN's output is used to adjust the weights of each neuron. For clarity, the output of the NN would look like equation 5.0.1, and a scheme is shown in figure 5.0.2

$$y = \sigma(Wx + b) \tag{5.0.1}$$

Where y is the output; x , the input; W , the weight; σ , the activation function; and b , a bias to fit better inputs and outputs.

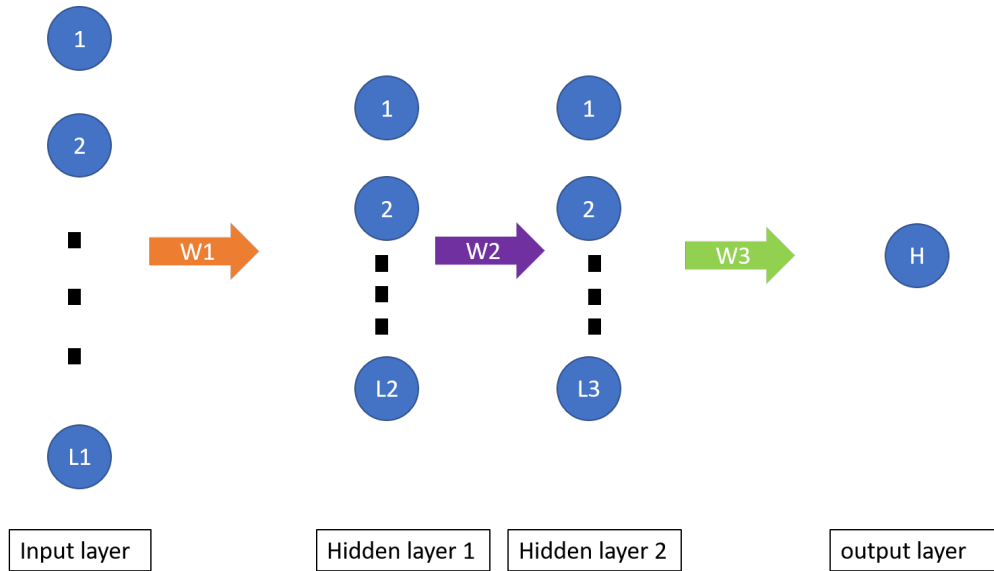


Figure 5.0.2: Neural network scheme. A NN with two hidden layers is presented here. Input is passed onto hidden layer 1 through the first set of weights. Then, from hidden layer 1 to hidden layer 2 by the second set of weights. And finally, to the output through the last set of weights.

So implementing a neural network would bring one main advantage. Once the NN is trained (with the simulator), it can substitute the simulator itself. Neural networks are, in general, far faster than any integrator because they reduce any problem to a series of products between input variables and weight matrices. Of course, training the NN will depend on the cavity configuration, but if, the simulator is fast enough, it should not take much time to run, for example, around a hundred simulations to train the NN.

Finally, one last thing that could be done is to use automatic differentiation [105, 106]. Automatic differentiation is a relatively novel differentiation method that is easier to implement and faster than symbolic differentiation and, at the same time, more accurate than numerical differentiation. For these reasons, its use has been increasing in the past few years, specially in the field of machine learning. Its working principle is relatively simple: it uses the chain rule to compute at the same time the evaluation of a function and its derivative. Of course, its implementation is more complex than that and if the reader is interested, I highly recommend having a look at reference [106], where further details of the method and how to implement it specifically in Matlab can be found. Apart from the previously mentioned advantages, another one is that it can be used to find the derivatives of a function when it has been implemented by a NN. Being able to calculate the derivative rapidly facilitates the implementation of other optimization methods that need the evaluation of the function and its derivative (unlike the Nelder-Mead method, that only requires the value of the function) and are more efficient and accurate than the Nelder-Mead algorithm.

Seeing the improvements that can still be made and the applications and research lines that might come out of this setup makes me believe that this ring fiber laser scheme holds a great potential and applicability and will be tremendously useful in a near future.

Appendix A: User Interface guide

When the program is run a window like that of figure 5.0.3 appears. This is the optimization window. By clicking on the right tab in the upper left corner, labeled with 'simulation', we can access the simulation window. We can switch from optimization mode to simulation mode by clicking on the corresponding tabs (see fig. 5.0.4)

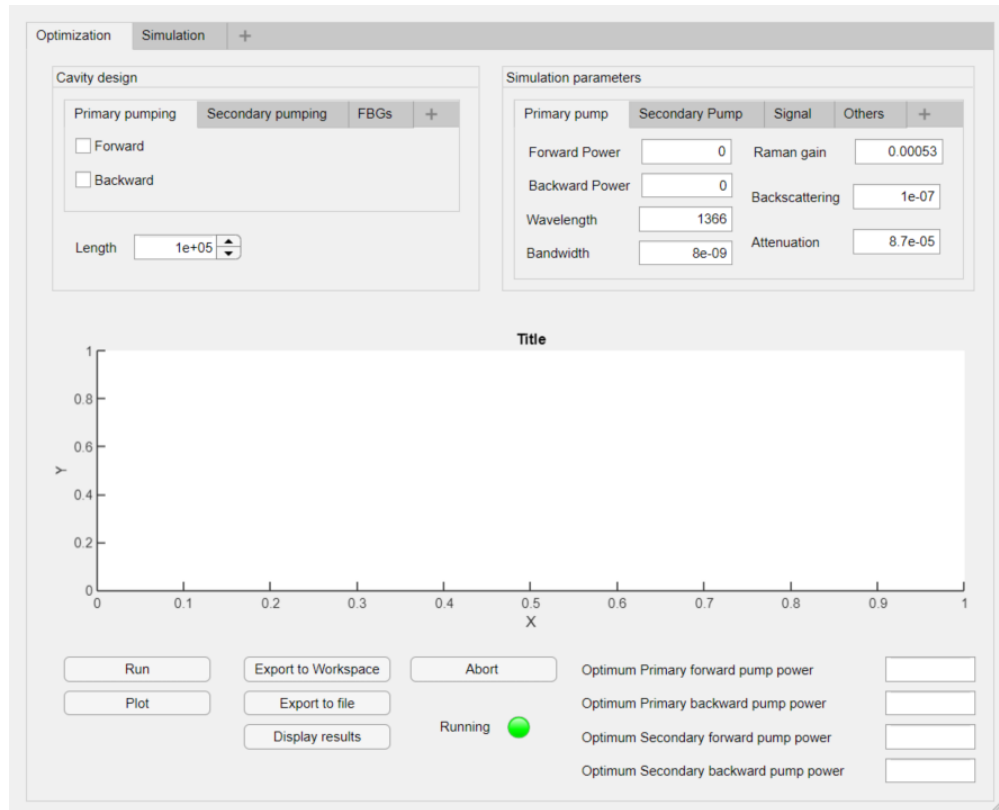


Figure 5.0.3: Initial window of the UI

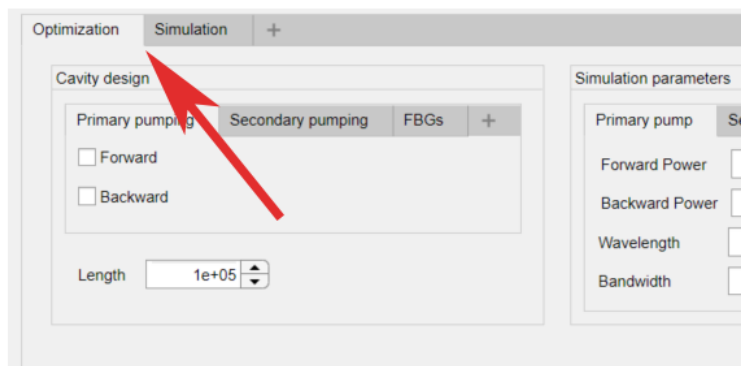


Figure 5.0.4: Simulation and optimization tabs in the UI

Optimization tab

In the optimization tab we can use the frame in the left of the UI to select the cavity design (fig 5.0.5). That is, we should specify if our system uses primary or secondary pumping mode. We can specify this by ticking the different boxes in this window. We can switch from tab to tab in this window to change the ‘Primary pumping’, ‘Secondary pumping’ and ‘FBGs’ configurations. In this last tab, we can select whether or not our system has FBGs and where they are (at the beginning and/or at the end). Lastly, in the bottom left corner of the ‘Cavity design’ frame, we can specify the length of the fiber span.

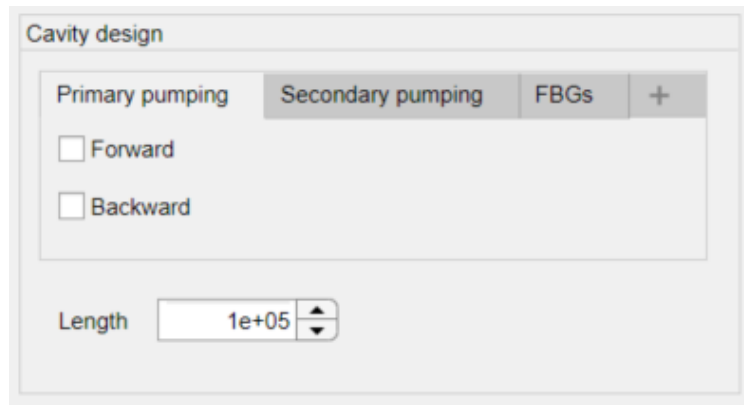


Figure 5.0.5: ‘Cavity design’ window in UI. Here we can see the ‘Cavity design’ tab from the UI, where we can specify the pumping mode, the position of FBGs and the length

Note that as long as there are two wavelengths apart from the signal it is a secondary pumping scheme, even if we choose to give the primary or secondary pump an initial value of zero. So, only if one is operating with just one pump wavelength should the ‘secondary pumping’ boxes be left unticked.

Once the pumping configuration is set, we can move to the ‘Simulation parameters’ tab (fig. 5.0.6). There we can modify the parameters of the simulation and adjust them to our system. Under the ‘Primary pump’ and ‘Secondary pump’ tabs, we can find the forward and backward powers; the wavelength; the bandwidth and the Raman, backscattering and attenuation coefficients for each of the pumps. In the ‘Signal’ tab, we can modify the power of the input signal, its wavelength and its bandwidth as well as its backscattering and attenuation coefficients. And in the ‘Others tab’, we can modify the initial Noise, temperature and tolerance and the reflectances and bandwidth of the FBGs.

On the bottom left corner of the optimization window, we can see a series of buttons (see fig. 5.0.7a) with which we can operate the interface. The ‘Run’ button gets the optimization started. Once it has finished, we can use the ‘Plot’ button to print a graph of the results in the central figure. The ‘Export to workspace’ and ‘Export to file’ buttons will respectively generate the corresponding variables in your MATLAB[®] workspace or a text file. The ‘Display results’ button will show the values of primary and secondary forward and backward pumping in the empty fields on the bottom right corner (see fig. 5.0.7b). Finally, the ‘Abort’ button will stop the simulation. We can use this if we have made a mistake when introducing the parameters for example or if it is taking too long. Right below the ‘Abort’ button, there is a light labeled ‘Running’. It is green when the UI is opened and turns red when the optimization is running. Then, when the optimization is finished, it turns green again to let the user know the work is done and results can now be plotted and displayed. If the abort button is pushed, the light will turn orange

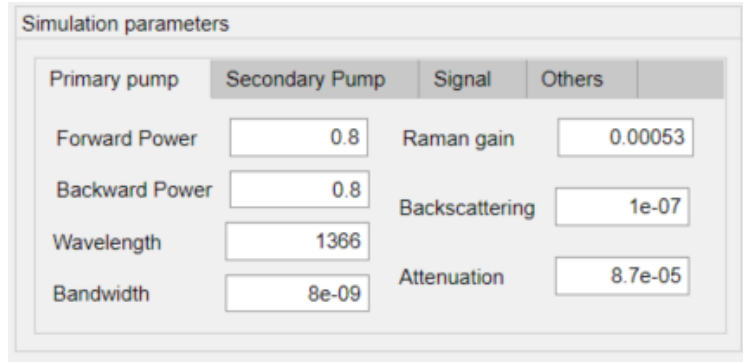
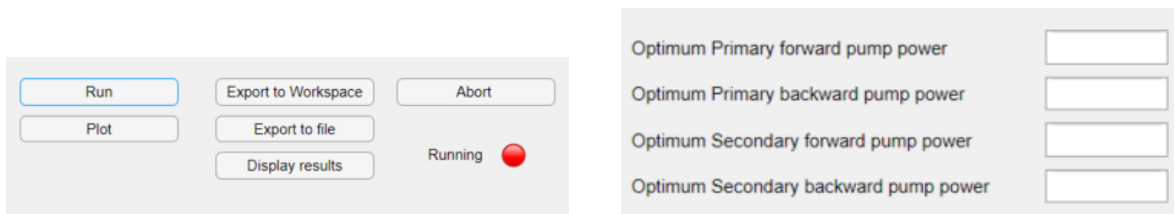


Figure 5.0.6: ‘Simulation parameters’ window in UI. Here we can see modify different parameters from the primary pump, secondary pump and signal.



(a) Buttons to get the interface running, get results, etc

(b) Fields where results appear after the ‘Display results’ button is clicked

Figure 5.0.7: Operating the interface: buttons and results management

Simulation tab

The simulation tab (fig. 5.0.8) is very similar to the optimization tab. It has a main tab where we can modify the same things we could change in the optimization tab (see fig. 5.0.9). Under this box, we can find the buttons to run the simulation and export results (fig. 5.0.10). The ‘Save’ button at the right, exports the results to a text file. The rest of the buttons have the same functions as in the ‘Optimization’ tab.

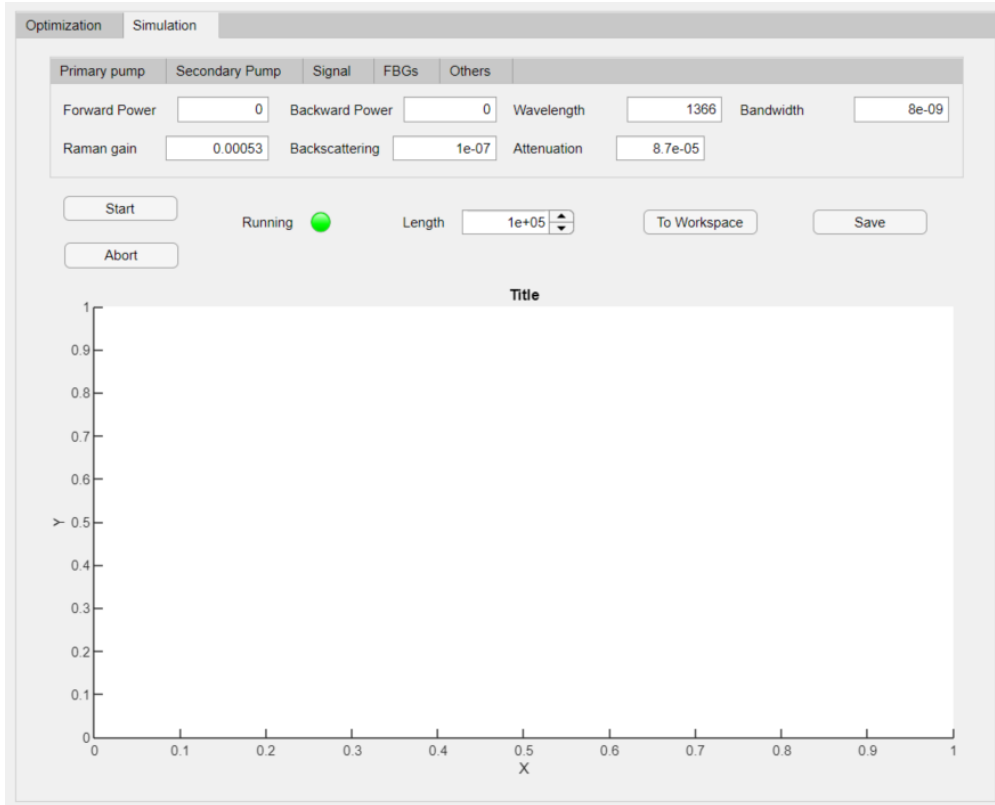


Figure 5.0.8: ‘Simulation’ tab in the simulator feature of the UI. Here we can specify the parameters that we are using in the laboratory and run a simulation



Figure 5.0.9: ‘Simulation parameters’ tab in the simulator feature of the UI. As in the ‘Optimization’ tab, here we can modify all the relevant parameters of the simulation



Figure 5.0.10: Buttons to operate the UI in the ‘Simulation’ tab. They are fundamentally the same as in the ‘Optimization’ tab.

Results and what to expect from the program

The results that are output to a text file or the workspace are an array named 'results' and two arrays named 'z' and 'x'. The components in 'results' are: primary forward pump power, primary backward pump power, secondary forward pump power, secondary backward pump power, percentage of error in the signal output power with respect to the input, forward propagating noise at the beginning and backward propagating noise at the end. The two arrays labeled 'z' and 'x' generated hold the data of distance and power at every distance step of the seven variables that appear in the model. These same arrays are the ones that the 'To Workspace' and 'To file' buttons generate in the 'Optimization' tab. The only difference between the two modes is the 'Display results' feature

When we run either the simulator or the optimizer, the first thing that appears on the workspace is a statement saying 'caseis = ' and a number under it. This is left there on purpose to let the user know what case (configuration) is being used. The legend for the cases is the following:

- Case 1: No pumping
- Case 2: Primary backward pumping
- Case 3: Secondary backward pumping
- Case 4: Primary forward pumping
- Case 5: Secondary forward pumping
- Case 6: Primary bidirectional pumping
- Case 7: Secondary backward, primary forward pumping
- Case 8: Secondary forward, primary backward pumping
- Case 9: Secondary bidirectional pumping

After this message, when using the simulator, it should not take long until the light turns green in the UI. However, a progress bar has been included that lets the user know when 10%, 20%, etc of the maximum iterations have been reached. There is a chance that a singular Jacobian is found during the simulation. If that is the case, a message will be printed saying 'Singular Jacobian found' and the simulation process will stop. If this happens, the user should try again with slightly different parameters. If after the maximum number of iterations have been reached, the simulator has not gotten to a satisfactory solution, an error will be thrown saying 'Convergence could not be reached'. This is an unlikely case, but if it happened, the recommendation is to slightly change the power values.

In the case of the optimizer, it is a little different. After the message stating the case is printed, the optimizer will print the simplex at some points and alert whether or not it meets the termination and divergence criteria. Also, during the iterative process it will most likely print a lot of warning messages on orange saying that tolerance could not be met or a singular Jacobian has been found. These warnings can be ignored.

Appendix B: The code

Because my main goal was to build a robust, versatile and user-friendly code and it is, indeed what has taken most of the hours of work, I think it should be included here, so the reader can see how everything I

have talked about has been implemented and even change it at will to suit another application or improve its performance. Because the code is implemented in an UI, it is divided in ‘Callbacks’ and ‘Functions’. Callbacks are lines of code that are executed when the user clicks a certain button. For instance, when the user clicks the buttons ‘Start’ or ‘Run’ in the simulation and optimization tabs respectively, the lines in the corresponding callback are executed. The ‘Functions’ are pieces of code that might be invoked during the callback execution.

Dividing the code this way keeps things much cleaner and easier to modify if needed and, in fact, it is good practice to avoid long functions in the code and use instead smaller subfunctions that can be called from the main function.

Because the code ends up being rather large and has lines that can not be broken up in two or more, it is not explicitly included in this document. Rather than that, to keep things neat and clean, a link to a Github repository is included right bellow and in reference [107]

<https://github.com/FernandoSolisFernandez/Lossless-transmission-system-simulator-optimizer/blob/main/User%20Interface%20code>

References

- [1] Hal Hellman. *Lasers*. Tech. rep. US Atomic Energy Commission (AEC), 1968.
- [2] K Charles Kao and George A Hockham. “Dielectric-fibre surface waveguides for optical frequencies”. In: *Proceedings of the Institution of Electrical Engineers*. Vol. 113. 7. IET. 1966, pp. 1151–1158.
- [3] Govind P Agrawal. *Fiber-optic communication systems*. Vol. 222. John Wiley & Sons, 2012.
- [4] Juan Diego Ania-Castañón. “Quasi-lossless transmission using second-order Raman amplification and fibre Bragg gratings”. In: *Optics Express* 12.19 (2004), pp. 4372–4377.
- [5] Anthony E. Siegman. *Lasers*. Stanford University Science Books, 1986.
- [6] Valerii Ter-Mikirtychev. *Fundamentals of fiber lasers and fiber amplifiers*. Springer, 2019.
- [7] Tetsuo Sakka, Kotaro Saito, and Yukio H Ogata. “Laser Ablation Processing of Solid Surfaces Immersed in Water”. In: *Novel Materials Processing by Advanced Electromagnetic Energy Sources: Proceedings of the International Symposium on Novel Materials Processing by Advanced Electromagnetic Energy Sources (MAPEES’04)*. Elsevier. 2005, p. 209.
- [8] Kenneth L. Busch. “Mass Spectrometry”. In: *Encyclopedia of Physical Science and Technology (Third Edition)*. Ed. by Robert A. Meyers. Third Edition. New York: Academic Press, 2003, pp. 145–158.
- [9] M. Bellini. “Harmonic Generation Frequency Conversion”. In: *Encyclopedia of Condensed Matter Physics*. Ed. by Franco Bassani, Gerald L. Liedl, and Peter Wyder. Oxford: Elsevier, 2005, pp. 303–311.
- [10] Chia Wei Hsu et al. “Observation of trapped light within the radiation continuum”. In: *Nature* 499.7457 (2013), pp. 188–191.
- [11] Pei-Lin Hsiung et al. “Optical coherence tomography using a continuous-wave, high-power, Raman continuum light source”. In: *Optics express* 12.22 (2004), pp. 5287–5295.
- [12] Bin Xu et al. “Research on Infrared Laser Leak Detection for Natural Gas Pipeline”. In: *International Pipeline Conference*. Vol. 45127. American Society of Mechanical Engineers. 2012, pp. 711–715.
- [13] EU Rafailov and E Avrutin. “Ultrafast pulse generation by semiconductor lasers”. In: *Semiconductor lasers*. Elsevier, 2013, pp. 149–217.
- [14] OE Martinez, RL Fork, and James P Gordon. “Theory of passively mode-locked lasers including self-phase modulation and group-velocity dispersion”. In: *Optics letters* 9.5 (1984), pp. 156–158.
- [15] Michael G. Littman and Xiao Wang. “Pulsed Lasers”. In: *Atomic, Molecular, and Optical Physics: Electromagnetic Radiation*. Ed. by F.B. Dunning and Randall G. Hulet. Academic Press, 1997, pp. 137–169.
- [16] Eugene Hecht. *Optics*. 5th ed. Pearson, 2017.
- [17] Oleksiy Shulika and Igor Sukhoivanov. *Advanced lasers: Laser physics and technology for applied and fundamental science*. Vol. 193. Springer, 2015.
- [18] John Crisp and Barry Elliott. “What makes the light stay in the fiber?” In: *Introduction to Fiber Optics (Third Edition)*. Ed. by John Crisp and Barry Elliott. Third Edition. Oxford: Newnes, 2005, pp. 10–17.
- [19] ddp13fiberoptics. *Fiber optic cable propagation mode*. Last accessed 3 March 2021. 1999. URL: <https://ddp13fiberoptics.wordpress.com/fiber-optic-cable/propagation-mode/>.
- [20] J. Hecht. *Understanding Fiber Optics*. Laser Light Press, 2015.
- [21] Rongqing Hui. *Introduction to fiber-optic communications*. Academic Press, 2019.
- [22] RH Stolen. “Fiber raman lasers”. In: *Fiber and Integrated Optics*. Springer, 1979, pp. 157–182.

- [23] Jong Chow et al. “Multiwavelength generation in an erbium-doped fiber laser using in-fiber comb filters”. In: *IEEE Photonics Technology Letters* 8.1 (1996), pp. 60–62.
- [24] SV Chernikov et al. “Supercontinuum self-Q-switched ytterbium fiber laser”. In: *Optics letters* 22.5 (1997), pp. 298–300.
- [25] Charles J Koester and Elias Snitzer. “Amplification in a fiber laser”. In: *Applied optics* 3.10 (1964), pp. 1182–1186.
- [26] ddp13fiberoptics. *Ring Resonators*. Last accessed 24 April 2021. 2019. URL: https://www.rp-photonics.com/ring_resonators.html.
- [27] Govind P. Agrawal. *Nonlinear fiber optics*. 6th ed. Elsevier Inc., 2019.
- [28] Joseph C Kolecki. *An introduction to tensors for students of physics and engineering*. National Aeronautics and Space Administration, Glenn Research Center, 2002.
- [29] Pavel Grinfeld. *Introduction to tensor analysis and the calculus of moving surfaces*. Springer, 2013.
- [30] Gerd Keiser. “Optical fiber communications”. In: Wiley Online Library, 2003.
- [31] Dietrich Marcuse. *Theory of dielectric optical waveguides*. Elsevier, 2013.
- [32] Allan W Snyder and John Love. *Optical waveguide theory*. Springer Science & Business Media, 2012.
- [33] John A Buck. “Fundamentals of optical fibers”. In: 50 (2004).
- [34] Bing Li and G Jogesh Babu. “Convolution Theorem and Asymptotic Efficiency”. In: *A Graduate Course on Statistical Inference*. Springer, 2019, pp. 295–327.
- [35] Jonathan M. Blackledge. “Chapter 2 - 2D Fourier Theory”. In: *Digital Image Processing*. Ed. by Jonathan M. Blackledge. Woodhead Publishing, 2005, pp. 30–49.
- [36] Svetlana A Malinovskaya, Tom Collins, and Vishesh Patel. “Ultrafast manipulation of Raman transitions and prevention of decoherence using chirped pulses and optical frequency combs”. In: *Advances in Quantum Chemistry* 64 (2012), pp. 211–258.
- [37] Halina Abramczyk. “Pulse Amplification”. In: *Introduction to Laser Spectroscopy*. Ed. by Halina Abramczyk. Amsterdam: Elsevier Science, 2005, pp. 147–160.
- [38] A. S. Weling et al. “Generation of tunable narrow-band THz radiation from large aperture photoconducting antennas”. In: *Applied Physics Letters* 64.2 (1994), pp. 137–139.
- [39] P Maine et al. “Generation of ultrahigh peak power pulses by chirped pulse amplification”. In: *IEEE Journal of Quantum electronics* 24.2 (1988), pp. 398–403.
- [40] Karen Marie Hilligsøe et al. “Supercontinuum generation in a photonic crystal fiber with two zero dispersion wavelengths”. In: *Optics Express* 12.6 (2004), pp. 1045–1054.
- [41] Stuart May, Matteo Clerici, and Marc Sorel. “Supercontinuum generation in dispersion engineered AlGaAs-on-insulator waveguides”. In: *Scientific Reports* 11.1 (2021), pp. 1–7.
- [42] Hideyuki Sotobayashi et al. “Supercontinuum generation and its applications”. In: *Active and Passive Optical Components for WDM Communications V*. Vol. 6014. International Society for Optics and Photonics. 2005, 60140T.
- [43] C Dunsby and PMW French. “Biophotonics applications of supercontinuum generation”. In: *Supercontinuum Generation in Optical Fibers* (2010), pp. 349–372.
- [44] Alexis Labruyère et al. “Compact supercontinuum sources and their biomedical applications”. In: *Optical Fiber Technology* 18.5 (2012), pp. 375–378.
- [45] Adrian Podoleanu et al. “Supercontinuum applications in high resolution non invasive optical imaging”. In: *CLEO: Applications and Technology*. Optical Society of America. 2018, AW3S–1.
- [46] SV Smirnov et al. “Supercontinuum in telecom applications”. In: *The Supercontinuum Laser Source*. Springer, 2016, pp. 371–403.

- [47] JP Gordon and H Kogelnik. “PMD fundamentals: Polarization mode dispersion in optical fibers”. In: *Proceedings of the National Academy of Sciences* 97.9 (2000), pp. 4541–4550.
- [48] Andrea Galtarossa and Curtis R Menyuk. *Polarization mode dispersion*. Vol. 1. Springer Science & Business Media, 2006.
- [49] Miguel Gonzalez-Herraez and Thibaut Sylvestre. “Nonlinear Effects in Optical Fibers”. In: *Photonic Crystal Fibers*. Ed. by Luc Thevenaz. EPFL Press, 2011, pp. 145–170. ISBN: 978-1-4398-3517-3.
- [50] Alex McMillan et al. “Wave mixing in single-mode optical fibers”. In: *Experimental Methods in the Physical Sciences*. Vol. 45. Elsevier, 2013, pp. 411–465.
- [51] A. Podoleanu. “Optical sources for optical coherence tomography (OCT)”. In: *Lasers for Medical Applications*. Ed. by Helena Jelínková. Woodhead Publishing, 2013, pp. 253–285.
- [52] R Caro and M Gower. “Phase conjugation by degenerate four-wave mixing in absorbing media”. In: *IEEE Journal of Quantum Electronics* 18.9 (1982), pp. 1376–1380.
- [53] Osamu Aso, Masateru Tadakuma, and Shu Namiki. “Four-wave mixing in optical fibers and its applications”. In: *dEp* 1 (1999), p. 2.
- [54] Noor Umami Hazirah Hani Zalkepali et al. “Generation of Four-Wave Mixing in a Highly Non-Linear Optical Fiber Using a Tunable Dual Wavelength Fiber Laser Source”. In: *Journal of Science and Technology* 10.2 (2018).
- [55] Chandrasekhara Venkata Raman. “A new radiation”. In: *Indian Journal of physics* 2 (1928), pp. 387–398.
- [56] Roger H Stolen, Clinton Lee, and R_K Jain. “Development of the stimulated Raman spectrum in single-mode silica fibers”. In: *JOSA B* 1.4 (1984), pp. 652–657.
- [57] Wesley R Browne and John J McGarvey. “The Raman effect and its application to electronic spectroscopies in metal-centered species: Techniques and investigations in ground and excited states”. In: *Coordination Chemistry Reviews* 251.3-4 (2007), pp. 454–473.
- [58] Ruchita S Das and YK Agrawal. “Raman spectroscopy: recent advancements, techniques and applications”. In: *Vibrational spectroscopy* 57.2 (2011), pp. 163–176.
- [59] Qiang Tu and Chang Chang. “Diagnostic applications of Raman spectroscopy”. In: *Nanomedicine: Nanotechnology, Biology and Medicine* 8.5 (2012), pp. 545–558.
- [60] Thomas W Bocklitz et al. “Raman based molecular imaging and analytics: a magic bullet for biomedical applications!?” In: *Analytical Chemistry* 88.1 (2016), pp. 133–151.
- [61] Mengjie Yu et al. “Raman lasing and soliton mode-locking in lithium niobate microresonators”. In: *Light: Science & Applications* 9.1 (2020), pp. 1–7.
- [62] Eric J Heller, Robert Sundberg, and David Tannor. “Simple aspects of Raman scattering”. In: *The Journal of Physical Chemistry* 86.10 (1982), pp. 1822–1833.
- [63] Johannes Arnoldus Koningstein. *Introduction to the Theory of the Raman Effect*. Springer Science & Business Media, 2012.
- [64] No Bloembergen. “The stimulated Raman effect”. In: *American Journal of Physics* 35.11 (1967), pp. 989–1023.
- [65] John Scott Russell. *Report on Waves: Made to the Meetings of the British Association in 1842-43*. 1845.
- [66] Philippe Emplit et al. “Picosecond steps and dark pulses through nonlinear single mode fibers”. In: *Optics communications* 62.6 (1987), pp. 374–379.
- [67] Akira Hasegawa and Frederick Tappert. “Transmission of stationary nonlinear optical pulses in dispersive dielectric fibers. I. Anomalous dispersion”. In: *Applied Physics Letters* 23.3 (1973), pp. 142–144.

- [68] S Novikov et al. *Theory of solitons: the inverse scattering method*. Springer Science & Business Media, 1984.
- [69] Mark J Ablowitz et al. *Solitons, nonlinear evolution equations and inverse scattering*. Vol. 149. Cambridge university press, 1991.
- [70] Lokenath Debnath. “A brief historical introduction to solitons and the inverse scattering transform—a vision of Scott Russell”. In: *International Journal of Mathematical Education in Science and Technology* 38.8 (2007), pp. 1003–1028.
- [71] Miki Wadati. “Introduction to solitons”. In: *Pramana* 57.5 (2001), pp. 841–847.
- [72] Yuri S Kivshar and Govind P Agrawal. *Optical solitons: from fibers to photonic crystals*. Academic press, 2003.
- [73] Akira Hasegawa. “Optical solitons in fibers”. In: *Optical solitons in fibers*. Springer, 1989, pp. 1–74.
- [74] Yuri S Kivshar and Barry Luther-Davies. “Dark optical solitons: physics and applications”. In: *Physics reports* 298.2-3 (1998), pp. 81–197.
- [75] Linn F Mollenauer and James P Gordon. *Solitons in optical fibers: fundamentals and applications*. Elsevier, 2006.
- [76] David S Ricketts and Donhee Ham. *Electrical solitons: theory, design, and applications*. CRC Press, 2018.
- [77] Arnold Markovich Kosevich, BA Ivanov, and AS Kovalev. “Magnetic solitons”. In: *Physics Reports* 194.3-4 (1990), pp. 117–238.
- [78] Xin-Hong Jia et al. “Towards fully distributed amplification and high-performance long-range distributed sensing based on random fiber laser”. In: *OFS2012 22nd International Conference on Optical Fiber Sensors*. Vol. 8421. International Society for Optics and Photonics. 2012, p. 842127.
- [79] Zinan Wang et al. “175km phase-sensitive OTDR with hybrid distributed amplification”. In: *23rd international conference on optical fibre sensors*. Vol. 9157. International Society for Optics and Photonics. 2014, p. 9157D5.
- [80] Mercedes Alcón-Camas and Juan Diego Ania-Castañón. “RIN transfer in 2nd-order distributed amplification with ultralong fiber lasers”. In: *Optics Express* 18.23 (2010), pp. 23569–23575.
- [81] ZN Wang et al. “Ultra-long phase-sensitive OTDR with hybrid distributed amplification”. In: *Optics letters* 39.20 (2014), pp. 5866–5869.
- [82] Francesca Gallazzi. “Ultralong continuous wave and ultrafast fibre lasers at telecommunication wavelengths”. PhD thesis. Universidad de Alcalá, 2020.
- [83] Juan Diego Ania-Castañón and SK Turitsyn. “Noise and gain optimisation in bi-directionally pumped dispersion compensating amplifier modules”. In: *Optics communications* 224.1-3 (2003), pp. 107–111.
- [84] William H Press et al. *Numerical recipes 3rd edition: The art of scientific computing*. Cambridge university press, 2007.
- [85] P. DeVries, P.L. DeVries, and J. Hasbun. *A First Course in Computational Physics*. Jones & Bartlett Learning, 2011.
- [86] RD Russell and Lawrence F Shampine. “A collocation method for boundary value problems”. In: *Numerische Mathematik* 19.1 (1972), pp. 1–28.
- [87] Tsung Yen Na. *Computational methods in engineering boundary value problems*. Academic press, 1980.
- [88] Christian Grossmann, Hans-Görg Roos, and Martin Stynes. *Numerical treatment of partial differential equations*. Vol. 154. Springer, 2007.
- [89] Arieh Iserles. “Finite difference schemes”. In: *A First Course in the Numerical Analysis of Differential Equations*. 2nd ed. Cambridge University Press, 2008, pp. 139–170.

- [90] John A Nelder and Roger Mead. “A simplex method for function minimization”. In: *The computer journal* 7.4 (1965), pp. 308–313.
- [91] G.R. Liu and S.S. Quek. “Modeling Techniques”. In: *The Finite Element Method (Second Edition)*. Ed. by G.R. Liu and S.S. Quek. Second Edition. Oxford: Butterworth-Heinemann, 2014, pp. 301–345.
- [92] Jeffrey C Lagarias et al. “Convergence properties of the Nelder–Mead simplex method in low dimensions”. In: *SIAM Journal on optimization* 9.1 (1998), pp. 112–147.
- [93] Marco A Luersen and Rodolphe Le Riche. “Globalized Nelder–Mead method for engineering optimization”. In: *Computers & structures* 82.23-26 (2004), pp. 2251–2260.
- [94] Christopher John Price, Ian D Coope, and David Byatt. “A convergent variant of the Nelder–Mead algorithm”. In: *Journal of optimization theory and applications* 113.1 (2002), pp. 5–19.
- [95] John E Dennis Jr and Daniel J Woods. *Optimization on microcomputers. the nelder-mead simplex algorithm*. Tech. rep. 1985.
- [96] Lixing Han and Michael Neumann. “Effect of dimensionality on the Nelder–Mead simplex method”. In: *Optimization Methods and Software* 21.1 (2006), pp. 1–16.
- [97] Fuchang Gao and Lixing Han. “Implementing the Nelder-Mead simplex algorithm with adaptive parameters”. In: *Computational Optimization and Applications* 51.1 (2012), pp. 259–277.
- [98] Stanford University. *Ring Resonators*. Last accessed 02 May 2021. 2019. URL: <https://web.stanford.edu/group/sisl/k12/optimization/M0-unit5-pdfs/5.6penaltyfunctions.pdf>.
- [99] Ross Pleban et al. *SSPROP Matlab toolbox*. Last accessed 08 May 2021. URL: <https://photonics.umd.edu/software/ssprop/>.
- [100] AS Miller, BH Blott, et al. “Review of neural network applications in medical imaging and signal processing”. In: *Medical and Biological Engineering and Computing* 30.5 (1992), pp. 449–464.
- [101] Ido Seginer. “Some artificial neural network applications to greenhouse environmental control”. In: *Computers and Electronics in Agriculture* 18.2-3 (1997), pp. 167–186.
- [102] FAN Fernandes and LMF Lona. “Neural network applications in polymerization processes”. In: *Brazilian Journal of Chemical Engineering* 22.3 (2005), pp. 401–418.
- [103] Bo K Wong and Yakup Selvi. “Neural network applications in finance: A review and analysis of literature (1990–1996)”. In: *Information & Management* 34.3 (1998), pp. 129–139.
- [104] Warren S McCulloch and Walter Pitts. “A logical calculus of the ideas immanent in nervous activity”. In: *The bulletin of mathematical biophysics* 5.4 (1943), pp. 115–133.
- [105] Atilim Gunes Baydin et al. “Automatic differentiation in machine learning: a survey”. In: *Journal of machine learning research* 18 (2018).
- [106] Richard D Neidinger. “Introduction to automatic differentiation and MATLAB object-oriented programming”. In: *SIAM review* 52.3 (2010), pp. 545–563.
- [107] Fernando Solís Fernández. *Lossless transmission system simulator/optimizer*. Last accessed 28 May 2021. URL: <https://github.com/FernandoSolisFernandez/Lossless-transmission-system-simulator-optimizer-/blob/main/User%20Interface%20code>.